Universiteit Leiden
The Netherlands

Role of integrin adhesions in cellular mechanotransduction

Balcıoğlu, H.E.

Citation
Balcıoğlu, H. E. (2016, March 8). *Role of integrin adhesions in cellular mechanotransduction*. Retrieved from https://hdl.handle.net/1887/38405

Version:	Corrected Publisher's Version
License:	Licence agreement concerning inclusion of doctoral thesis in the Institutional Repository of the University of Leiden
Downloaded from:	https://hdl.handle.net/1887/38405

Note: To cite this publication please use the final published version (if applicable).

Cover Page

Universiteit Leiden

Leiden University Repository

The handle http://hdl.handle.net/1887/38405 holds various files of this Leiden University dissertation

Author: Balcıoğlu, Hayri Emrah
Title: Role of integrin adhesions in cellular mechanotransduction
Issue Date: 2016-03-08

Role of Integrin Adhesions in Cellular Mechanotransduction

PROEFSCHRIFT

ter verkrijging van
de graad van Doctor aan de Universiteit Leiden,
op gezag van Rector Magnificus, prof. mr. C.J.J.M. Stolker,
volgens besluit van het College voor Promoties
te verdedigen op 8 Maart 2016
klokke 13:45 uur

door

Hayri Emrah Balcıoğlu

geboren te Şişli, Turkije
in 1986

Promotiecommissie

Promotor:	Prof. dr. B. vd Water
Promotor:	Prof. dr. T. Schmidt
Co-Promotor:	Dr. E.H.J. Danen
Overige leden:	Prof. dr. P.H. vd Graaf
	Prof. dr. M. Danhof
	Prof. dr. A. Sonnenberg
	Prof. dr. P. ten Dijke (LUMC, Leiden)
	Prof. dr. G. Koenderink (AMOLF, Amsterdam)
	Dr. ir. S.J.T. van Noort
	Dr. C. Storm (TU Eindhoven)

©2016 Hayri Emrah Balcıoğlu. All rights reserved.
Cover: GEβ1 cell immunostained for paxillin (green) and f-actin (red) and a tumoroid in 3D collagen network imaged with reflection microscopy

ISBN 978-94-6295-460-1
An electronic version of this thesis can be found at
https://openaccess.leidenuniv.nl
Printed by: Proefschriftmaken.nl || Uitgeverij BOXPress

This research was conducted at the Division of Toxicology of the Leiden Academic Centre for Drug Research, Leiden University, Leiden, The Netherlands.

Het onderzoek beschreven in dit proefschrift is onderdeel van het wetenschappelijke programma van de Stichting voor Fundamenteel Onderzoek der Materie (FOM), die financieel wordt gesteund door de Nederlandse organisatie voor Wetenschappelijk Onderzoek (NWO).

"will you *understand* what I'm going to tell you? ... No, you're not going to be able to understand it. ... That is because *I* don't understand it. Nobody does. ... while I am describing to you *how* Nature works, you won't understand *why* Nature works that way. But you see, nobody understands that. I can't explain why Nature behaves in this peculiar way."

Richard Feynman, QED: The Strange Theory of Light and Matter (1985)

Ailem için.

Contents

1 Introduction: Cell Matrix Adhesions - Feeling The Force 1

1.1 Mechanics of mechanosensing 3
1.2 The mechanical scaffolds: the cytoskeleton and the ECM . 3
1.3 Cell matrix adhesions at the heart of force sensing 7
1.4 Cell matrix adhesions in cell fate decisions 12
1.5 Concluding remarks 14
1.6 Aim and outline of this thesis 16

2 Mechanics of Angiogenesis 35

2.1 Introduction 37
2.2 Results 38
2.2.1 Tumor spheroids in 3D collagen induce the reorientation of surrounding collagen 38
2.2.2 Remote tumor-induced collagen network reorientation correlates with local cell migration capacity and requires Rho kinase-myosin activity 38
2.2.3 Endothelial spheroids orient in response to tumor-oriented collagen network 42
2.2.4 Endothelial response to oriented collagen network requires physical coupling with tumor 47
2.3 Discussion 47
2.4 Materials and methods 50
2.4.1 Cell culture 50
2.4.2 Automated sequential microprinting of tumor- and endothelial cells in ECM scaffolds 51
2.4.3 Collagen gel imaging 51
2.4.4 Laser severing assay 52
2.4.5 Image analysis 52

2.5 Acknowledgements 54
2.6 Supplemental figures 55

3 Role of Integrins in Mechanotransduction 65
3.1 Introduction 67
3.2 Results 69
3.2.1 Cells adhering through αvβ3 show more robust cytoskeletal reorganization in response to cyclic stretch as compared to cells using α5β1 69
3.2.2 Cells expressing α5β1 or αvβ3 each support cell spreading in response to substrate stiffening 71
3.2.3 Cells adhering through αvβ3 form cell-matrix adhesions at lower substrate stiffness compared to cells adhering through α5β1 72
3.2.4 Cells adhering through α5β1 or αvβ3 each mediate traction forces that are regulated in response to altered substrate rigidity 75
3.2.5 Cells adhering through α5β1 preferentially support centripetal force application and long actin filaments in an actomyosin contractility-dependent manner 76
3.3 Discussion 79
3.4 Materials and methods 81
3.4.1 Fluorescence-activated cell sorting (FACS) analysis 81
3.4.2 Cell culture 81
3.4.3 Cyclic cell stretching 82
3.4.4 Characterization of stretcher strain field 83
3.4.5 PAA substrates 83
3.4.6 Analysis of stiffness of PAA gels by rheology 84
3.4.7 PAA and PDMS adhesion assay 85
3.4.8 Assays using PDMS micropillars 85
3.4.9 Immunostaining 86
3.4.10 Microscopy 86
3.4.11 Image analysis 87
3.4.12 Pillar deflection analysis 88
3.4.13 Statistical analysis 88
3.5 Acknowledgements 89
3.6 Supplemental figures 90

4 Quantitative dSTORM on Cell-Matrix Adhesions 101
4.1 Introduction 103
4.2 Results 104
4.2.1 dSTORM on cell matrix adhesion proteins 104
4.2.2 Combination of dSTORM and cellular traction force measurements 104
4.2.3 From dSTORM localizations to molecule counts . 106
4.2.4 Relating the abundance of cell matrix adhesion proteins to traction forces 109
4.3 Discussion 112
4.4 Materials and methods 115
4.4.1 Cell culture and transduction 115
4.4.2 Micropillar preparation and cell seeding 116
4.4.3 Fixation and immunostaining 116
4.4.4 Imaging and analysis 117
4.4.5 Statistic analysis 120
4.5 Acknowledgements 120
4.6 Supplemental materials 121
4.6.1 Obtaining the cdf 121
4.6.2 Relation between variance and squared mean . . . 121
4.6.3 Simulation for a combined statistics with secondary antibody labeling 121

5 Migration and Traction Force 131
5.1 Introduction 133
5.2 Results 134
5.2.1 Larger adhesions and altered adhesion dynamics in response to knockdown of TPM1, PPP1R12B, RAC2 or HIPK3 134
5.2.2 Knockdown of TPM1, PPP1R12B, RAC2 or HIPK3 inhibits tumor cell migration 135
5.2.3 Knockdown of PPP1R12B, RAC2 and HIPK3 results in higher traction forces and slower force turnover 135
5.3 Discussion 140
5.4 Materials and methods 142
5.4.1 Cell culture 142
5.4.2 Cell transfection with siRNA 142
5.4.3 Automated microscopy 143
5.4.4 Image analysis 143

5.4.5 Random cell migration assay 144
5.4.6 Traction force microscopy with silicon elastomeric micropillar post arrays 144
5.4.7 Statistic analysis 146
5.5 Acknowledgements 146
5.6 Authors' contribution 146
5.7 Supplemental figures 148

6 General Discussion **155**

Summary **167**

Özet **171**

Samenvatting **175**

List of Abbreviations **179**

Publications **181**

Curriculum Vitae **183**

Chapter 1

Introduction: Cell matrix adhesions - feeling the force [1]

[1] This chapter is partially based on: Karin A Jansen; Dominique M Donato; Hayri E Balcıoğlu; Thomas Schmidt; Erik HJ Danen; Gijsje H Koenderink, A guide to mechanobiology: Where biology and physics meet., *Biochimica et biophysica acta. 2015*

Abstract

In their natural context, cells are in contact with the extracellular matrix (ECM) that provides cells with chemical and physical cues. The physical properties of the ECM control cell survival, proliferation, and differentiation, and its deregulation can contribute to pathologies such as fibrosis and cancer. Transmembrane receptors of the integrin family couple the ECM network to the intracellular cytoskeletal network. Integrins sense and transmit biophysical cues in both directions, providing mechanical homeostasis between cells and ECM. Here, we discuss recent advances in our understanding of the integrin-associated mechanotransduction complex within cell-matrix adhesions and how this, in concert with chemosensory signaling pathways, controls cell fate.

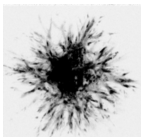

Cells are able to sense and respond to physical as well as chemical aspects of their surrounding extracellular matrix (ECM) to maintain homeostasis with their environment. The physical aspect of this interaction determines normal cell function, stem cell differentiation and tissue homeostasis [1, 2], while deregulation can contribute to onset and progression of cancer [3]. Forces also play a crucial role in embryogenesis [4, 5] and cells in our body are constantly under force; e.g. cell-cell forces in epithelial tissues, compression and tension due to muscle contraction, shear forces in vasculature, lung epithelium and intestines. Therefore, in addition to its importance in cancer research, manipulating the mechanical properties of the ECM has become a powerful tool in stem cell research and tissue engineering.

1.1 Mechanics of mechanosensing

Several signal transducers have been implicated in the ability of cells to sense and respond to extracellular forces, including ion channels, cell matrix adhesion complexes and membrane-associated phospholipases [6, 7]. In any case, a force-transmitting cytoskeleton is essential for cells to sense the mechanical properties of the environment. The microtubules (MT) [8], actin cytoskeleton [9] and intermediate filaments (IF) [10] have all been implicated in cellular mechanotransduction. Indeed, Rho GTPases, the enzymes in control of cytoskeletal organization [11], play important roles in cellular sensing of- and responding to force [12, 13].

1.2 The mechanical scaffolds: the cytoskeleton and the ECM

Cytoskeletal networks, enable cells to maintain their shape and mechanical strength [14]. Of the three cytoskeletal systems; MTs, IFs and actin cytoskeleton, the emphasis has been on actin cytoskeleton that is responsible for traction force generation [15]. The actin cytoskeleton forms a continuous network between the nucleus and, via the adhesion complex, the ECM [16] (Figure 1.1). Cells, prominently on 2D substrates, form long contractile actomyosin structures termed stress fibers that apply traction forces via myosin molecular motors pulling on polarized actin filaments [15]. Formation and organization of such stress fibers

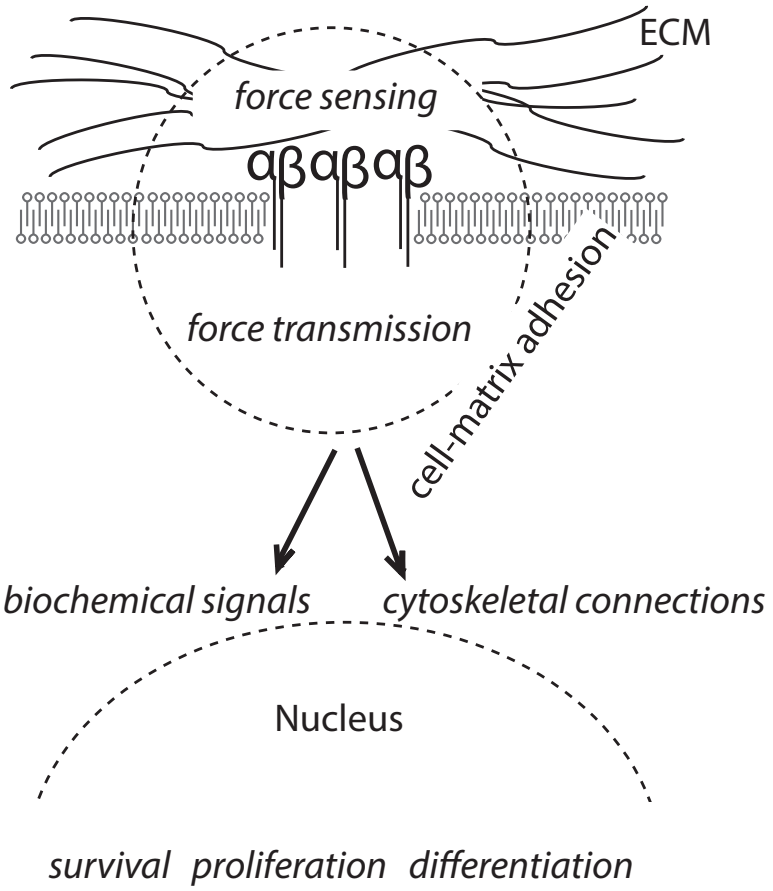

Figure 1.1
Mechanical cues from the environment dictate cell fate decisions. *Cartoon depicting force sensing, transmission, and translation into biological response through cell matrix adhesions.*

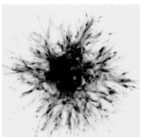

are stiffness dependent [17, 18]; and the formation of adhesion complexes is dependent on the actin cytoskeleton [19].

Purified networks of actin and intermediate filaments increase their stiffness under the influence of force. In other words, these networks strain-stiffen in response to mechanical shear or stretch [20–22]. This phenomenon allows cells to actively stiffen their actin cytoskeleton on hard substrates [18]. Moreover, strain-stiffening of IFs is thought to prevent excess deformation of cells and epithelial tissues [21, 22].

Microtubules (MTs) are not so widely studied in the context of mechanotransduction but MTs also influence cell-matrix adhesions by regulating traction forces via crosstalk with the actomyosin machinery and it has been shown that both on 2D substrates [23, 24] and in 3D collagen gels [25, 26], MT depolymerization causes increased traction forces and thereby adhesion maturation [27].

ECM properties play an important role in mechanosensing. Cells can sense the global (i.e. macroscopic) and local (e.g. fiber) matrix stiffness, matrix topography [28], the porosity [29] and dimensionality as well as actively change the physical properties of the ECM [30, 31]. In fibrous collagen or fibrin networks, cells can sense to a length scale of ∼200 µm [32, 33], whereas on 2D flexible gels, this distance is reduced to a few tens of microns [34, 35]. The organization of ECM network is tailored to the function of each tissue, for instance collagen fibers are thick and aligned in stiff tissues like tendon to ensure tensile strength, whereas they are thin and organized in a meshwork in cornea to ensure optical transparency. During disease progression and aging the physiological organization of the ECM is subject to changes and ECM is increasingly recognized as an active player and potential therapeutic target in diseases such as fibrosis, atherosclerosis and cancer [36–40].

The ECM forms a scaffold for cells to adhere to and acts as a reservoir for growth factors, cytokines and proteolytic enzymes. ECM structures can be 2D (e.g. basement membrane) as well as 3D (connective tissue) and cell matrix adhesion proteins regulate cell motility on both of these ECM environments [41].

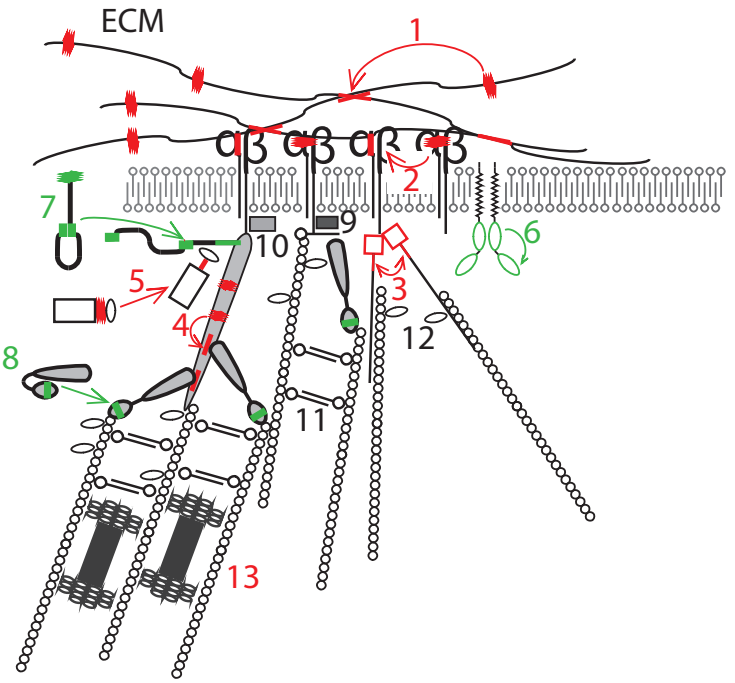

Figure 1.2
Cell matrix adhesions as hotspots for bidirectional mechanotransduction. *Elements associated with cell matrix adhesions that act as force sensors; e.g. change conformation/interactions in response to force are indicated in red. Elements that are implicated in force transmission but have not (yet) been directly implicated as force sensors are indicated in green. 1) When cytoskeletal contractility, through integrins, stretches fibronectin fibers; cryptic sites are exposed that cause enhanced cross-linking; 2) intracellular or extracellular forces cause conformational changes in the integrin head domain of some integrins driving strengthening of a catch bond with ECM; 3) kinetics of filamin dimerization change under force, which affects its actin and integrin binding; 4) stretching of flexible domains in talin exposes cryptic vinculin (8)-binding sites; 5) stretching of the linker domain in p130Cas may expose phosphorylation sites, which can trigger new protein-protein interactions; 6) force-dependent unfolding of the zipper-like autoinhibitory domains in RPTPalpha may underlie its role in rigidity sensing; 7) force-dependent breaking of an autoinhibitory intramolecular interaction involving the FERM domain and/or stretching of its adhesion targeting domain may trigger FAK activation and explain its role in force transmission; 8) myosin contractility-dependent interaction of vinculin head and tail domains is important for its role in mechanotransduction; 9-12) ILK, paxillin, alpha-actinin and zyxin have been implicated in rigidity sensing but it is not known whether they undergo conformational change in response to physiological force; 13) extracellular forces, through cell matrix adhesions enhance actomyosin contractility thereby balancing intra- and extracellular forces in the cell matrix adhesions and coupling through physical linkage to the nuclear envelope.*

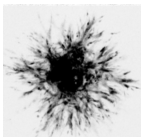

1.3 Cell matrix adhesions at the heart of force sensing

The regions where cells are in close physical contact with their environment and connect to the actin cytoskeleton - the "cell matrix adhesions" - appear to be hotspots for mechanotransduction [42] (Figure 1.2). Within cell matrix adhesions, clustered integrin transmembrane receptors bind ECM components with their globular head domains and connect to the actin cytoskeleton through their short cytoplasmic tails [43–45]. Coupling to the cytoskeleton is indirect, involving a large, regulated protein complex that connects the integrin tails to f-actin fibers [43]. Cell matrix adhesions are mechanosensitive structures [46–48] that may also be centers for protein synthesis through force dependent recruitment of ribosomes [49]. The activity of Rho GTPases is regulated by force responsive signaling cascades in cell matrix adhesions [50]. In turn, Rho GTPase-mediated alterations in cytoskeletal tension affect growth and turnover of cell-matrix adhesions [51, 52].

Cell matrix adhesions have a well-preserved nanoarchitecture [53], their size correlates with cell migration speed in 2D [54] and the presence of cell matrix adhesions in 3D ECM environments has been established [55–57]. The tight connection between force and cell matrix adhesions has been studied using laser tweezers [58], traction force microscopy on deformable gels [59], micropillar arrays [60, 61] and bead displacement maps in 3D ECM networks [62].

Integrins recruit more than 150 different proteins to the cell-ECM adhesion complex, many of which are Lin11, Isi-1, Mec-3 (LIM) domain proteins that were recruited to the adhesion in a force responsive manner [63]. Integrins as well as several integrin-associated proteins that reside in cell matrix adhesions have also been shown to act as mechanotransducers [64]: they change conformation and/or expose new protein-binding sites when stretched by force. This allows cell matrix adhesions to alter intermolecular interactions that affect signaling pathways and connections to the actin cytoskeleton in response to force, thereby ensuring a balance between extracellular (ECM) and intracellular (cytoskeletal) forces. Indeed, the molecular architecture and size of cell matrix adhesions depend on myosin-derived cellular contractility [65, 66]. Key force sensors associated with cell matrix adhesions are described in Figure 1.2. Notably, for several additional cell matrix adhesion-associated proteins,

despite their important role in adhesion and migration, such as tensin, parvins, kindlins; neither conformational changes in response to force nor direct implication in force transmission has been demonstrated thus far.

Integrins are bi-directional transmembrane signaling receptors. Intracellular proteins bind to the tail region of integrins, thus causing conformational changes in the head region that increases affinity for its extracellular ligands (inside-out signaling) and ligand binding triggers conformational changes that activate intracellular signaling cascades (outside-in signaling). Integrins are heterodimers of an α and a β subunit and so far 24 different heterodimers formed by combinations of 18 different α subunits and 8 β subunits have been identified [45]. Most integrins recognize multiple ligands, for instance, integrin αvβ3 can bind to vitronectin, fibronectin and fibrinogen through the RGD-binding motif [67]. Additionally, in 3D environments, integrins are required for the fibrillogenesis of various ECM proteins [68, 69].

Integrins play a central role in environment sensing: integrin binding to the ECM promotes integrin clustering and recruitment of additional proteins into cell matrix adhesions [70], and through cytoplasmic linker proteins integrins connect to the actin cytoskeleton, which in turn is physically connected to the nucleus [71]. The spacing and pattern of integrin ligands controls cell spreading and cell matrix adhesion maturation [72]. It has been shown that clustering of integrins to form adhesion complexes requires a certain minimum ligand density [72–76] and that forces supported by individual integrin-RGD pair increases with reduced ligand spacing [77]. In addition, integrins go through force dependent binding/unbinding cycles, which regulate the activity of Rho GTPases, cell matrix adhesion formation, and integrin turnover [78, 79].

Mechanical loading has been shown to influence the lifetime of some integrin-ECM bonds. For instance αIIbβ3, exhibits slip-bond behavior characterized by a decreased lifetime with increasing load [80], whereas the integrin α5β1 heterodimer forms catch bonds with the ECM protein, fibronectin: the bonds are strengthened in response to external (ECM-driven) or internal (cytoskeleton-derived) force application [81, 82]. This force-dependent strengthening of catch bonds between α5β1 and fibronectin is necessary to create downstream signaling cascades [83] and theoretical modeling has shown that catch bond clusters can act as autonomous mechanosensors [84, 85].

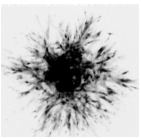

Different integrin heterodimers that bind to the same ECM protein have been shown to respond differently to applied force. Cells adhering to fibronectin substrates through αvβ3 versus α5β1 integrins, for instance, differ in traction force generation [86, 87], dynamics [88], and adhesion [88, 89]. These integrins activate different intracellular signaling cascades [87, 90] and interchanging the ligand binding domains reverses the signaling phenotype [91, 92]. Similarly, expression of αvβ6 integrins in the presence or absence of α5β1 changes traction force generation [84]. Different splice variants of α6β1 also give rise to different phenotypes due to the two distinct cytoplasmic domains [93]. Thus cells can regulate their mechanosensitivity by modifying the integrin expression profile.

ILK (integrin linked kinase) is a pseudokinase that is part of the ILK-Pinch-Parvin (IPP) complex that plays critical roles in coupling integrins to the f-actin cytoskeleton in cell matrix adhesions [94]. ILK is directly recruited to integrin beta1 and beta3 cytoplasmic domains and is crucial for actin rearrangement, cell polarization, spreading, migration, proliferation, survival and tumor metastasis [95]. The ILK protein itself has not been shown to directly respond to force but it is recruited to cell matrix adhesions in a myosin II activity-dependent manner [96].

Talin and ***vinculin*** are adaptor proteins located in the cell matrix adhesions that have a mechanosensitive interaction. The talin head domain activates integrin through binding to its beta tail causing dissociation of the alpha and beta cytoplasmic domains [97]. Talin also directly connects integrins to the actin cytoskeleton. Talin is important for force-induced adhesion strengthening through interactions with integrin alphavbeta3 [88]. Vinculin is recruited to cell matrix adhesions in a force dependent manner [66, 98] and mediates cell matrix adhesion growth through binding to talin and f-actin [99]. Vinculin is required for force-induced cell matrix adhesion stabilization [100] and overall cell responses to environment stiffness [101, 102] possibly through Src-mediated phosphorylation at residues Y100 and Y1065 [103]. Despite enhancing cellular traction forces, vinculin is not required for force transmission at cell matrix adhesions but myosin contractility-dependent interaction of the vinculin head and tail domains is important for cellular mechanotransduction [102, 104]. Experiments with isolated talin and vinculin molecules showed that application of physiological forces to talin molecules leads to exposure of cryptic vinculin-binding sites [105]. This unfolding of talin has also been observed in isolated cells [106]. Possibly through this in-

teraction, vinculin stabilizes talin in an unfolded conformation and its localization shifts from integrin proximal to actin proximal region with increasing force [107]. Notably, vinculin interacts with several other cell matrix adhesion proteins and can be recruited to cell matrix adhesions upon force application in a talin-independent manner as well (see paxillin section).

Filamin and ***alpha-actinin*** are f-actin crosslinking proteins that can also directly bind integrin to actin filaments [108]. The filamin A-integrin interaction requires force [109], can stimulate activation of Rho GTPases in a force dependent manner [110], and is necessary for cells to induce collagen gel contraction [111]. Filamin A can unfold and change actin-binding dynamics under force [112]. Filamin A and talin bind to the same region in the integrin cytoplasmic tail, which might suggest a competition between filamin A and talin for integrin binding [113]. However knockdown of filamin A causes, in addition to an increased number of force-induced apoptotic cells, a reduction in force-induced beta1 integrin activation and a reduction in recruitment of talin and vinculin molecules to the adhesion [114]. Alpha-actinin, competes with talin for integrin beta3 tail binding but cooperates with talin when binding the integrin beta1 tail [115]. Alpha-actinin is not required for cell matrix adhesion force generation but it controls cell matrix adhesion maturation through its role in generating an actin network [9] and in connecting this network to the integrin mediated adhesions [115].

Zyxin recruits actin polymerizing proteins to integrin-mediated adhesions [116]. It changes binding kinetics and induces actin polymerization at cell matrix adhesions under force [117, 118]. Zyxin is also known to mobilize from cell matrix adhesions to actin fibers upon stretch [119] in a force-dependent manner [120]. Upon force-dependent relocalization to actin fibers, zyxin, together with alpha-actinin plays a role in actin stress fiber maintenance [121, 122].

p130Cas is a member of the Cas (Crk-associated substrate) family of proteins that is localized to cell matrix adhesions. p130Cas plays a role in migration, cell cycle control, apoptosis, differentiation and cancer development [123, 124]. Stretching the p130Cas protein in vitro increases its tyrosine phosphorylation, which is known to influence adhesion formation and actin dynamics [125, 126]. p130Cas phosphorylation is also important in cellular reorientation upon cyclic stretch [127] and coupling of the cytoskeleton to the adhesion during migration [128]. Studies of

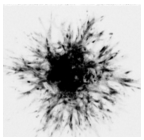

vinculin knockout cells and vinculin mutants unable to bind to p130Cas, have shown that vinculin is necessary for p130Cas to respond to changes in substrate rigidity [129].

FAK (Focal Adhesion Kinase) is a protein-tyrosine kinase that is present in cell matrix adhesions. FAK regulates the activity of Rho GTPases and its kinase activity increases in response to extracellular forces [130]. Modification of an autoinhibitory intramolecular interaction involving the FAK four-point-one, ezrin, radixin, moesin (FERM) domain may be involved in this regulatory mode [7]. Direct evidence from *in vitro* studies demonstrating that FAK is a mechanoresponsive protein is not available but computer simulations have predicted that the cell matrix adhesion targeting (FAT) domain of FAK protein will extend under physiological force and this might regulate its interaction with paxillin [131]. There is evidence that FAK can be activated in a tension dependent or independent manner through its interaction with different integrins [132]. Indeed, FAK is recruited to cell matrix adhesions in a myosin contractility-dependent manner [66].

Paxillin is a multidomain adaptor protein that is essential for cell matrix adhesion formation, plays an important role for cell migration in 2D and 3D [131, 133] and mediates force induced Rho GTPase activity [134]. Paxillin phosphorylation, but not its localization to cell matrix adhesions, depends on myosin II activity [66]. This force dependent phosphorylation of paxillin is regulated by FAK activity, which in turn regulates vinculin recruitment to cell matrix adhesions, adhesion assembly and turnover, and cellular response to changes in ECM stiffness [135, 136].

RPTP-alpha (receptor-like protein tyrosine kinase alpha) is a transmembrane protein that co-localizes with alphav integrins at the leading edge of migrating cells and takes part in force-dependent formation and strengthening of cell matrix adhesions [137, 138]. RPTP-alpha might be able to respond directly to mechanical stimuli through force-dependent unfolding of its zipper-like autoinhibitory domains [139]. RPTP-alpha-dependent rigidity sensing influences neuronal migration [140] and is required for cells to exert forces on the ECM [61].

ECM proteins, similar to intracellular cell matrix adhesion proteins discussed above, can be stretched when force is applied and expose cryptic binding sites or growth factors [141]. The ***fibronectin*** matrix is an example of an ECM that is modified as force is applied to it. Fi-

bronectin is a globular ECM protein that is highly abundant in plasma and produced by cells during active processes such as tissue regeneration, angiogenesis and tumor invasion. Fibronectin is assembled into a fibrillar network via interactions with integrins and syndecan receptors [69]. Rho GTPase activity is required to generate the contractile force for fibronectin fibrilogenesis and assembly of a fibronectin matrix. The fibronectin fibrillar network stiffens with applied force [142]. This stiffening is probably due to cryptic binding sites for intramolecular interactions within the network that become exposed under force [143, 144].

Taken together, integrins and several associated cell matrix adhesion proteins undergo conformational changes in response to force. This leads to new protein-protein interactions within cell matrix adhesions, strengthened interaction with the cytoskeleton, and cytoskeletal network stiffening when extracellular force is applied. Vice versa, enhanced cytoskeletal tension - likely through the same complex of proteins - exerts forces on ECM proteins (such as fibronectin), which induces ECM reorganization through enhanced protein unfolding and protein-protein interactions, causing ECM stiffening. Thus, integrin-containing cell matrix adhesions act as key protein complexes that mediate bidirectional force transduction across the plasma membrane to ensure physical homeostasis between cells and ECM.

1.4 Cell matrix adhesions in cell fate decisions

Cell survival and proliferation is supported by ECM attachment in a manner that requires an intact actomyosin network and the ability of cells to spread [145, 146]. Crucial determinants of cell cycle progression, including mitogen-activated protein(MAP) kinase activity, cyclin D expression, and cyclin-dependent kinase (cdk) inhibitor levels are not properly regulated when cells attach to soft, rather than stiff collagen matrices leading these cells into quiescence [147]. Integrin signaling through FAK is one mechanosensitive mechanism involved: on rigid but not soft ECM substrates FAK is activated causing Rac-mediated cyclin D1 gene induction, cyclin D1-dependent phosphorylation of the retinoblastoma(Rb) protein, and passage through the restriction point into synthesis(S) phase [148]. ECM stiffness also controls endothelial cell proliferation during angiogenesis *in vitro* and *in vivo*: in this case Rho-dependent regulation of the balance between two mutually antagonistic

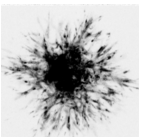

transcription factors that influence expression of the vascular endothelial growth factor receptor (VEGFR) is the mechanoresponsive switch [149].

Stem cell differentiation is one of the processes where mechanotransduction has been shown to have a major impact [150]. Cellular mechanosensing drives mesenchymal stem cell differentiation, with soft substrates promoting neuronal- and stiff substrates promoting osteoblast lineage specification [1]. Traction forces and integrin signaling regulate cell stemness [151]. On the one hand sensing of global rigidity was hypothesized to be involved [1]. On the other hand, the underlying mechanism was reported to involve differences in ligand anchoring density: stiffer hydrogels provide a denser network of ECM protein anchorage points and the resulting larger resistance to integrin-mediated cellular pulling force is sensed by the cells and controls cell fate decisions [152]. Similarly, in 3D environments, the cell-mediated degradation of the ECM resulted in larger traction forces and higher osteogenesis [153]. The spacing and patterning of integrin ligands, through its regulation of cytoarchitecture, controls mechanical properties of mesenchymal stem cells that would be expected to affect differentiation [72, 154]. In embryonic stem cells, substrate stretching has provided somewhat confusing results with evidence for stretch supporting either differentiation or stemness [155–157]. In agreement with a need to balance cellular and extracellular forces, the ability to stimulate actomyosin contractility through RhoA signaling is important for *in vivo* differentiation of lung epithelium [158]. Given the importance for these findings to the field of tissue engineering and stem cell therapeutics, cell culture techniques have been developed where substrate rigidity can be fine-tuned to control the balance between pluripotency, differentiation, and lineage specification. This includes patterned substrates [159], 2D and 3D substrates with different rigidities [160–162], or substrates with dynamically controlled rigidity [163].

Tumor progression is another aspect in which integrin-mediated mechanotransduction plays a critical role [164]. Tumor malignancy is affected by ECM stiffness with increasing ECM rigidity promoting invasive growth through force-induced integrin- [39], FAK- [165, 166], Rho- and extracellular signal-regulated kinases(ERK)-signaling [40] and actomyosin contractility [167]. RPTP-alpha-dependent rigidity sensing also supports cancer cell invasion [168]. Integrin antagonists, which would disrupt the ability of cell matrix adhesion to act as mechanotransduc-

ing units, are considered to be promising anticancer therapeutics [169]. Interfering with integrin-mediated adhesions can reduce the ability of metastatic tumor cells to proteolytically degrade ECM during invasion [170] and it can increase tumor cell sensitivity to radiotherapy [171]. However, the role of integrins in different cancer types / oncogenic backgrounds is complex [172] and blocking integrin adhesions have been shown to both induce [173–175] and block [176] cancer progression.

Other biological processes - In the zebrafish, mutations in ILK interfere with the ability of cardiomyocytes to sense mechanical stretch and respond to it by upregulating crucial factors that regulate calcium waves [177]. Silencing beta-parvin phenocopied the ILK mutation, together providing genetic evidence that the integrin-IPP complex is important in heart function. This interaction is also important in the development and functionality of the mammalian heart [178] and has been implicated in cardiomyopathy in humans [179]. Integrin-mediated mechanosensing also plays an important role in normal vascular physiology and atherosclerosis. Changes in fluid shear stress affect endothelial cell biology in developing and adult bloodvessels. It has been proposed that the glycocalyx, receptors, and ion channels at the luminal surface all participate in shear stress sensing and the resulting tension is transmitted (i.e. via the cytoskeleton) to integrin-mediated cell-matrix adhesions at the basal cell surface. These adhesions subsequently act as mechanotransducers and activate signaling pathways to adapt to the altered blood flow [180].

1.5 Concluding remarks

It has become evident over the past years that mechanical cues from the ECM control physiology and pathology in a wide range of biological settings. It is clear that integrin-mediated adhesion sites are important mediators of bidirectional force transmission that connect the ECM and cytoskeleton. The force-regulated conformations and associations within cell matrix adhesions are partly resolved and many more molecular interactions that are subject to force modulation are expected to be discovered. Another aspect that is only partially understood is how mechanical signaling in cell matrix adhesions is coupled to cell fate decisions. The cytoskeleton connects integrins to LINC (linker of nucleoskeleton and cytoskeleton) complexes in the nuclear envelope. There, nesprin proteins

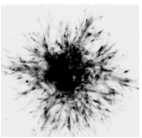

in the outer membrane connect to microtubules, actin fibers, and intermediate filaments while Sad1 and UNC84 (SUN) domain proteins in the inner membrane bind the nuclear lamina [181]. Since chromatin-binding proteins and DNA are attached to the nuclear lamina, extracellular mechanical stress may be propagated into the chromatin and affect gene expression through conformational regulation of DNA and associated proteins. However, although extracellular forces, through integrins are mechanically linked to changes in nuclear orientation and shape [71], direct evidence for such purely mechanical coupling between ECM and gene expression is lacking.

Mechanical perturbations are translated into biochemical signaling in cell matrix adhesions. Therefore the molecular composition of the adhesion is important for cellular mechanosensing. Studies relating myosin activity to protein localization and turnover rates have shown that the adhesion structure itself is force dependent [66, 117, 118]. Additionally, super resolution microscopy has also allowed the study of force dependent nanoscale architecture of adhesion protein vinculin [107]. However force-molecular recruitment relation in cell-matrix adhesions is unknown. This relation can be unraveled through a reliable method that addresses the abundance of adhesion molecules. Cell-matrix adhesions that are coupled to the ECM via different integrins have differential mechanoresponse [88]. Cellular expression profile of integrins also dictate activated signaling pathways and regulate cellular force application [86, 87]. However how different integrins regulate cellular response to mechanical cues remains to be addressed.

Integrin expression profile and role of mechanical cues have also been addressed in relation to cancer [39, 40]. ECM-tumor cell interaction as well as the ECM itself is deregulated in cancer and such changes affect cancer progression [3]. Understanding the altered mechanoresponse in cancer may help develop new therapeutic interventions. Extensive crosstalk with various other signaling pathways further complicates the concerted effect of physical and chemical stimuli. Therefore it is necessary to isolate the effect of mechanosensing that is cell type and protein expression independent to understand how the physical tumor-ECM communication might affect hallmarks of cancer such as activation of invasion, metastasis and angiogenesis.

1.6 Aim and outline of this thesis

With the studies described in this thesis, I aimed to further the understanding of the mechanism and importance of cellular mechanotransduction. The focus was on integrin mediated adhesions and their roles in inside-out and outside-in mechanosensing. In chapter 2, the role of physical signaling in tumor progression is studied. Using automated sequential microprinting of tumor and endothelial cells in 3D collagen gels in combination with reflection microscopy it is shown that; i) tumor expansion and tumor induced collagen organization are highly correlated, ii) this relation is dependent on cellular force generation but is resistant to depletion of collagen-binding integrins, iii) the remote organization of collagen induced by the tumor steers directional migration of endothelial cells, iv) this directional migration is impaired upon severing the physical connection between the tumor and endothelial cells. The physical signaling by the tumor is thus shown to influence tumor expansion and angiogenesis. Chapter 3 focusses on fibronectin binding integrins α5β1 and αvβ3 and describes their differential role in outside-in and inside-out cellular mechanosensing. It shows that cells expressing either of these integrins are able to reorganize their cytoskeleton upon cyclic stretch and induce ECM stiffness driven cellular spreading with similar efficiencies. Likewise, these integrins are shown to support similar magnitudes of cellular traction force generation and stiffness dependent regulation of cellular traction forces. However, cells that express αvβ3 are identified to form adhesions on softer substrates and to be able to better organize their actin cytoskeleton upon cyclic stretch and maintain this organization at higher strain rates. In contrast, cells that express α5β1 are shown to support more centripetally oriented traction forces in a ROCK/myosin activity dependent manner that also supports generation of longer actin fibers. Therefore it is shown that differential expression of fibronectin binding integrins regulate cellular plasticity by fine tuning sensing-force application capacities through differential regulation of ROCK/myosin signaling and actin cytoskeleton. In chapter 4 the relation between molecular composition of the adhesion, the force generation and environment stiffness is shown. Using a new approach to quantify the number of molecules in a cellular structure, the recruitment of adhesion proteins talin, paxillin, vinculin and FAK is studied in relation to force application and environment stiffness. Chapter 5 studies the cellular mechanotransduction in context of cancer cell migration and adhesion

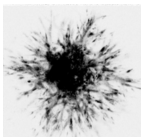

structure. Genes that are identified as regulators of cell-matrix adhesion and cancer cell migration are shown to regulate cellular traction force generation mechanisms. Formation of larger adhesions, reduced cellular migration, higher traction force generation and slow force turnover rates are identified to be interrelated. Lastly, in chapter 6 the overall conclusions of the studies in this thesis and future perspectives are described.

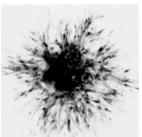

Bibliography

[1] Adam J Engler et al. "Matrix Elasticity Directs Stem Cell Lineage Specification". In: *Cell* 126.4 (2005).

[2] A Wayne Orr et al. "Mechanisms of Mechanotransduction". In: *Developmental Cell* 10.1 (2006).

[3] Pengfei Lu, Valerie M Weaver, and Zena Werb. "The extracellular matrix: A dynamic niche in cancer progression". In: *The Journal of Cell Biology* 196.4 (2012).

[4] Thibaut Brunet et al. "Evolutionary conservation of early mesoderm specification by mechanotransduction in Bilateria." In: *Nature communications* 4 (2013).

[5] Otger Campàs et al. "Quantifying cell-generated mechanical forces within living embryonic tissues." In: *Nature Methods* 11.2 (2014).

[6] Akiko Mammoto, Tadanori Mammoto, and Donald E Ingber. "Mechanosensitive mechanisms in transcriptional regulation". In: *Journal of Cell Science* 125.13 (2012).

[7] Simon W Moore, Pere Roca-Cusachs, and Michael P Sheetz. "Stretchy proteins on stretchy substrates: the important elements of integrin-mediated rigidity sensing." In: *Developmental Cell* 19.2 (2010).

[8] Kenneth A Myers et al. "Distinct ECM mechanosensing pathways regulate microtubule dynamics to control endothelial cell branching morphogenesis." In: *The Journal of Cell Biology* 192.2 (2011).

[9] Patrick W Oakes et al. "Tension is required but not sufficient for focal adhesion maturation without a stress fiber template". In: *The Journal of Cell Biology* 196.3 (2012).

[10] Colin P Johnson et al. "Forced unfolding of proteins within cells." In: *Science (New York, N.Y.)* 317.5838 (2007).

[11] Aron B Jaffe and Alan Hall. "Rho GTPases: Biochemistry and biology". In: *Annual Reviews of Cell Biology* 21 (2005).

[12] Benjamin D Matthews et al. "Cellular adaptation to mechanical stress: role of integrins, Rho, cytoskeletal tension and mechanosensitive ion channels". In: *Journal of Cell Science* 119.3 (2006).

[13] Michele A Wozniak et al. "ROCK-generated contractility regulates breast epithelial cell differentiation in response to the physical properties of a three-dimensional collagen matrix". In: *The Journal of Cell Biology* 163.3 (2003).

[14] Fabio Zampieri, Matteo Coen, and Giulio Gabbiani. "The Prehistory of the Cytoskeleton Concept". In: *Cytoskeleton* 71.8 (2014).

[15] Keith Burridge and Erika S Wittchen. "The tension mounts: Stress fibers as force-generating mechanotransducers". In: *The Journal of Cell Biology* 200.1 (2013).

[16] Ning Wang, Jessica D Tytell, and Donald E Ingber. "Mechanotransduction at a distance: mechanically coupling the extracellular matrix with the nucleus". In: *Nature Reviews. Molecular cell biology* 10.1 (2009).

[17] Mirjam Ochsner et al. "Dimensionality controls cytoskeleton assembly and metabolism of fibroblast cells in response to rigidity and shape." In: *PLoS One* 5.3 (2010).

[18] Jérôme Solon et al. "Fibroblast adaptation and stiffness matching to soft elastic substrates." In: *Biophysical Journal* 93.12 (2007).

[19] Ulrich S Schwarz and Margaret L Gardel. "United we stand: integrating the actin cytoskeleton and cell-matrix adhesions in cellular mechanotransduction." In: *Journal of Cell Science* 125.Pt 13 (2012).

[20] PA Janmey et al. "Viscoelastic properties of vimentin compared with other filamentous biopolymer networks." In: *The Journal of Cell Biology* 113.1 (1991).

[21] Michael Schopferer et al. "Desmin and vimentin intermediate filament networks: their viscoelastic properties investigated by mechanical rheometry." In: *Journal of Molecular Biology* 388.1 (2009).

[22] Cornelis Storm et al. "Nonlinear elasticity in biological gels." In: *Nature* 435.7039 (2005).

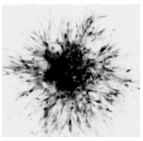

[23] Barbara A Danowski. "Fibroblast contractility and actin organization are stimulated by microtubule inhibitors". In: *Journal of Cell Science* 93 (1989).

[24] Andrew Rape, Wei-hui H Guo, and Yu-li L Wang. "Microtubule depolymerization induces traction force increase through two distinct pathways." In: *Journal of cell science* 124.Pt 24 (2011).

[25] Areum Kim and Matthew W Petroll. "Microtubule regulation of corneal fibroblast morphology and mechanical activity in 3-D culture". In: *Experimental Eye Research* 85.4 (2007).

[26] Michael S Kolodney and Elliot L Elson. "Contraction due to microtubule disruption is associated with increased phosphorylation of myosin regulatory light chain". In: *Proceedings of the National Academy of Sciences of the United States of America* 92.22 (1995).

[27] Daniel HJ Ng et al. "Microtubule-Dependent Modulation of Adhesion Complex Composition". In: *PLoS One* 9.12 (2014).

[28] Ahmed Ballo et al. "Nanostructured model implants for in vivo studies: influence of well-defined nanotopography on de novo bone formation on titanium implants". In: *International Journal of Nanomedicine* 6 (2011).

[29] Amit Pathak and Sanjay Kumar. "Independent regulation of tumor cell migration by matrix stiffness and confinement". In: *Proceedings of the National Academy of Sciences of the United States of America* 109.26 (2012).

[30] Karin A Jansen et al. "Cells Actively Stiffen Fibrin Networks by Generating Contractile Stress". In: *Biophysical Journal* 105.10 (2013).

[31] Jessamine P Winer, Shaina Oake, and Paul A Janmey. "Nonlinear Elasticity of Extracellular Matrices Enables Contractile Cells to Communicate Local Position and Orientation". In: *PLoS One* 4.7 (2009).

[32] Xiaoyue Ma et al. "Fibers in the Extracellular Matrix Enable Long-Range Stress Transmission between Cells". In: *Biophysical Journal* 104.7 (2013).

[33] Mathilda S Rudnicki et al. "Nonlinear Strain Stiffening Is Not Sufficient to Explain How Far Cells Can Feel on Fibrous Protein Gels". In: *Biophysical Journal* 105.1 (2013).

[34] Amnon Buxboim et al. "How deeply cells feel: methods for thin gels". In: *Journal of Physics: Condensed Matter* 22.19 (2010).

[35] John M Maloney et al. "Influence of inite thickness and stiffness on cellular adhesion-induced deformation of compliant substrata". In: *Physical review. E, Statistical, nonlinear, and soft matter physics* 78.4 Pt 1 (2008).

[36] Craig E Barcus et al. "Stiff Collagen Matrices Increase Tumorigenic Prolactin Signaling in Breast Cancer Cells". In: *Journal of Biological Chemistry* 288.18 (2013).

[37] Ovijit Chaudhuri et al. "Extracellular matrix stiffness and composition jointly regulate the induction of malignant phenotypes in mammary epithelium". In: *Nature Materials* 13.10 (2014).

[38] Cedric Gaggioli et al. "Fibroblast-led collective invasion of carcinoma cells with differing roles for RhoGTPases in leading and following cells". In: *Nature Cell Biology* 9.12 (2007).

[39] Kandice R Levental et al. "Matrix Crosslinking Forces Tumor Progression by Enhancing Integrin Signaling". In: *Cell* 139.5 (2009).

[40] Matthew J Paszek et al. "Tensional homeostasis and the malignant phenotype". In: *Cancer Cell* 8.3 (2005).

[41] Stephanie I Fraley et al. "A distinctive role for focal adhesion proteins in three-dimensional cell motility." In: *Nature Cell Biology* 12.6 (2010).

[42] Benjamin Geiger, Joachim P Spatz, and Alexander D Bershadsky. "Environmental sensing through focal adhesions". In: *Nature Reviews* 10.1 (2009).

[43] Cord Brakebusch and Reinhard Fässler. "The integrin-actin connection, an eternal love affair". In: *The EMBO Journal* 22.10 (2003).

[44] Keith Burridge et al. "Focal Adhesions: Transmembrane Junctions Between the Extracellular Matrix and the Cytoskeleton". In: *Annual Review of Cell Biology* 4.1 (1988).

[45] Richard O Hynes. "Integrins: Bidirectional, allosteric signaling machines". In: *Cell* 110.6 (2002).

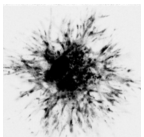

[46] Daniel Choquet, Dan P Felsenfeld, and Michael P Sheetz. "Extracellular Matrix Rigidity Causes Strengthening of Integrin-Cytoskeleton Linkages". In: *Cell* 88.1 (1997).

[47] Ben-Zion Katz et al. "Physical State of the Extracellular Matrix Regulates the Structure and Molecular Composition of Cell-Matrix Adhesions". In: *Molecular Biology of the Cell* 11.3 (2000).

[48] Masha Prager-Khoutorsky et al. "Fibroblast polarization is a matrix-rigidity-dependent process controlled by focal adhesion mechanosensing." In: *Nature Cell Biology* 13.12 (2011).

[49] Marina E Chicurel et al. "Integrin binding and mechanical tension induce movement of mRNA and ribosomes to focal adhesions." In: *Nature* 392.6677 (1998).

[50] J Thomas Parsons, Alan R Horwitz, and Martin A Schwartz. "Cell adhesion: integrating cytoskeletal dynamics and cellular tension." In: *Nature Reviews. Molecular Cell Biology* 11.9 (2010).

[51] Stephan Huveneers and Erik HJ Danen. "Adhesion signaling - crosstalk between integrins, Src and Rho". In: *Journal of Cell Science* 122.8 (2009).

[52] Daniel Riveline et al. "Focal Contacts as Mechanosensors Externally Applied Local Mechanical Force Induces Growth of Focal Contacts by an Mdia1-Dependent and Rock-Independent Mechanism". In: *The Journal of Cell Biology* 153.6 (2001).

[53] Pakorn Kanchanawong et al. "Nanoscale architecture of integrin-based cell adhesions." In: *Nature* 468.7323 (2010).

[54] Dong-Hwee Kim and Denis Wirtz. "Focal adhesion size uniquely predicts cell migration". In: *The FASEB Journal* 27.4 (2013).

[55] Chi-Li L Chiu et al. "Nanoimaging of focal adhesion dynamics in 3D." In: *PLoS One* 9.6 (2014).

[56] Edna Cukierman et al. "Taking cell-matrix adhesions to the third dimension." In: *Science (New York, N.Y.)* 294.5547 (2001).

[57] Kristopher E Kubow and Alan R Horwitz. "Reducing background fluorescence reveals adhesions in 3D matrices." In: *Nature Cell Biology* 13.1 (2011).

[58] Catherine G Galbraith, Kenneth M Yamada, and Michael P Sheetz. "The relationship between force and focal complex development". In: *The Journal of Cell Biology* 159.4 (2002).

[59] Nathalie Q Balaban et al. "Force and focal adhesion assembly: a close relationship studied using elastic micropatterned substrates". In: *Nature Cell Biology* 3.5 (2001).

[60] Jianping Fu et al. "Mechanical regulation of cell function with geometrically modulated elastomeric substrates." In: *Nature Methods* 7.9 (2010).

[61] Saba Ghassemi et al. "Cells test substrate rigidity by local contractions on submicrometer pillars." In: *Proceedings of the National Academy of Sciences of the United States of America* 109.14 (2012).

[62] Wesley R Legant et al. "Measurement of mechanical traction exerted by cells in three-dimensional matrices". In: *Nature Methods* 7.12 (2010).

[63] Mark A Smith, Laura M Hoffman, and Mary C Beckerle. "LIM proteins in actin cytoskeleton mechanoresponse". In: *Trends in Cell Biology* 24.10 (2014).

[64] Hiroaki Hirata et al. "Non-channel mechanosensors working at focal adhesion-stress fiber complex." In: *Pflügers Archiv European Journal of Physiology* 467.1 (2015).

[65] Kristopher E Kubow, Sarah K Conrad, and Rick A Horwitz. "Matrix Microarchitecture and Myosin II Determine Adhesion in 3D Matrices". In: *Current biology: CB* 23.17 (2013).

[66] Ana M Pasapera et al. "Myosin II activity regulates vinculin recruitment to focal adhesions through FAK-mediated paxillin phosphorylation." In: *The Journal of cell biology* 188.6 (2010).

[67] Jonathan D Humphries, Adam Byron, and Martin J Humphries. "Integrin ligands at a glance". In: *Journal of Cell Science* 119.19 (2006).

[68] Karl E Kadler, Adele Hill, and Elizabeth G Canty-Laird. "Collagen fibrillogenesis: fibronectin, integrins, and minor collagens as organizers and nucleators". In: *Current Opinion in Cell Biology* 20.5 (2008).

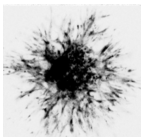

[69] Yong Mao and Jean E Schwarzbauer. "Fibronectin fibrillogenesis, a cell-mediated matrix assembly process". In: *Matrix Biology* 24.6 (2005).

[70] Cheng-han H Yu et al. "Early integrin binding to Arg-Gly-Asp peptide activates actin polymerization and contractile movement that stimulates outward translocation." In: *Proceedings of the National Academy of Sciences of the United States of America* 108.51 (2011).

[71] Andrew J Maniotis, Christopher S Chen, and Donald E Ingber. "Demonstration of mechanical connections between integrins cytoskeletal filaments, and nucleoplasm that stabilize nuclear structure". In: *Proceedings of the National Academy of Sciences of the United States of America* 94.3 (1997).

[72] Elisabetta Cavalcanti-Adam et al. "Cell Spreading and Focal Adhesion Dynamics Are Regulated by Spacing of Integrin Ligands". In: *Biophysical Journal* 92.8 (2009).

[73] Marco Arnold et al. "Activation of Integrin Function by Nanopatterned Adhesive Interfaces". In: *ChemPhysChem* 5.3 (2004).

[74] Jinghuan Huang et al. "Impact of order and disorder in RGD nanopatterns on cell adhesion". In: *Nano Letters* 9.3 (2009).

[75] Stephen P Massia and Jeffrey A Hubbell. "An RGD spacing of 440 nm is sufficient for integrin alpha v beta 3-mediated fibroblast spreading and 140 nm for focal contact and stress fiber formation." In: *The Journal of Cell Biology* 114.5 (1991).

[76] Guillaume Saux et al. "Spacing of integrin ligands influences signal transduction in endothelial cells". In: *Biophysical journal* 101.4 (2011).

[77] Yang Liu et al. "Nanoparticle Tension Probes Patterned at the Nanoscale: Impact of Integrin Clustering on Force Transmission". In: *Nano Letters* 14.10 (2014).

[78] Christophe Guilluy et al. "The Rho GEFs LARG and GEF-H1 regulate the mechanical response to force on integrins." In: *Nature Cell Biology* 13.6 (2011).

[79] Eileen Puklin-Faucher and Michael P Sheetz. "The mechanical integrin cycle". In: *Journal of Cell Science* 122.2 (2009).

[80] Rustem I Litvinov et al. "Dissociation of Bimolecular alpha(IIb)beta(3)-Fibrinogen Complex under a Constant Tensile Force". In: *Biophysical Journal* 100.1 (2011).

[81] Fang Kong et al. "Cyclic mechanical reinforcement of integrin-ligand interactions". In: *Molecular Cell* 49.6 (2013).

[82] Feiya Y Li et al. "Force measurements of the alpha(5)beta(1) integrin-fibronectin interaction". In: *Biophysical Journal* 84.2 (2003).

[83] Julie C Friedland, Mark H Lee, and David Boettiger. "Mechanically activated integrin switch controls alpha5beta1 function". In: *Science* 323.5914 (2009).

[84] Alberto Elosegui-Artola et al. "Rigidity sensing and adaptation through regulation of integrin types". In: *Nature Materials* 13.6 (2014).

[85] Elizaveta A Novikova and Cornelis Storm. "Contractile Fibers and Catch-Bond Clusters: a Biological Force Sensor?" In: *Biophysical Journal* 105.6 (2013).

[86] Grace L Lin et al. "Activation of beta 1 but not beta 3 integrin increases cell traction forces". In: *FEBS Letters* 587.6 (2013).

[87] Herbert B Schiller et al. "beta1- and alphav-class integrins cooperate to regulate myosin II during rigidity sensing of fibronectin-based microenvironments." In: *Nature Cell Biology* 15.6 (2013).

[88] Pere Roca-Cusachs et al. "Clustering of alpha(5)beta(1) integrins determines adhesion strength whereas alpha(v)beta(3) and talin enable mechanotransduction". In: *Proceedings of the National Academy of Sciences of the United States of America* 106.38 (2009).

[89] Alexander Fuhrmann et al. "Cation Type Specific Cell Remodeling Regulates Attachment Strength". In: *PLoS One* 9.7 (2014).

[90] Dominic P White, Patrick T Caswell, and Jim C Norman. "alpha-v beta-3 and alpha-5 beta-1 integrin recycling pathways dictate downstream Rho kinase signaling to regulate persistent cell migration". In: *The Journal of Cell Biology* 177.3 (2007).

[91] Erik HJ Danen et al. "The fibronectin-binding integrins alpha5beta1 and alphavbeta3 differentially modulate RhoA-GTP loading, organization of cell matrix adhesions, and fibronectin fibrillogenesis". In: *The Journal of Cell Biology* 159.6 (2002).

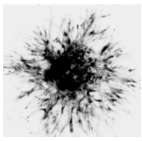

[92] Hui Miao et al. "Differential regulation of Rho GTPases by beta1 and beta3 integrins: the role of an extracellular domain of integrin in intracellular signaling". In: *Journal of Cell Science* 115.10 (2002).

[93] Hira Goe et al. "Regulated Splicing of the alpha6 Integrin Cytoplasmic Domain Determines the Fate of Breast Cancer Stem Cells". In: *Cell Reports* 7.3 (2014).

[94] Sara A Wickström et al. "The ILK/PINCH/parvin complex: the kinase is dead, long live the pseudokinase!" In: *The EMBO journal* 29.2 (2010).

[95] Moritz Widmaier et al. "Integrin-linked kinase at a glance". In: *Journal of Cell Science* 125.8 (2012).

[96] Herbert B Schiller et al. "Quantitative proteomics of the integrin adhesome show a myosin II-dependent recruitment of LIM domain proteins". In: *EMBO Reports* 12.3 (2011).

[97] Seiji Tadokoro et al. "Talin binding to integrin beta tails: a final common step in integrin activation." In: *Science (New York, N.Y.)* 302.5642 (2003).

[98] Hiroaki Hirata et al. "Force-dependent vinculin binding to talin in live cells: a crucial step in anchoring the actin cytoskeleton to focal adhesions". In: *Am J Physiol Cell Physiol* 306.6 (2014).

[99] Jonathan D Humphries et al. "Vinculin controls focal adhesion formation by direct interactions with talin and actin". In: *The Journal of Cell Biology* 179.5 (2007).

[100] Casten Grashoff et al. "Measuring mechanical tension across vinculin reveals regulation of focal adhesion dynamics". In: *Nature* 466.7303 (2010).

[101] Gerold Diez et al. "Head/tail interaction of vinculin influences cell mechanical behavior". In: *Biochemical and Biophysical Research Communications* 406.1 (2011).

[102] Andrew W Holle et al. "In situ mechanotransduction via vinculin regulates stem cell differentiation". In: *Stem Cells* 31.11 (2013).

[103] Vera Auernheimer et al. "Vinculin phosphorylation at residues Y100 and Y1065 is required for cellular force transmission." In: *Journal of Cell Science* 128.18 (2015).

[104] David W Dumbauld et al. "How vinculin regulates force transmission." In: *Proceedings of the National Academy of Sciences of the United States of America* 110.24 (2013).

[105] Armando del Rio et al. "Stretching Single Talin Rod Molecules Activates Vinculin Binding". In: *Science* 323.5914 (2009).

[106] Felix Margadant et al. "Mechanotransduction in vivo by repeated talin stretch-relaxation events depends upon vinculin." In: *PLoS Biology* 9.12 (2011).

[107] Lindsay B Case et al. "Molecular mechanism of vinculin activation and nanoscale spatial organization in focal adhesions." In: *Nature Cell Biology* 17.7 (2015).

[108] Alex-Xianghua X Zhou, John H Hartwig, and Levent M Akyürek. "Filamins in cell signaling, transcription and organ development." In: *Trends in Cell Biology* 20.2 (2010).

[109] Harvey S Chen, Kevin S Kolahi, and Mohammad RK Mofrad. "Phosphorylation Facilitates the Integrin Binding of Filamin under Force". In: *Biophysical Journal* 97.12 (2009).

[110] Allen J Ehrlicher et al. "Mechanical strain in actin networks regulates FilGAP and integrin binding to filamin A." In: *Nature* 478.7368 (2011).

[111] Scott Gehler et al. "Filamin A-beta 1 Integrin Complex Tunes Epithelial Cell Response to Matrix Tension". In: *Molecular Biology of the Cell* 20.14 (2009).

[112] Hyungsuk Lee et al. "Cytoskeletal Deformation at High Strains and the Role of Cross-link Unfolding or Unbinding". In: *Cellular and Molecular Bioengineering* 2.1 (2009).

[113] Tiila Kiema et al. "The Molecular Basis of Filamin Binding to Integrins and Competition with Talin". In: *Molecular Cell* 21.3 (2005).

[114] Vanessa I Pinto et al. "Filamin A protects cells against force-induced apoptosis by stabilizing talin- and vinculin-containing cell adhesions". In: *The FASEB Journal* 28.1 (2014).

[115] Pere Roca-Cusachs et al. "Integrin-dependent force transmission to the extracellular matrix by alpha-actinin triggers adhesion maturation." In: *Proceedings of the National Academy of Sciences of the United States of America* 110.15 (2013).

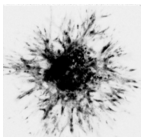

[116] David A Nix et al. "Targeting of Zyxin to Sites of Actin Membrane Interaction and to the Nucleus". In: *Journal of Biological Chemistry* 276.37 (2001).

[117] Hiroaki Hirata, Hitoshi Tatsumi, and Masahiro Sokabe. "Mechanical forces facilitate actin polymerization at focal adhesions in a zyxin-dependent manner". In: *Journal of Cell Science* 121.17 (2008).

[118] Tanmay P Lele et al. "Mechanical forces alter zyxin unbinding kinetics within focal adhesions of living cells". In: *Journal of Cellular Physiology* 207.1 (2006).

[119] Masaaki Yoshigi et al. "Mechanical force mobilizes zyxin from focal adhesions to actin filaments and regulates cytoskeletal reinforcement". In: *The Journal of Cell Biology* 171.2 (2005).

[120] Julien Colombelli et al. "Mechanosensing in actin stress fibers revealed by a close correlation between force and protein localization". In: *Journal of Cell Science* 122.10 (2009).

[121] Laura M Hoffman et al. "Stretch-induced actin remodeling requires targeting of zyxin to stress fibers and recruitment of actin regulators". In: *Molecular Biology of the Cell* 23.10 (2012).

[122] Mark A Smith et al. "A Zyxin-Mediated Mechanism for Actin Stress Fiber Maintenance and Repair". In: *Developmental Cell* 19.3 (2010).

[123] Angela Barrett et al. "p130Cas: A key signalling node in health and disease". In: *Cellular Signalling* 25.4 (2013).

[124] Radoslav Janoštiak Radoslavtiak et al. "Mechanosensors in integrin signaling: The emerging role of p130Cas". In: *European Journal of Cell Biology* 93.10-12 (2014).

[125] Leslie M Meenderink et al. "P130Cas Src-binding and substrate domains have distinct roles in sustaining focal adhesion disassembly and promoting cell migration". In: *PLoS One* 5.10 (2010).

[126] Yasuhiro Sawada et al. "Force sensing by mechanical extension of the Src family kinase substrate p130Cas". In: *Cell* 127.5 (2006).

[127] Verena Niediek et al. "Cyclic stretch induces reorientation of cells in a Src family kinase- and p130Cas-dependent manner". In: *European Journal of Cell Biology* 91.2 (2012).

[128] Hiroaki Machiyama et al. "Displacement of p130Cas from focal adhesions links actomyosin contraction to cell migration". In: *Journal of Cell Science* 127.16 (2014).

[129] Radoslav Janoštiak et al. "CAS directly interacts with vinculin to control mechanosensing and focal adhesion dynamics". In: *Cellular and Molecular Life Sciences* 71.4 (2013).

[130] Alok Tomar and David D Schlaepfer. "Focal adhesion kinase: switching between GAPs and GEFs in the regulation of cell motility". In: *Current Opinion in Cell Biology* 21.5 (2009).

[131] Michael C Brown and Christopher E Turner. "Paxillin: Adapting to Change". In: *Physiological Reviews* 84.4 (2004).

[132] Jihye Seong et al. "Distinct biophysical mechanisms of focal adhesion kinase mechanoactivation by different extracellular matrix proteins." In: *Proceedings of the National Academy of Sciences of the United States of America* 110.48 (2013).

[133] Nicholas O Deakin and Christopher E Turner. "Paxillin inhibits HDAC6 to regulate microtubule acetylation, Golgi structure, and polarized migration". In: *The Journal of Cell Biology* 206.3 (2014).

[134] Grzegorz Gawlak et al. "Paxillin mediates stretch-induced Rho signaling and endothelial permeability via assembly of paxillin-p42/44MAPK-GEF-H1 complex." In: *FASEB Journal* 28.7 (2014).

[135] Sergey V Plotnikov et al. "Force fluctuations within focal adhesions mediate ECM-rigidity sensing to guide directed cell migration." In: *Cell* 151.7 (2012).

[136] Ronen Zaidel-Bar et al. "A paxillin tyrosine phosphorylation switch regulates the assembly and form of cell-matrix adhesions". In: *Journal of Cell Science* 120.1 (2007).

[137] Guoying Jiang et al. "Rigidity sensing at the leading edge through alpha(v)beta(3) Integrins and RPTP alpha". In: *Biophysical Journal* 90.5 (2006).

[138] Götz von Wichert et al. "RPTP-alpha acts as a transducer of mechanical force on alphav/beta3-integrin-cytoskeleton linkages". In: *The Journal of Cell Biology* 161.1 (2003).

[139] Guoqiang Jiang, Jeroen den Hertog, and Tony Hunter. "Receptor-like protein tyrosine phosphatase alpha homodimerizes on the cell surface." In: *Molecular and Cellular Biology* 20.16 (2000).

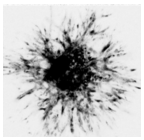

[140] Ana Kostic, Jan Sap, and Michael P Sheetz. "RPTPalpha is required for rigidity-dependent inhibition of extension and differentiation of hippocampal neurons". In: *Journal of Cell Science* 120.21 (2007).

[141] Bojun Li et al. "Mesenchymal stem cells exploit extracellular matrix as mechanotransducer." In: *Scientific Reports* 3 (2013).

[142] Enrico Klotzsch et al. "Fibronectin forms the most extensible biological fibers displaying switchable force-exposed cryptic binding sites". In: *Proceedings of the National Academy of Sciences of the United States of America* 106.43 (2009).

[143] Andres F Oberhauser et al. "The mechanical hierarchies of fibronectin observed with single-molecule AFM." In: *Journal of molecular biology* 319.2 (2002).

[144] Michael L Smith et al. "Force-induced unfolding of fibronectin in the extracellular matrix of living cells." In: *PLoS Biology* 5.10 (2007).

[145] Christopher S Chen et al. "Geometric control of cell life and death." In: *Science (New York, N.Y.)* 276.5317 (1997).

[146] Judah Folkman and Anne Moscona. "Role of cell shape in growth control." In: *Nature* 273.5661 (1978).

[147] Jeanne Fringer and Frederick Grinnell. "Fibroblast quiescence in floating or released collagen matrices: contribution of the ERK signaling pathway and actin cytoskeletal organization." In: *Journal of Biological Chemistry* 276.33 (2001).

[148] Eric A Klein et al. "Cell-Cycle Control by Physiological Matrix Elasticity and In Vivo Tissue Stiffening". In: *Current Biology* 19.18 (2009).

[149] Akiko Mammoto et al. "A mechanosensitive transcriptional mechanism that controls angiogenesis." In: *Nature* 457.7233 (2009).

[150] Tadanori Mammoto and Donald E Ingber. "Mechanical control of tissue and organ development". In: *Development* 137.9 (2010).

[151] Hermes Taylor-Weiner, Neeraja Ravi, and Adam J Engler. "Traction forces mediated by integrin signaling are necessary for definitive endoderm specification". In: *Journal of Cell Science* 128.10 (2015).

[152] Britta Trappmann et al. "Extracellular-matrix tethering regulates stem-cell fate". In: *Nature Materials* 11.7 (2012).

[153] Sudhir Khetan et al. "Degradation-mediated cellular traction directs stem cell fate in covalently crosslinked three-dimensional hydrogels". In: *Nature Materials* 12.5 (2013).

[154] Evelyn KF Yim et al. "Nanotopography-induced changes in focal adhesions, cytoskeletal organization, and mechanical properties of human mesenchymal stem cells". In: *Biomaterials* 31.6 (2010).

[155] Farhan Chowdhury et al. "Material properties of the cell dictate stress-induced spreading and differentiation in embryonic stem cells." In: *Nature Materials* 9.1 (2010).

[156] Rie Horiuchi et al. "Cyclic mechanical strain maintains Nanog expression through PI3K/Akt signaling in mouse embryonic stem cells". In: *Experimental Cell Research* 318.14 (2012).

[157] Somen Saha et al. "Inhibition of human embryonic stem cell differentiation by mechanical strain". In: *Journal of Cellular Physiology* 206.1 (2006).

[158] Kimberly A Moore et al. "Control of basement membrane remodeling and epithelial branching morphogenesis in embryonic lung by Rho and cytoskeletal tension". In: *Developmental Dynamics* 232.2 (2005).

[159] Evelyn Yim, Stella W Pang, and Kam W Leong. "Synthetic nanostructures inducing differentiation of human mesenchymal stem cells into neuronal lineage". In: *Experimental Cell Research* 313.9 (2007).

[160] Sirio Dupont et al. "Role of YAP/TAZ in mechanotransduction". In: *Nature* 474.7350 (2011).

[161] Nathaniel Huebsch et al. "Harnessing traction-mediated manipulation of the cell/matrix interface to control stem-cell fate". In: *Nature Materials* 9.6 (2010).

[162] Yubing Sun et al. "Mechanics regulates fate decisions of human embryonic stem cells." In: *PLoS One* 7.5 (2012).

[163] Jennifer L Young and Adam J Engler. "Hydrogels with time-dependent material properties enhance cardiomyocyte differentiation in vitro". In: *Biomaterials* 32.4 (2011).

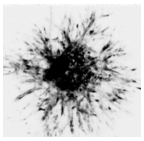

[164] Jiangling Xiong, Hayri E Balcıoğlu, and Erik HJ Danen. "Integrin signaling in control of tumor growth and progression". In: *The International Journal of Biochemistry & Cell Biology* 45.5 (2013).

[165] Götz von Wichert et al. "Focal adhesion kinase mediates defects in the force-dependent reinforcement of initial integrin-cytoskeleton linkages in metastatic colon cancer cell lines". In: *European journal of cell biology* 87.1 (2007).

[166] Paolo P Provenzano et al. "Matrix density-induced mechanoregulation of breast cell phenotype, signaling and gene expression through a FAK-ERK linkage." In: *Oncogene* 28.49 (2009).

[167] Michael S Samuel et al. "Actomyosin-Mediated Cellular Tension Drives Increased Tissue Stiffness and beta-Catenin Activation to Induce Epidermal Hyperplasia and Tumor Growth". In: *Cancer Cell* 19.6 (2011).

[168] Denis Krndija et al. "Substrate stiffness and the receptor-type tyrosine-protein phosphatase alpha regulate spreading of colon cancer cells through cytoskeletal contractility." In: *Oncogene* 29.18 (2010).

[169] Jay S Desgrosellier et al. "An integrin alpha(v)beta(3)-c-Src oncogenic unit promotes anchorage-independence and tumor progression." In: *Nature Medicine* 15.10 (2009).

[170] Brian T Beaty et al. "beta1 integrin regulates Arg to promote invadopodial maturation and matrix degradation." In: *Molecular Biology of The Cell* 24.11 (2013).

[171] Iris Eke et al. "beta1 Integrin/FAK/cortactin signaling is essential for human head and neck cancer resistance to radiotherapy". In: *Journal of Clinical Investigation* 122.4 (2012).

[172] Jordi Puigvert et al. "Cross-Talk between Integrins and Oncogenes Modulates Chemosensitivity". In: *Molecular Pharmacology* 75.4 (2009).

[173] Kim Moran-Jones, Anita Ledger, and Matthew J Naylor. "beta1 integrin deletion enhances progression of prostate cancer in the TRAMP mouse model." In: *Scientific Reports* 2 (2012).

[174] Jenny G Parvani et al. "Targeted inactivation of beta1 integrin induces beta3 integrin switching, which drives breast cancer metastasis by TGF-beta." In: *Molecular Biology of the Cell* 24.21 (2013).

[175] Hoa H Truong et al. "beta1 integrin inhibition elicits a prometastatic switch through the TGFbeta-miR-200-ZEB network in E-cadherin-positive triple-negative breast cancer." In: *Science Signaling* 7.312 (2014).

[176] Norma E Ramirez et al. "The alpha2beta1 integrin is a metastasis suppressor in mouse models and human cancer." In: *The Journal of Clinical Investigation* 121.1 (2011).

[177] Garnet Bendig et al. "Integrin-linked kinase, a novel component of the cardiac mechanical stretch sensor, controls contractility in the zebrafish heart". In: *Genes & Development* 20.17 (2006).

[178] Gregory E Hannigan, John G Coles, and Shoukat Dedhar. "Integrin-linked kinase at the heart of cardiac contractility, repair, and disease." In: *Circulation research* 100.10 (2007).

[179] Ralph Knöll et al. "Laminin-alpha 4 and integrin-linked kinase mutations cause human cardiomyopathy via simultaneous defects in cardiomyocytes and endothelial cells". In: *Circulation* 116.5 (2007).

[180] Cornelia Hahn and Martin A Schwartz. "Mechanotransduction in vascular physiology and atherogenesis." In: *Nature Reviews. Molecular Cell Biology* 10.1 (2009).

[181] Rui P Martins et al. "Mechanical Regulation of Nuclear Structure and Function". In: *Annual Review of Biomedical Engineering* 14.1 (2012).

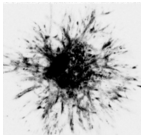

Chapter 2

Tumor-induced remote ECM network orientation steers angiogenesis [1]

[1] This chapter is based on: Hayri E Balcıoğlu, Bob vd Water and Erik HJ Danen, Tumor-induced remote ECM network orientation steers angiogenesis. *submitted: Scientific Reports*

Abstract

Tumor angiogenesis promotes tumor growth and metastasis. Here, we use automated sequential microprinting of tumor and endothelial cells in extracellular matrix (ECM) scaffolds to study its mechanical aspects. Quantitative reflection microscopy shows that tumor spheroids induce radial orientation of the surrounding collagen fiber network up to a distance of five times their radius. Across a panel of ∼20 different human tumor cell lines, remote collagen orientation is correlated with local tumor cell migration behavior. Tumor induced collagen orientation requires contractility but is remarkably resistant to depletion of collagen-binding integrins. Microvascular endothelial cells undergo directional migration towards tumor spheroids once they are within the tumor-oriented collagen fiber network. Laser ablation experiments indicate that an intact physical connection of the oriented network with the tumor spheroid is required for mechanical sensing by the endothelial cells. Together our findings show that remote physical manipulation of the ECM network by the tumor steers angiogenesis.

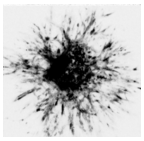

2.1 Introduction

Tumor-associated angiogenesis is one of the hallmarks of cancer [1, 2]. The chemotactic aspect of this pathology has been well studied. Oncogenic signaling pathways and hypoxia occurring in tumors activate the release of growth factors, such as vascular endothelial growth factor (VEGF), which triggers the formation of new microvascular sprouts from pre-existing vessels. Inhibitors against this paracrine interaction, targeting mainly the VEGF receptor (VEGFR) on endothelial cells, have entered the clinic [3, 4].

Angiogenesis involves proliferation and migration of endothelial cells [5]. During angiogenesis, endothelial cells migrate through a 3D extracellular matrix (ECM) network that is rich in collagen. Migration efficiency and the mode of migration (e.g. the extent of integrin-dependency and the requirement of matrix metalloproteases) are determined by ECM properties including ligand density, stiffness, fiber crosslinking, and pore size [6–8]. These ECM properties are typically altered in tumor areas, e.g. ECM stiffening has been observed in tumor tissue [9, 10].

The ECM network may control angiogenesis in several ways. First, it acts as an organizing platform for growth factor distribution, activation, and presentation [11]. In vitro assays have shown that tissue deformation can regulate angiogenesis through spatial organization of activity of the VEGF pathway [12]. In addition, cells receive mechanical cues from the ECM through integrin-based cell-matrix adhesions [13–15]. In vivo studies have demonstrated that angiogenesis is an integral response to chemical and mechanical cues [16].

Here we use sequential microprinting of tumor and microvascular endothelial cells to investigate their mechanical interaction through ECM scaffolds. We use quantitative reflection microscopy analysis to study tumor-induced collagen orientation. We show that tumor spheroids can orient a collagen network to a distance of up to 5 times the tumor radius - far beyond the area of tumor expansion and cell migration. Furthermore, we demonstrate that microvascular endothelial cells sense and respond to such orientation provided that the oriented ECM is physically connected to the tumor spheroid. Together, our data indicates that ECM network reorientation acts as a remote mechanical cue to steer angiogenesis.

2.2 Results

2.2.1 Tumor spheroids in 3D collagen induce the reorientation of surrounding collagen

4T1 breast cancer spheroids were microprinted in collagen gels (Figure 2.1A) and their outgrowth and migration was monitored after 48 hours (Figure 2.1B). A spheroid mask was generated to define the final spheroid area including core spheroid and migrated cells (Figure 2.1C). Reflection microscopy was performed to analyze the collagen network surrounding this final spheroid area (Figure 2.1D). In 2 days the tumor spheroid radius (including core and migrated cells) had increased ∼4-fold (Figure 2.1A,B). Concomitantly, reflection microscopy showed that the surrounding collagen network contained an increase in radially oriented fibers (Figure 2.1D, 2.2A). Indeed, quantitative image analysis showed an increase in collagen fibers with an orientation parameter ∼1 (dark red; denoting collagen directed radially towards the tumor spheroid center) close to the spheroid boundary (Figure 2.2A). By contrast, in areas distant from the spheroid, the number of fibers with an orientation parameter ∼1 equaled the number of fibers with an orientation parameter ∼0 (dark blue; denoting collagen oriented tangential to the tumor spheroid radius) (Figure 2.2A). Quantification of collagen fiber orientation throughout the gel relative to the distance from the final tumor spheroid edge (dashed red circle in Figure 2.1C,D) indicated that tumor spheroids that expanded from an average radius of 116±21 µm to 527±54 µm had caused radial orientation of collagen fibers up to 2.65 mm from the spheroid edge (i.e. 95% confidence interval >0.5 indicating orientation was significantly different from random) (Figure 2.2B). Thus, tumor spheroids induced remote orientation of collagen fibers up to distances of 5 times the spheroid radius.

2.2.2 Remote tumor-induced collagen network reorientation correlates with local cell migration capacity and requires Rho kinase-myosin activity

To address the role of collagen-binding integrins (mainly α1β1, α2β1) in tumor-induced collagen orientation we made use of cells stably expressing shRNAs targeting ITGB1, which express strongly reduced (∼90%) levels of β1 integrins [17]. For 4T1 cells, depletion of β1 integrins reduced

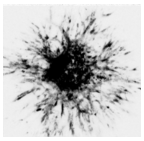

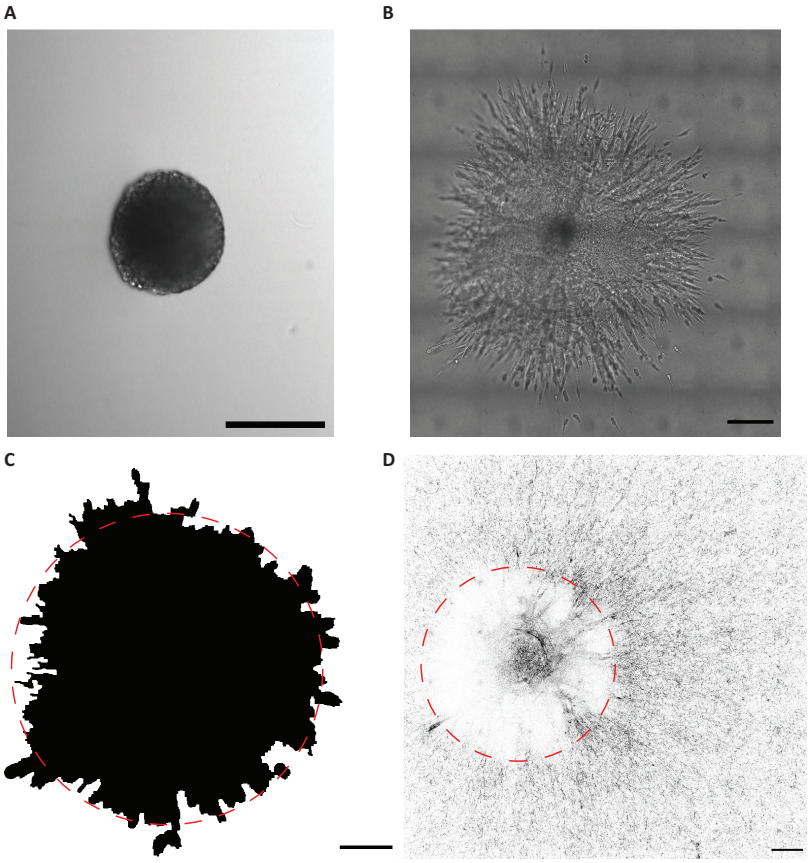

Figure 2.1
4T1 breast cancer spheroid expansion and collagen network organization. *(A-B) 4T1 tumor spheroid at the day of injection (A) and 48 hours after injection (B). (C) Spheroid mask covering core spheroid and migrating cells at 48 hours, which was used as boundary for collagen organization calculations (red dashed circle). (D) Inverted reflection microscopy image with tumor border marked with red dashed circle, showing radial orientation of surrounding collagen. Scale bar, 200 µm.*

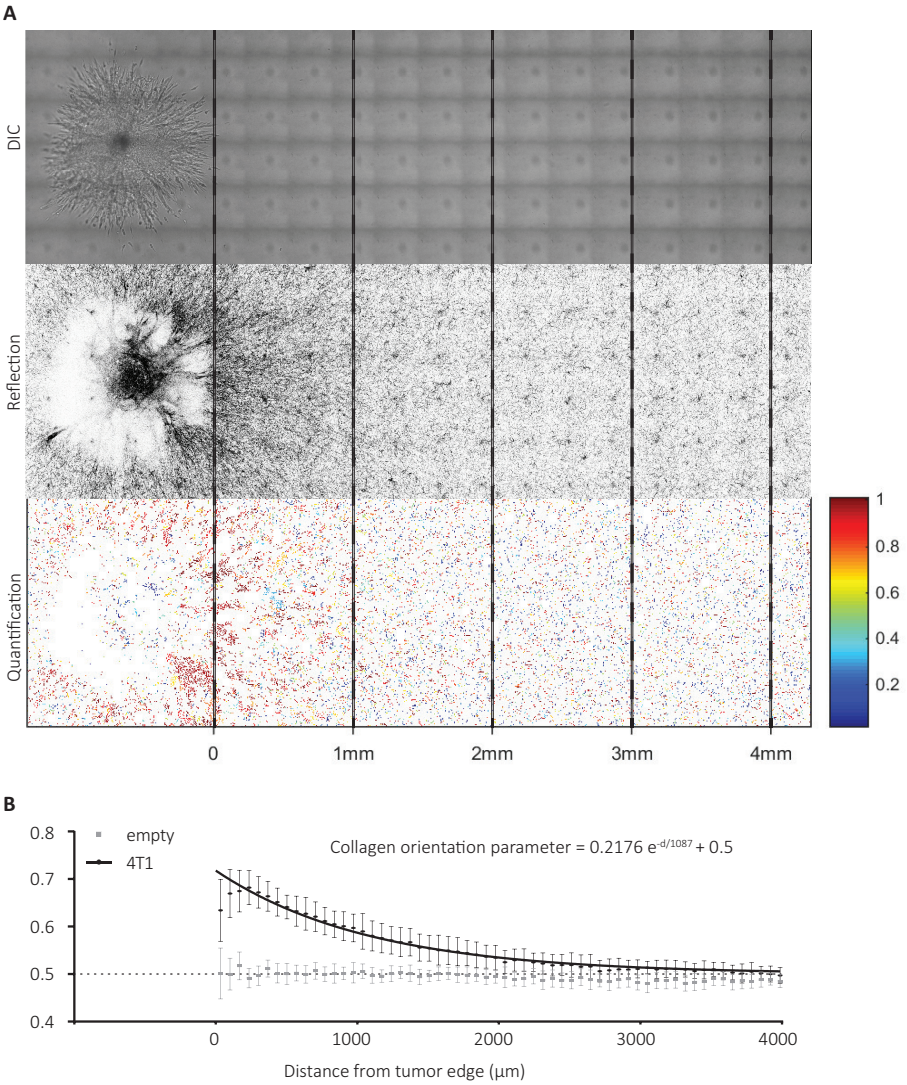

Figure 2.2

4T1 breast cancer spheroids cause long distance radial orientation of surrounding collagen. *(A) Brightfield (top) and reflection microscopy (middle) images of collagen-embedded spheroid 48 hours post injection and corresponding collagen orientation detection (bottom). Red, radially oriented collagen fibers; blue, tangential collagen fibers. Dashed lines note the indicated distances from tumor spheroid border. Note the dense red at distance 0-1mm with gradually increasing randomness of colors at increasing distances. (B) Collagen orientation parameter calculated 48 hours after injection at the indicated distances from individual tumor spheroid borders for 29 4T1 injections (black circles) and 22 empty wells (gray squares) from 5 independent experimental replicas with standard deviations. The fit equation (black line) is shown.*

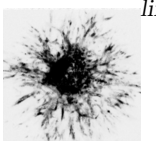

spheroid expansion through collective migration and induced migration of individual cells, as described before [17] (Figure 2.3A). This was accompanied by reduced collagen orientation (measured beyond the area of spheroid expansion - cell migration) (Figure 2.3B). Similar results were obtained for HCC70-derived tumor spheroids (Figure S1A,B). By contrast, control MDA-MB-468 and BT20 tumor spheroids showed little migration whereas depletion of β1 integrins in these cells enhanced spheroid expansion through a mix of collective and single cell migration (Figure 2.3C and S1C). In these cases, depletion of β1 integrins led to an increased remote collagen orientation (Figure 2.3D and S1D). Lastly, in HCC1806 cells β1 integrin depletion caused a shift from relatively ineffective collective migration to similarly weak single cell migration and this did not affect the capacity of the tumor spheroids to cause collagen orientation (Figure 2.3E,F). Together, these results indicated that the capacity of tumor cells to orient the collagen network was not affected by a reduction in collagen-binding integrins per se. Rather, changes in integrin expression caused decreased or increased tumor cell migration at the spheroid edge, which correlated with decreased or increased remote collagen orientation capacity, respectively.

We next tested a larger panel of carcinoma and sarcoma cell lines for their capacity to orient surrounding collagen (Figure S2). In line with the results obtained with 4T1 cells, irrespective of the origin of the cell line, β1 integrin expression level, or migration strategy; there was a strong correlation between remote collagen orientation capacity and spheroid expansion (average initial spheroid radius for all cell lines was 113±29 µm) (Figure 2.4A,B). Spheroid expansion as measured included spheroid growth and migration and tumor cell types showing the largest spheroid expansions typically displayed strong migration activity. To investigate the role of cytoskeletal contractility, pharmacological inhibition of myosin II or Rho kinase that acts upstream of myosin II activity was used for the duration of the experiment. Treatment of 4T1 spheroids with a myosin II inhibitor caused a ∼15% decrease in final spheroid radius and reduced collective migration activity that was accompanied by a 50% reduction in remote collagen orientation (Figure 2.4C,D and S3). Inhibition of Rho kinase led to a ∼8% decrease in final spheroid radius and caused a switch from collective migration to individual cell migration that was accompanied by a 70% reduction in remote collagen orientation (Figure 2.4C,D and S3). These results showed that inhibition of Rho kinase-

myosin II-mediated contractility has moderate effects on cell migration at the spheroid edge but strongly attenuates remote collagen orientation.

2.2.3 Endothelial spheroids orient in response to tumor-oriented collagen network

HMEC-1 human microvascular endothelial cells were injected at various defined x-y distances from 4T1 spheroids at 48 hours post 4T1 injection (Figure 2.5A and S4). The resulting endothelial spheroids were monitored by DIC 24 hours later and the direction of the tumor spheroid was marked (red arrow head) (Figure 2.5B). Endothelial spheroid masks were generated to study the orientation of their long axis (Figure 2.5C; blue arrows) and relate this to the relative position of the tumor spheroid (Figure 2.5C; red arrows). Alignment of the endothelial spheroid in the direction of the tumor spheroid was observed for injections within the 2.65mm collagen orientation area whereas this was lost for endothelial cells injected beyond this zone (Figure 2.5D).

Next, HMEC-1 cells were injected at varying distances from tumor spheroids derived from the panel of cell lines described above (Figure 2.6A). In accordance with the large variation in collagen orientation distance among these lines (Figure 2.4), the distance to which HMEC-1 cells could sense and respond to these spheroids differed strongly. Across the panel of cell lines, HMEC-1 spheroids present within a zone of strong tumor-oriented collagen were directed towards the tumor spheroid whereas direction of HMEC-1 spheroids was random if they were outside of this zone (Figure 2.6B-D). HMEC-1 directionality was induced in response to collagen orientation significantly above average as measured for all tested HMEC-1 injection coordinates (Figure 2.6B). This level of orientation was reached by 4T1, HCC70, Hs578t, SAOS2, U20S, MOS and KPD but not BT20 or MDA-MB-468 cells. In accordance with data shown above (Figure 2.3; S1) β1 integrin-depletion reduced above-threshold collagen orientation measurements for 4T1 and HCC 70 cells whereas this was induced for BT20 and MDA-MB-468 cells in response to ITGB1 silencing. Likewise, HMEC-1 spheroid elongation correlated with tumor-induced collagen orientation (Figure 2.6E,F) and combining HMEC-1 spheroid direction and elongation parameters showed a strong and significant HMEC orientation response to tumor-oriented collagen (Figure 2.6G,H).

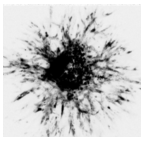

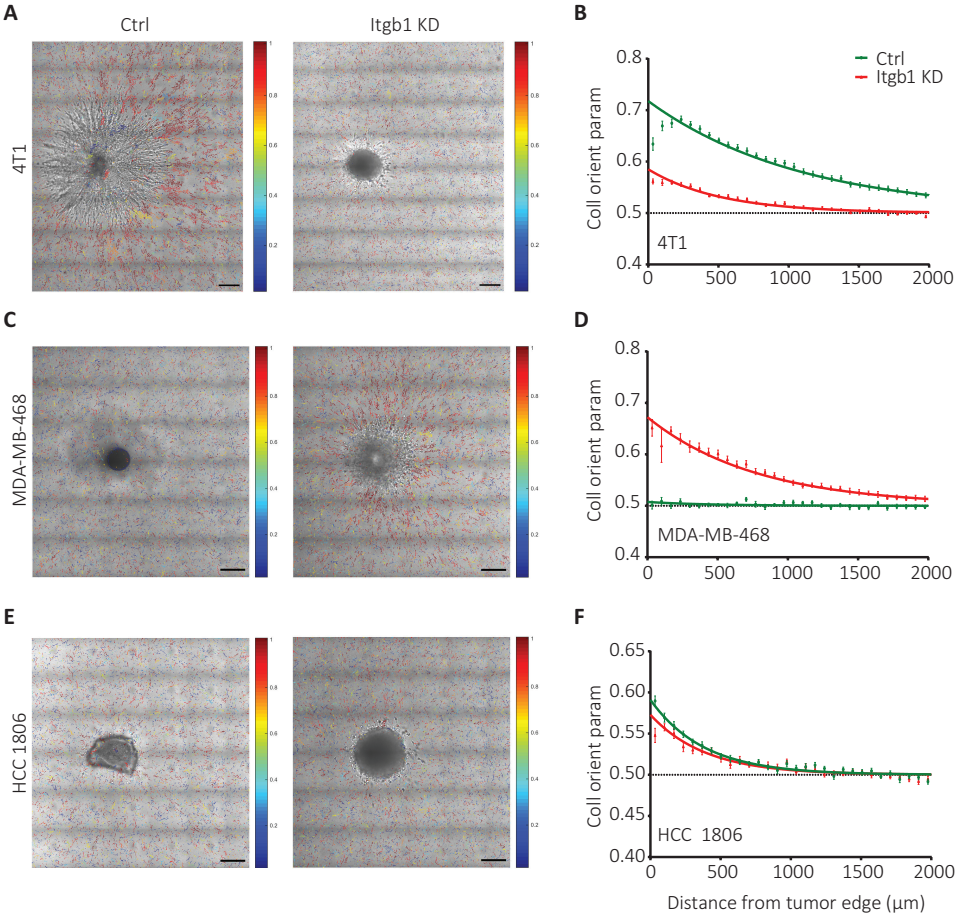

Figure 2.3

Distinct effects of β1 integrin downregulation on tumor spheroid cell migration and collagen orientation. *(A,C,E) Collagen orientation images merged with brightfield images taken 48 hours after injecting the indicated cell lines with or without shRNA targeting ITGB1. (B,D,F) Collagen orientation measured at a range of distances from tumor border for 4T1 shctrl (B, green; n=29), 4T1 shITGB1 (B, red; n=29), MDA-MB-468 WT (D, green; n=16), MDA-MB-468 shITGB1 (D, red; n=21), HCC 1806 shctrl (F, green; n=20), and HCC 1806 shITGB1 (F, red; n=21) tumor spheroids 48 hours after injection mean ± standard deviation with exponential fits (solid lines) from at least four independent experimental replicas is shown. Scale bar, 200 µm.*

A

$$\text{Orientation} = (Y_0 - 0.5)\, e^{-d/L_0} + 0.5$$

Cell line	Y_0	L_0(µm)	Integrated Orientation (µm)	Tumor Radius (µm)
4T1 shCtrl	0,7176	1089	236,9664	527
4T1 shb1	0,585	513,4	43,639	263,35
MDA-MB-468 WT	0,5468	491,8	23,01624	149,95
MDA-MB-468 shb1	0,6822	891	162,3402	348,55
HCC 1806 shCtrl	0,5854	359,4	30,69276	173,45
HCC 1806 shb1	0,5763	438,5	33,45755	246,7
HCC 70 shCtrl	0,5639	487,3	31,13847	141,15
HCC 70 shb1	0,5745	318,2	23,7059	150,1
BT20 shCtrl	0,6353	567,2	76,74216	190,45
BT20 shb1	0,628	862,5	110,4	278,95
BT549	0,5077	336,6	2,59182	143,2
HCC 1937	0,6523	354,2	53,94466	150,45
HS578T	0,7323	951,2	220,96376	357,85
MDA-MB-453	0,5191	519,4	9,92054	119,2
SAOS2	0,7053	857,8	176,10634	412,1
SKBR7	0,6561	549,3	85,74573	243,65
MOS	0,681	535,5	96,9255	223,5
U2OS	0,7013	660,6	132,97878	303
143b	0,6155	373,1	43,09305	235,8
ZK58	0,5978	273,8	26,77764	183,25
KPD	0,6143	524,8	59,98464	300,45
6647	0,5198	297,2	5,88456	138,05
CHP100	0,5468	253,9	11,88252	137,7

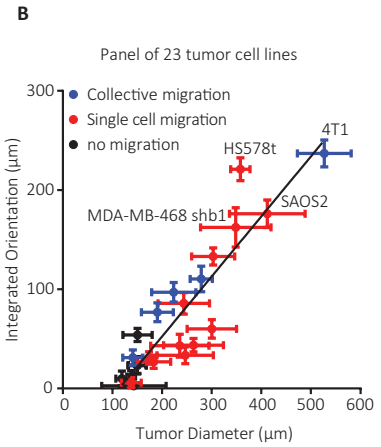

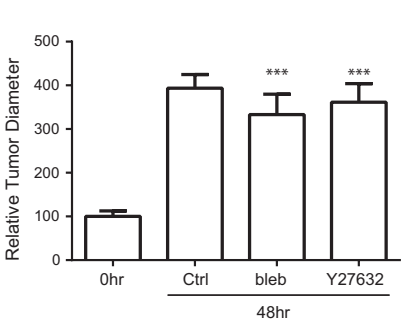

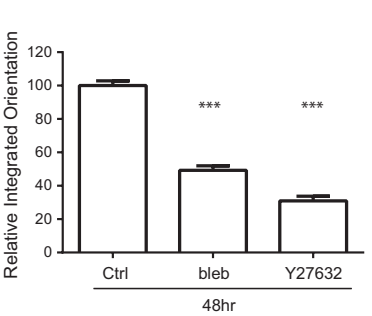

Figure 2.4

Tumor induced collagen orientation and tumor expansion are interrelated and depend on ROCK-myosin II-induced contractility. *(A) Table showing the fit parameters Y_0 and L_0, the area under the fitted curve (integrated orientation) and the tumor radius 48 hours after injection for indicated cell lines. (B) Graph showing relation between tumor radius at 48 hours post injection and integrated collagen orientation parameter for cell lines depicted in table A with distinct modes of migration as indicated based on DIC images. Plot shows mean, standard deviation and linear fit (Y=0.605(±0.06)X-68.65(±15.6); R^2=0.8251). (C,D) Bar graphs showing mean and standard deviation of relative 4T1 tumor radius normalized to tumor size at 0hr (C), and relative integrated collagen orientation at 48 hours normalized to control (D) for no treatment (Ctrl; n=55), 10 µM blebbistatin (bleb; n=53) and 10 µM Y27632 (Y27632; n=46). Combined data from three independent experiments is shown. ***; $p<0.0005$ according to Mann-Whitney test (C) or unpaired t-test (D) compared to control at 48 hours.*

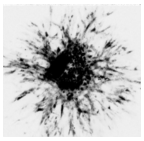

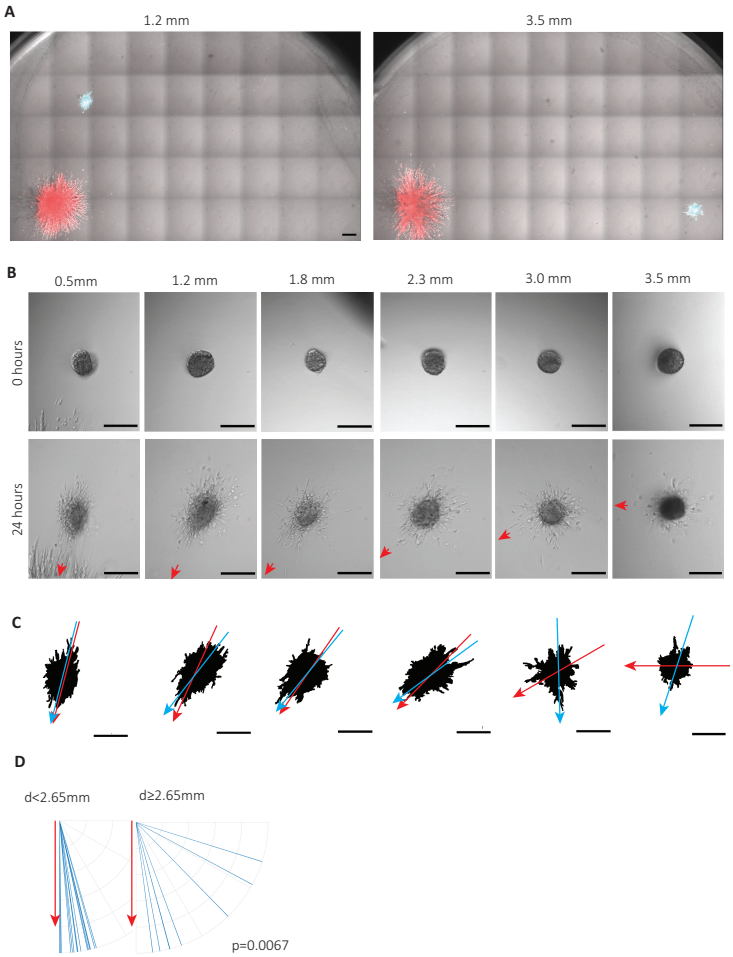

Figure 2.5

HMEC-1 microvascular endothelial cells injected within 4T1 remote area of oriented collagen show directional migration towards tumor spheroid. *(A) Merged brightfield/fluorescence images taken at t=72 hours showing CellTracker green CMFDA-labeled HMEC-1 cells injected at t=48 hours at the indicated distances from the spheroid border of CellTracker Orange CMRA-labeled 4T1 cells injected at t=0 hours. (B) Representative DIC images of HMEC-1 spheroids at the day of injection (top) or 24 hours after injection (bottom) at indicated distances from 4T1 tumor spheroids. The red arrows point towards the center of 4T1 tumor spheroid. (C) HMEC-1 spheroid masks generated for images shown in B (bottom). Blue arrow indicates major axis of the mask; red arrow points to 4T1 tumor spheroid center. (D) Major axis orientation of HMEC-1 spheroids (blue lines) injected at distances from 4T1 spheroid edge less (n=15; left) or more than 2.65 mm (n=8; right) plotted against the direction of the 4T1 tumor spheroid (set vertically for each experiment; red arrow). Data obtained from four independent experiments; P value calculated using Mann-Whitney test; scale bar, 200 µm.*

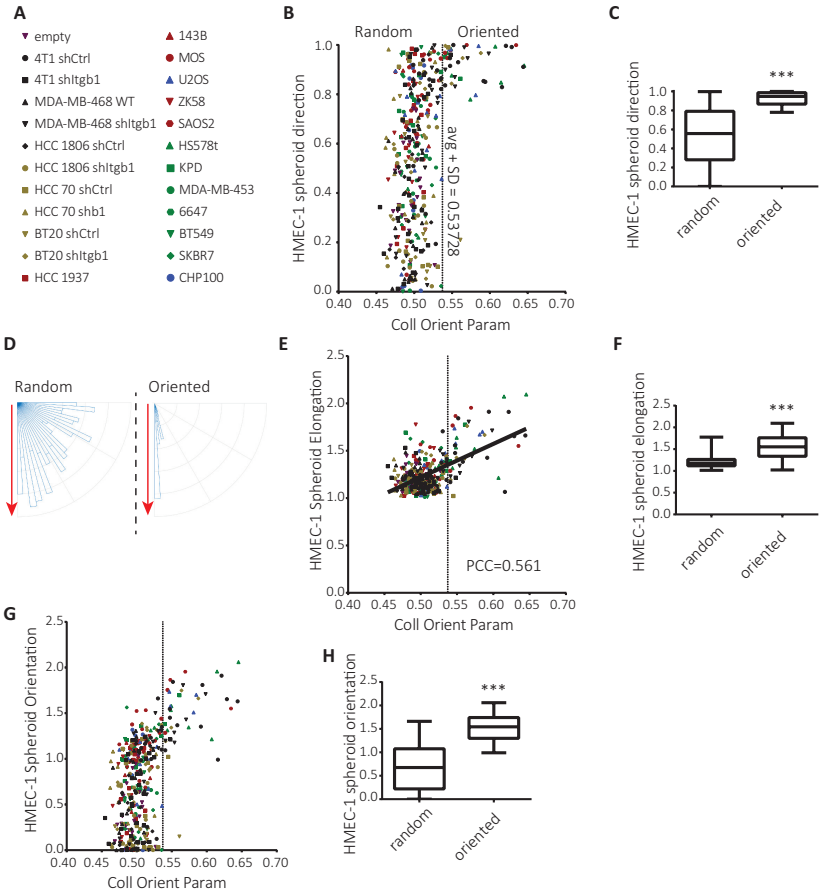

Figure 2.6

Directional HMEC-1 migration towards tumor spheroid when injected within area of tumor-oriented collagen for panel of tumor cell lines. *(A) Panel of cell lines used with corresponding symbols. (B, E, G) Direction (B), elongation (E) and orientation (G) of HMEC-1 spheroids measured 24 hours after HMEC-1 injection at varying distances from panel of tumor spheroids (A) plotted against collagen orientation parameter at the corresponding distances (obtained in each case from reflection microscopy 48 hours after tumor cell injection just prior to HMEC-1 injection). Dashed line is drawn at one standard deviation above average collagen orientation parameter and indicates the threshold for "oriented collagen". (C, F, H) Box whisker graphs showing the minimum to maximum of direction (C), elongation (F) and orientation (H) of HMEC-1 spheroids injected in regions of oriented collagen vs regions of random collagen. (D) Major axis direction of HMEC-1 injections in oriented collagen vs random collagen plotted against the direction of the tumor spheroids (set vertically for each experiment; red arrow). ***; $p<0.0005$ according to Mann-Whitney test. PCC: calculated Pearson product-moment correlation coefficient.*

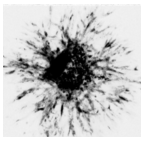

2.2.4 Endothelial response to oriented collagen network requires physical coupling with tumor

To address if physical connections between the tumor spheroid and the oriented collagen network remained important for guidance of endothelial cells, the spheroid was physically disconnected after the collagen network had been oriented. For this purpose, two HMEC-1 spheroids were injected at the same distance from the tumor spheroid at opposite sides and laser cutting of collagen fibers was applied close to the tumor edge, between the tumor and one of the HMEC-1 spheroids (Figure 2.7A). Orientation of the collagen network was maintained in areas disconnected from the tumor spheroid through laser ablation (Figure 2.7B,C). However, HMEC-1 cells injected in such areas no longer responded to collagen orientation: HMEC-1 spheroid direction, elongation, and the combined orientation parameter were decreased; resembling HMEC-1 behavior in non-oriented collagen areas (Figure 2.7D-F). Control HMEC-1 spheroids in the same well that were still connected to the tumor normally responded to oriented collagen. These findings demonstrate that an intact physical connection of the oriented ECM network with the tumor spheroid is required for orientation sensing by the endothelial cells.

2.3 Discussion

The tumor stroma plays an important role in initiation and progression of cancer [18]. Mechanical properties of the ECM can influence tumor cell behavior and have been linked to prognosis. ECM stiffness [19–21], pore size [22–24], crosslinking [25], fiber alignment [26, 27], as well as the presence of stromal contractile cells [28] have all been shown to influence aspects of cancer progression, including tumor growth and invasion. Vice-versa, tumor cells actively modify these ECM properties thereby promoting tumor growth, invasion, and metastasis potential [29–32].

Here, we use quantitative reflection microscopy analysis to study remote tumor-mediated collagen network orientation. We show that tumor spheroids reorient a surrounding collagen-based ECM network up to five times their radius. In a panel of cell lines the distance of collagen orientation correlates with spheroid expansion which is mainly caused by tumor invasion/migration. Such long range collagen reorganization has also been observed for mouse fibroblast explants [33]. Local ECM reorga-

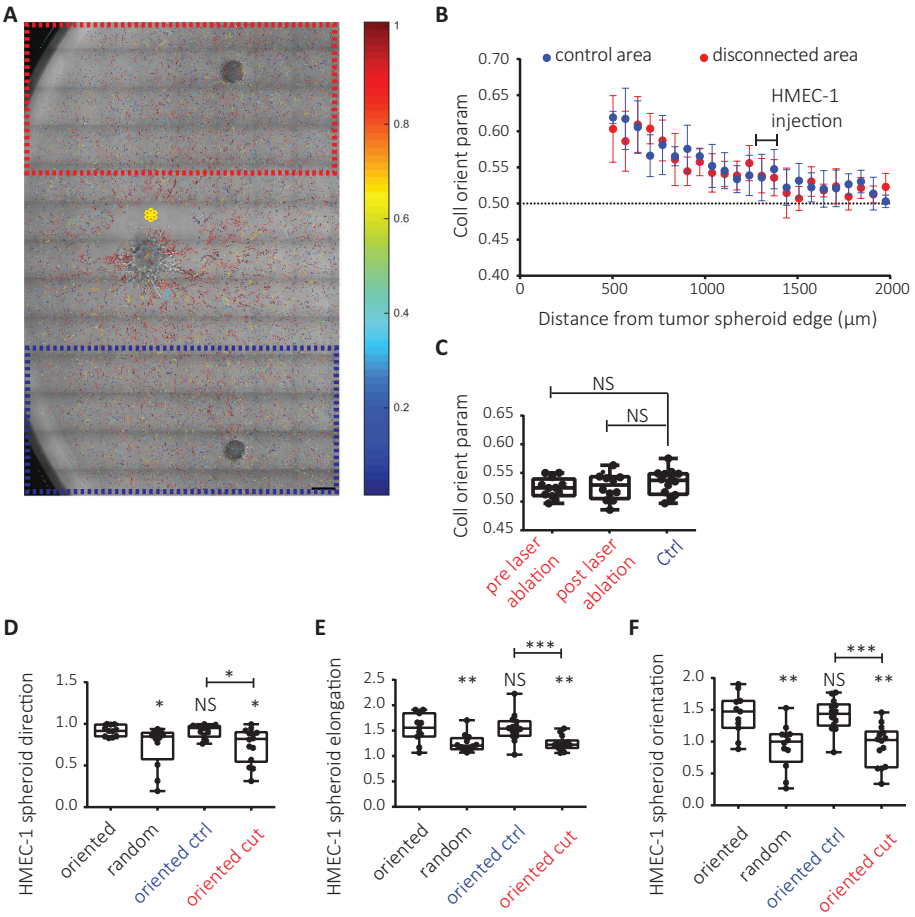

Figure 2.7

Endothelial response to tumor-oriented collagen network depends on physical connection of oriented collagen network with the tumor. *(A) Collagen orientation image superimposed on brightfield image showing 4T1 spheroid (left center) and two HMEC-1 spheroids at the top and bottom of the image at ∼1.4mm from the 4T1 injection. Yellow asterisk indicates area of laser ablation 48 hours post 4T1 injection just after HMEC-1 injection; red box, area disconnected from the tumor; blue box, control area. (B) Collagen orientation parameter (mean ± standard deviation) for control (blue) and disconnected (red) areas shown in (A) with HMEC-1 injections performed at the indicated region. (C) Box whisker graphs showing the minimum to maximum of collagen orientation parameter at HMEC-1 injection sites just prior to HMEC-1 injection for blue box in Figure A (Ctrl) and red box in Figure A before and after laser ablation. (D-F) Box whisker graphs showing the minimum to maximum of direction (D), elongation (E) and orientation (F) of HMEC-1 spheroids injected in oriented or random collagen regions (black legends; data for 4T1 cells from Figure 5) or injected in the blue box (oriented ctrl) or the disconnected red box (oriented cut) as indicated in A. NS, p>0.05; *, p< 0.05; **, p<0.01; ***, p<0.001 relative to oriented unless otherwise indicated; Mann-Whitney test; Scale bar, 200 µm.*

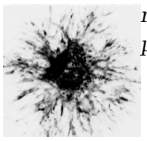

nization in areas containing tumor cells is driven by Rho kinase-Myosin II-mediated contractility [20, 34, 35]. Our findings indicate that traction forces applied by the tumor cells on the local collagen network drives ECM reorientation also in distant areas where tumor cells are absent. In fact, while consequences of contractility inhibition for local tumor cell migration are limited, which can be explained by tumor cell plasticity, remote ECM reorientation is strongly attenuated.

Antibody blocking experiments have shown that collagen-binding integrins mediate i) local tumor-induced collagen network reorganization [36], and ii) tumor cell-responses to mechanical ECM properties [25]. Gene silencing as used in our study may be less efficient than antibody blocking. Nevertheless, we observe highly distinct effects of β1 integrin silencing on collagen network reorientation. We and others have previously shown that depletion or blockade of β1 integrins can either inhibit migration or cause a switch from collective to single cell migration, e.g. through effects on TGF-β signaling [17, 37, 38]. Our current study shows that in tumors where collective migration is attenuated or switched to less abundant individual cell migration in response to β1 integrin silencing, collagen network reorientation is lost (e.g. 4T1); whereas in tumors where cell motility is normally very poor and β1 integrin silencing triggers more abundant (individual) cell migration, a concomitant increase in collagen network reorientation is observed (e.g. MDA-MB-468). The fact that β1 integrin silencing does not directly attenuate collagen organization may point to roles for other collagen-binding receptors. On stromal fibroblasts, syndecan-1 participates in ECM network alignment [39]. Likewise, syndecans or discoidin domain collagen receptors on tumor cells may be candidates for force-induced collagen reorganization in the context of strongly reduced integrin levels.

The experiments discussed above show that tumor spheroids can reorient the collagen network at relatively long distances, way beyond the area of tumor expansion and migration. We subsequently show that endothelial cells can sense such long-range orientation and respond by moving towards the tumor. It is known that mechanical ECM properties, such as density and stiffness regulate angiogenesis [40–43]. This may be explained by changes in the distribution of soluble factors or enhanced activity of the receptors for these factors [12, 44, 45]. Alternatively, physical aspects of the network may instruct endothelial cell behavior. Indeed, we show that tumor-mediated remote radial organi-

zation of collagen directs human microvascular endothelial cells. The correlation between levels of remote collagen organization and induction of endothelial cell directionality holds through for a panel of ∼20 different human cancer cell lines. Importantly, laser ablation of collagen fibers close to the tumor does not affect the architecture of the remote collagen network but leads to complete loss of endothelial cell responsiveness to such oriented ECM regions. This argues against a mechanism involving chemotactic signals. It also indicates that contact guidance, i.e. a preference for aligned collagen fibers, is insufficient. Rather, once the collagen network is organized, distant forces applied to the network by the tumor are critical for sensing and/or responding of endothelial cells.

Taken together, our study shows for the first time that a radial collagen network organization generated by the tumor relatively far beyond the area of tumor expansion and migration, not only forms migratory highways for tumor invasion but can also guide angiogenesis in a manner dependent on tumor generated traction forces. In coordination with soluble factors, this mechanical interaction might further direct microvascular sprouts towards the tumor. Hence, targeting tumor induced ECM remodeling may prevent both tumor invasion and angiogenesis.

2.4 Materials and methods

2.4.1 Cell culture

4T1 mouse breast cancer cells and BT20, BT549, HCC1806, HCC1937, HCC70, HS578t, MDA-MB-453, MDA-MB-468, and SKBR7 human breast cancer cells purchased from the American Type Culture Collection or provided by Dr. J Foekens, Erasmus Medical Center, Rotterdam NL [46] were grown in RPMI1640 medium supplemented with 10% fetal bovine serum (GIBCO, USA), 25 U/ml penicillin and 25 µg/ml streptomycin (Invitrogen). Human osteosarcoma cell lines MOS, U2OS, 143B, ZK58, SAOS2, and KPD were described previously [47] and grown in the same medium. Human Ewing sarcoma cell lines 6647 and CHP100 were provided by Dr. P. Hogendoorn, Leiden University Medical Center, Leiden NL, and maintained in IMDM cell culture medium (GIBCO) supplemented with 10% fetal bovine serum, 25 U/ml penicillin and 25 µg/ml streptomycin. Stable bulk-sorted ITGB1-silenced tumor cell lines were described previously [17]. HMEC-1 human microvascular endothelial cells [48] were cultured in MCDB131 medium (GIBCO) supplemented

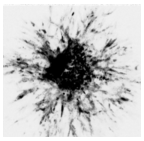

with 15% fetal bovine serum, 200 mM L-Glutamine, 10 µg/mL epidermal growth factor, 100 µg/mL hydrocortisone, 25 U/ml penicillin and 25 µg/ml streptomycin. All cells were cultured in a humidified incubator at 37°C with 5% CO_2.

2.4.2 Automated sequential microprinting of tumor- and endothelial cells in ECM scaffolds

Collagen type I solution was isolated from rat-tail collagen by acid extraction as described previously [49]. Collagen was diluted to 1 mg/mL in the culture medium containing 0.1 M Hepes (BioSolve) and fixed to pH 7.5 by addition of $NaHCO_3$ (stock 440 mM, Merck). 60 µL of this solution was then pipetted into a glass-bottom 96 well plate (Greiner) and incubated for 1 hour at 37°C to polymerize.

Automated injection of cell suspensions into the resulting collagen gels to generate arrays of cell spheroids with defined x-y-z position was performed as described using injection robotics from Life Science Methods, Leiden NL (http://www.lifesciencemethods.com) [17, 50]. Tumor spheroids of 113±29 µm initial radius were generated at 200 µm above the glass surface (average collagen gel height ∼1.5 mm) and incubated 48 hours with appropriate culture media for each cell line. Subsequently, medium was removed, HMEC-1 cells were injected at the same z-position at various defined x-y distances from the tumor spheroid, and wells were further incubated with HMEC-1 culture media for 24 hours (Figure S4).

For experiments where tumor spheroids were treated with Myosin II or Rho kinase inhibitors, media was supplemented with blebbistatin (Calbiochem cat. number 203389, Merck KGaA, Darmstadt, Germany) or Y27632 (Tocris cat. number 1254, Bristol, UK), respectively reaching 10 µM final concentration (medium+gel). For fluorescent imaging of 4T1 and HMEC-1, cells were incubated at 37°C with 1 µM CellTracker Orange CMRA or CellTracker Green CMFDA Dye, respectively for 15 minutes prior to injection.

2.4.3 Collagen gel imaging

Spheroids were imaged using a Nikon TE2000 confocal microscope equipped with a Prior stage controlled by NIS Element Software and with a temperature and CO_2-controlled incubator. Frame stitching was used when necessary. Differential interference contrast (DIC) images were captured

using a charged coupled device (CCD) camera with NIS software and 10x dry objective. Reflection microscopy of the entire well was performed by 5.4 mm x 5.4 mm stitching of images obtained using a 40x long distance water immersion objective by illuminating with a 561 nm laser coupled with a 561 nm blocking dichroic mirror for the detection.

2.4.4 Laser severing assay

After injecting HMEC-1 cells on both sides of the tumor spheroid at a distance of 1650 µm from the tumor spheroid center, laser severing was performed by applying 16 lines/second stimulation just outside of the tumor spheroid with infrared laser (Coherent Chameleon Discovery) at 790 nm wavelength at full power (∼3000 mW), using the 40x long distance water immersion lens, while manually scanning through the z plane over a duration of five minutes. This was repeated until all the collagen at one side of the tumor spheroid was cut.

2.4.5 Image analysis

All image analysis was performed using in house written Matlab scripts (Mathworks, Natick, MA, USA). DIC images were first put through a median filter to create a background illumination signal to which the original images were normalized. Normalized images were blurred and a mask for core detection was generated by thresholding for signal lower than two standard deviations below the mean and taking only the central binary image. Subsequently, a canny edge detection method was applied to the normalized image to mask the outer rim of the spheroid. This mask was dilated to include the area of single cell migration and combined with the core mask to capture the entire final spheroid.

For reflection image analysis, first a background image was calculated by applying a circular averaging filter of 10 pixel radius to the original image. This image was then subtracted from the original image and a customized rollingball filter was applied to extract fibrillar structures. The filter multiplied the signal with itself and used a local thresholding algorithm assigning pixels with squared intensities >0.5 standard deviations above mean squared intensity within 5px distance, to a collagen fiber. From this binary image, isolated pixels were removed, a binary closure was performed, and structures of >20 pixels and eccentricity >0.9 were assigned as fibers.

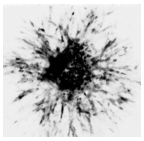

The directionality of a fiber was quantified by first manually determining the center of the tumor spheroid per image, and subsequently calculating for each fiber; the cosine square of the angle between the vector pointing from the tumor spheroid to the center of the collagen fiber and the orientation of the collagen fiber. The distance of a fiber to the tumor edge was calculated by subtracting the previously determined tumor spheroid radius (obtained from the DIC image analysis) from the distance of the fiber center to the tumor spheroid center. Fiber orientations were analyzed depending on their distance, in bins of 100px (67 µm). To this data a two-parameter single exponential plateauing at 0.5 was fitted with the equation Y=(p1-0.5)exp(-X/p2)+0.5 for x (distance) larger than 100 µm using GraphPad Prism 6 program (GraphPad Software, La Jolla, CA). Integrated orientation was calculated from the fit by taking the integral $\int_0^\infty (p1 - 0.5)exp(-X/p2)\,\mathrm{d}x$ which yielded the result (p1-0.5)*p2.

The collagen organization at the locations of HMEC-1 spheroids that were injected at designated distances from tumor center was determined by quantifying the collagen organization at that distance from the tumor spheroid before the HMEC-1 injections were performed, except when quantifying collagen orientation for the laser severing experiment for which the collagen organization was quantified both before HMEC-1 injection and after HMEC-1 injection/laser severing was performed. The HMEC-1 direction was determined by calculating the angle between the vector pointing from the HMEC-1 center to the tumor spheroid center and HMEC-1 long axis obtained from the injection mask, subtracting this angle from 90 degrees and dividing by 90 degrees so that HMEC-1 directed towards the tumor had a direction of 1 and directed perpendicularly had a direction 0. The elongation was calculated by dividing the long axis by the short axis length for the injection mask. Pearson product-moment correlation coefficient and linear fit were obtained using GraphPad Prism 6 software. The spheroid orientation was calculated by multiplying the direction with the elongation parameter.

To calculate significance between two conditions, the Mann-Whitney U test was used when comparing distribution data, and unpaired t-test was used when comparing integrated collagen orientation.

2.5 Acknowledgements

We thank Dr. Foekens and Dr. Hogendoorn for providing cell lines and Ms Tian Shu Fang (Division of Toxicology, Leiden Academic Center for Drug Research, Leiden, the Netherlands) for help setting up reflection microscopy technique.

Funding: Support for this work came from the Netherlands Organization for Scientific Research (FOM 09MMC03). **Authors' contributions:** H.E.B. performed the experiments and analyzed the data. B.v.d.W. provided imaging infrastructure and critically read the manuscript. H.E.B. and E.H.J.D designed the experiments, interpreted data and wrote the manuscript. **Competing interests:** The authors declare no competing interests.

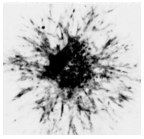

2.6 Supplemental figures

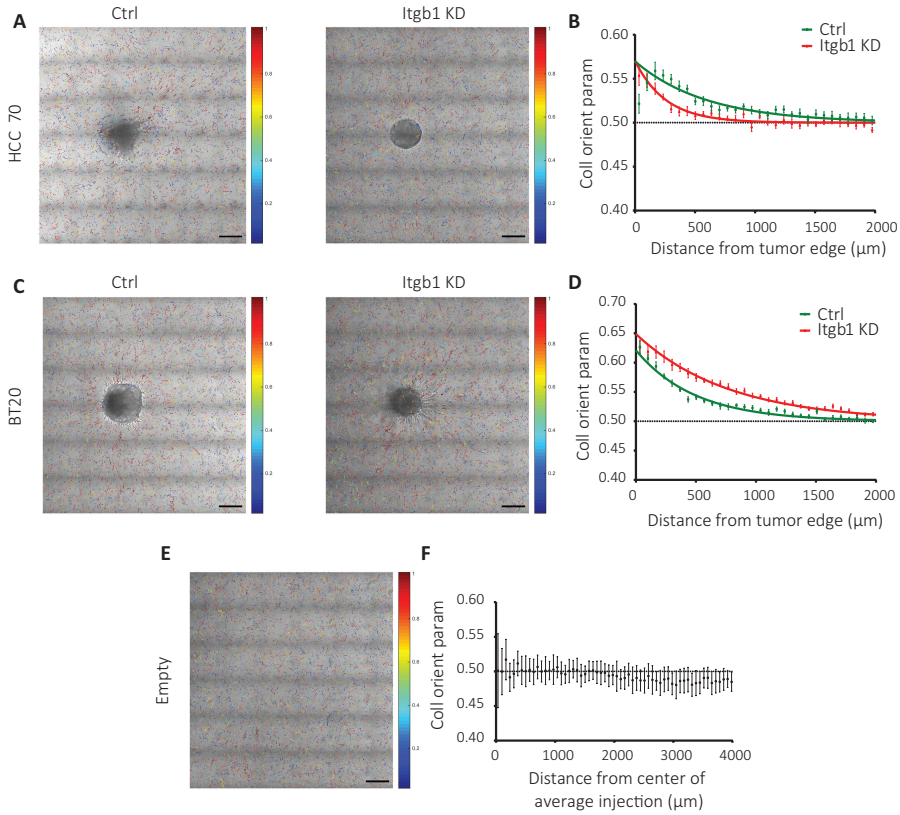

Figure S1

Effects of β1 integrin downregulation on tumor spheroid cell migration and collagen orientation. *(A,C,E) Collagen orientation images merged with brightfield images taken 48 hours after injecting the indicated cell lines with or without shRNA targeting ITGB1 (A,C) or without injection (E). (B,D,F) Collagen orientation measured at a range of distances from tumor border for HCC 70 shctrl (B, green; n=16), HCC 70 shITGB1 (B, red; n=15), BT20 shctrl (D, green; n=17), BT20 shITGB1 (D, red; n=17) tumor spheroids 48 hours after injection, and from the average injection location for empty well (F, black; n=22) at the same time point, mean ± standard deviation with exponential fits (solid lines) from at least three independent experimental replicas is shown. Scale bar, 200 µm.*

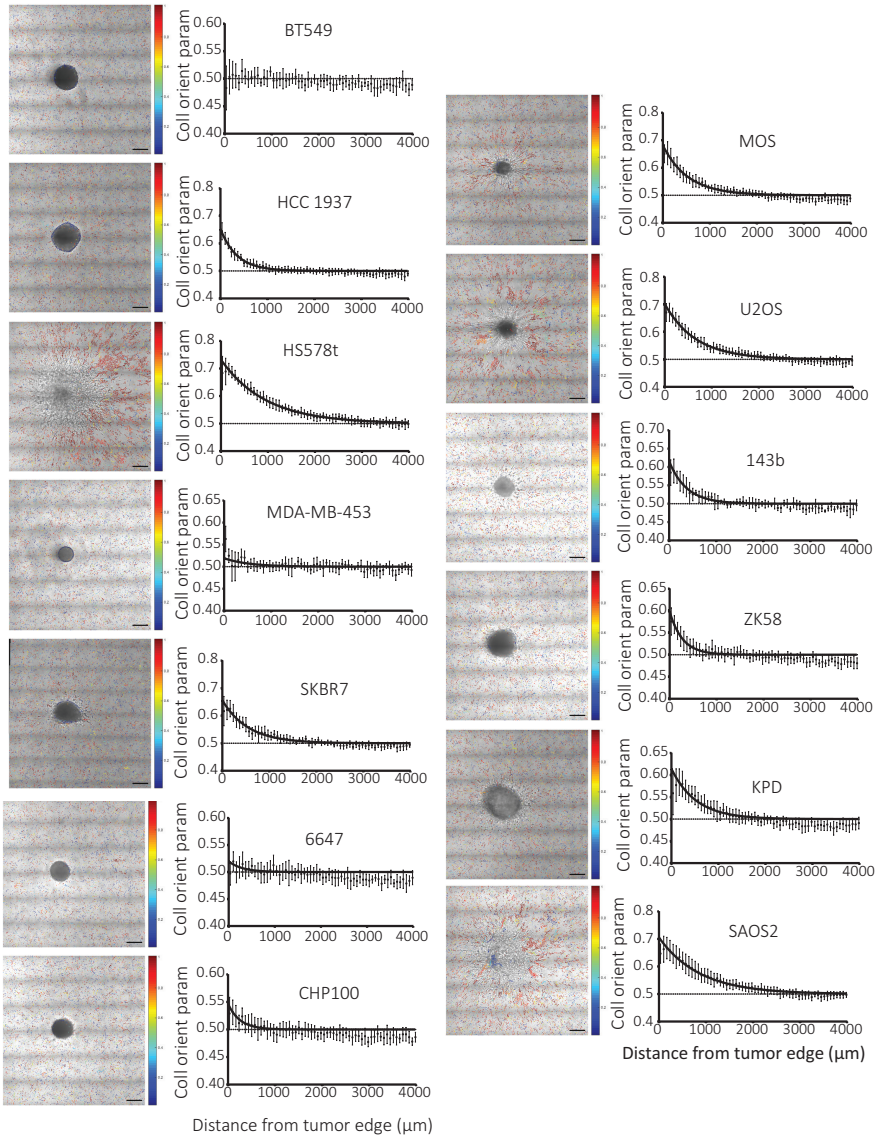

Figure S2

Collagen organization and tumor expansion for a panel of cell lines. *Collagen orientation images merged with brightfield images (left) taken 48 hours after injecting the indicated human breast cancer and sarcoma cells and corresponding collagen orientation measured at a range of distances from tumor border (right), mean ± standard deviation with exponential fits (solid lines) is shown. Scale bar, 200 µm.*

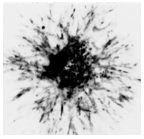

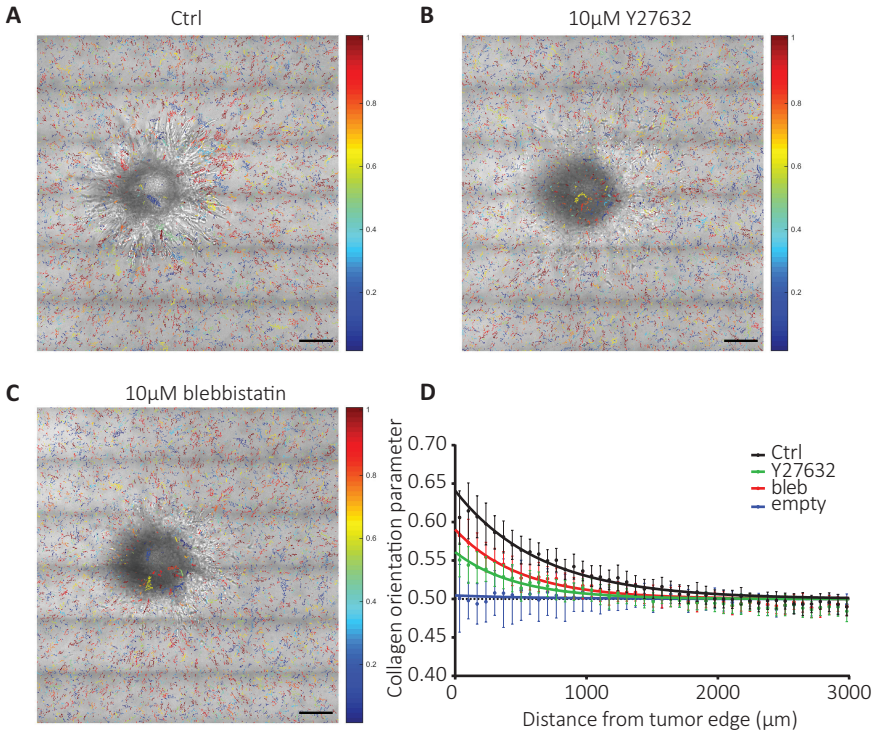

Figure S3

Effect of Y27632 and blebbistatin treatment on collagen organization. *(A-C) Collagen orientation images merged with brightfield images of 4T1 spheroids grown 48 hours in absence (A) or presence of 10 µM Y27632 (B) or 10 µM blebbistatin (C). (D) Collagen orientation measured at a range of distances from spheroid border for 4T1 injections after 48 hours without treatment (black, n=55), with 10 µM Y27632 (green, n=46) or 10 µM blebbistatin treatment (red, n=53) or from the average injection location for empty well (blue, n=23) at the same time point, mean ± standard deviation with exponential fits (solid lines) from three independent experimental replicas is shown. Scale bar, 200 µm.*

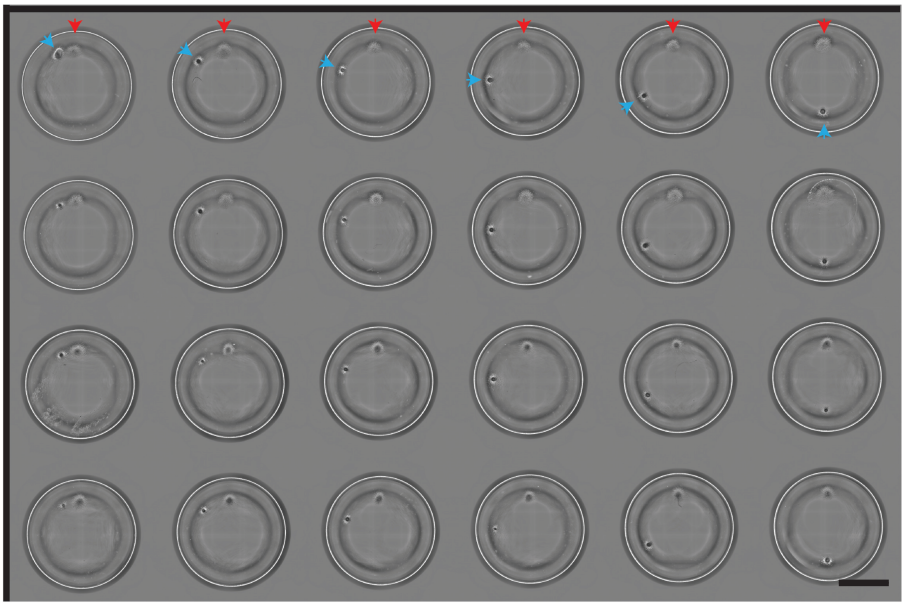

Figure S4

Automated sequential microinjection layout for tumor spheroid-HMEC-1 interaction. *Low magnification image of multiwell plate showing 4T1 cells (red arrow heads) injected at identical x-y-z position in each well followed by HMEC-1 cells (blue arrow heads) injected at varying distances, 48 hours later and incubated for an additional 24 hours. Scale bar, 3mm.*

Bibliography

[1] Judah Folkman. "Angiogenesis: an organizing principle for drug discovery?" In: *Nature Reviews Drug Discovery* 6.4 (2007).

[2] Douglas Hanahan and Robert A Weinberg. "Hallmarks of cancer: the next generation". In: *Cell* 144.5 (2011).

[3] Peter Carmeliet and Rakesh K Jain. "Molecular mechanisms and clinical applications of angiogenesis". In: *Nature* 473.7347 (2011).

[4] Sara Weis and David A Cheresh. "Tumor angiogenesis: molecular pathways and therapeutic targets". In: *Nature Medicine* 17.11 (2011).

[5] M M Sholley et al. "Mechanisms of neovascularization. Vascular sprouting can occur without proliferation of endothelial cells". In: *Laboratory Investigation* 51.6 (1984).

[6] Peter Friedl et al. "New dimensions in cell migration". In: *Nature Reviews. Molecular Cell Biology* 13.11 (2012).

[7] Tim Lämmermann et al. "Rapid leukocyte migration by integrin-independent flowing and squeezing". In: *Nature* 453.7191 (2008).

[8] Katarina Wolf et al. "Physical limits of cell migration: Control by ECM space and nuclear deformation and tuning by proteolysis and traction force". In: *The Journal of Cell Biology* 201.7 (2013).

[9] Laura Kass et al. "Mammary epithelial cell: Influence of extracellular matrix composition and organization during development and tumorigenesis". In: *The International Journal of Biochemistry & Cell Biology* 39.11 (2007).

[10] Michael W Pickup, Janna K Mouw, and Valerie M Weaver. "The extracellular matrix modulates the hallmarks of cancer". In: *EMBO Reports* 15.12 (2014).

[11] Richard O Hynes. "The extracellular matrix: Not just pretty fibrils". In: *Science (New York, N.Y.)* 326.5957 (2009).

[12] Nicolas C Rivron et al. "Tissue deformation spatially modulates VEGF signaling and angiogenesis". In: *Proceedings of the National Academy of Sciences of the United States of America* 109.18 (2012).

[13] Hayri E Balcıoğlu et al. "Integrin expression profile modulates orientation and dynamics of force transmission at cell matrix adhesions". In: *Journal of Cell Science* (2015).

[14] Frederick Grinnell and Matthew W Petroll. "Cell motility and mechanics in three-dimensional collagen matrices". In: *Annual Review of Cell and Developmental Biology* 26 (2010).

[15] Pere Roca-Cusachs, Thomas Iskratsch, and Michael P Sheetz. "Finding the weakest link - exploring integrin-mediated mechanical molecular pathways". In: *Journal of Cell Science* 125.13 (2012).

[16] Akiko Mammoto et al. "A mechanosensitive transcriptional mechanism that controls angiogenesis". In: *Nature* 457.7233 (2009).

[17] Hoa H Truong et al. "β1 integrin inhibition elicits a prometastatic switch through the TGFβ-miR-200-ZEB network in E-cadherin-positive triple-negative breast cancer". In: *Science Signaling* 7.312 (2014).

[18] Pengfei Lu, Valerie M Weaver, and Zena Werb. "The extracellular matrix: A dynamic niche in cancer progression". In: *Journal of Cell Biology* 196.4 (2012).

[19] Ovijit Chaudhuri et al. "Extracellular matrix stiffness and composition jointly regulate the induction of malignant phenotypes in mammary epithelium". In: *Nature Materials* 13.10 (2014).

[20] Matthew J Paszek et al. "Tensional homeostasis and the malignant phenotype". In: *Cancer Cell* 8.3 (2005).

[21] Robert W Tilghman et al. "Matrix Rigidity Regulates Cancer Cell Growth by Modulating Cellular Metabolism and Protein Synthesis". In: *PLoS One* 7.5 (2012).

[22] Shawn P Carey et al. "Biophysical control of invasive tumor cell behavior by extracellular matrix microarchitecture". In: *Biomaterials* 33.16 (2012).

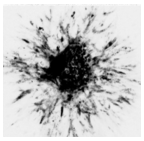

[23] Asja Guzman, Michelle J Ziperstein, and Laura J Kaufman. "The effect of fibrillar matrix architecture on tumor cell invasion of physically challenging environments". In: *Biomaterials* 35.25 (2014).

[24] Jiranuwat Sapudom et al. "The phenotype of cancer cell invasion controlled by fibril diameter and pore size of 3D collagen networks". In: *Biomaterials* 52 (2015).

[25] Kandice R Levental et al. "Matrix Crosslinking Forces Tumor Progression by Enhancing Integrin Signaling". In: *Cell* 139.5 (2009).

[26] Matthew W Conklin et al. "Aligned collagen is a prognostic signature for survival in human breast carcinoma". In: *The American Journal of Pathology* 178.3 (2011).

[27] Kristin M Riching et al. "3D collagen alignment limits protrusions to enhance breast cancer cell persistence". In: *Biophysical Journal* 107.11 (2014).

[28] Shalini Menon and Karen A Beningo. "Cancer cell invasion is enhanced by applied mechanical stimulation". In: *PLoS One* 6.2 (2011).

[29] Dewi Harjanto, Joseph S Maffei, and Muhammad H Zaman. "Quantitative analysis of the effect of cancer invasiveness and collagen concentration on 3D matrix remodeling". In: *PLoS One* 6.9 (2011).

[30] Casey M Kraning-Rush, Joseph P Califano, and Cynthia A Reinhart-King. "Cellular traction stresses increase with increasing metastatic potential". In: *PLoS One* 7.2 (2012).

[31] Daniel J McGrail et al. "Actomyosin tension as a determinant of metastatic cancer mechanical tropism". In: *Physical Biology* 12.2 (2015).

[32] Michael S Samuel et al. "Actomyosin-Mediated Cellular Tension Drives Increased Tissue Stiffness and beta-Catenin Activation to Induce Epidermal Hyperplasia and Tumor Growth". In: *Cancer Cell* 19.6 (2011).

[33] David Stopak and Albert K. Harris. "Connective tissue morphogenesis by fibroblast traction". In: *Developmental Biology* 90.2 (1982).

[34] Paolo P Provenzano et al. "Contact Guidance Mediated Three-Dimensional Cell Migration is Regulated by Rho/ROCK-Dependent Matrix Reorganization". In: *Biophysical Journal* 95.11 (2008).

[35] Jeffrey B Wyckoff et al. "ROCK- and myosin-dependent matrix deformation enables protease-independent tumor-cell invasion in vivo". In: *Current Biology* 16.15 (2006).

[36] James A Schiro et al. "Integrin alpha 2 beta 1 (VLA-2) mediates reorganization and contraction of collagen matrices by human cells". In: *Cell* 67.2 (1991).

[37] Yael Hegerfeldt et al. "Collective cell movement in primary melanoma explants: plasticity of cell-cell interaction, beta1-integrin function, and migration strategies". In: *Cancer Research* 62.7 (2002).

[38] Jenny G Parvani et al. "Targeted inactivation of beta1 integrin induces beta3 integrin switching, which drives breast cancer metastasis by TGF-beta." In: *Molecular Biology of the Cell* 24.21 (2013).

[39] Ning Yang et al. "Syndecan-1 in breast cancer stroma fibroblasts regulates extracellular matrix fiber organization and carcinoma cell motility". In: *The American Journal of Pathology* 178.1 (2011).

[40] Daniel R Croft et al. "Conditional ROCK activation in vivo induces tumor cell dissemination and angiogenesis". In: *Cancer Research* 64.24 (2004).

[41] Kaustabh Ghosh et al. "Tumor-derived endothelial cells exhibit aberrant Rho-mediated mechanosensing and abnormal angiogenesis in vitro". In: *Proceedings of the National Academy of Sciences of the United States of America* 105.32 (2008).

[42] Brooke N Mason et al. "Tuning three-dimensional collagen matrix stiffness independently of collagen concentration modulates endothelial cell behavior". In: *Acta Biomaterialia* 9.1 (2013).

[43] Amir Shamloo and Sarah C Heilshorn. "Matrix density mediates polarization and lumen formation of endothelial sprouts in VEGF gradients". In: *Lab on a Chip* 10.22 (2010).

[44] Yinying Dong et al. "Increasing matrix stiffness upregulates vascular endothelial growth factor expression in hepatocellular carcinoma cells mediated by integrin β1". In: *Biochemical and Biophysical Research Communications* 444.3 (2014).

[45] Jie Liu and Sudha Agarwal. "Mechanical signals activate vascular endothelial growth factor receptor-2 to upregulate endothelial cell proliferation during inflammation". In: *The Journal of Immunology* 185.2 (2010).

[46] Antoinette Hollestelle et al. "Distinct gene mutation profiles among luminal-type and basal-type breast cancer cell lines". In: *Breast Cancer Research and Treatment* 121.1 (2010).

[47] Zuzanna Baranski et al. "Aven-mediated checkpoint kinase control regulates proliferation and resistance to chemotherapy in conventional osteosarcoma". In: *The Journal of Pathology* 236.3 (2015).

[48] Edwin W Ades et al. "HMEC-1: Establishment of an immortalized human microvascular endothelial cell line". In: *The Journal of Investigative Dermatology* 99.6 (1992).

[49] Navneeta Rajan et al. "Preparation of ready-to-use, storable and reconstituted type I collagen from rat tail tendon for tissue engineering applications". In: *Nature Protocols* 1.6 (2006).

[50] Hoa H Truong et al. "Automated microinjection of cell-polymer suspensions in 3D ECM scaffolds for high-throughput quantitative cancer invasion screens". In: *Biomaterials* 33.1 (2012).

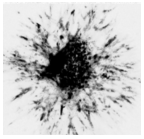

Chapter 3

Integrin expression profile modulates orientation and dynamics of force transmission at cell-matrix adhesions [1]

[1] This chapter is based on: Hayri E Balcıoğlu, Hedde van Hoorn, Dominique M Donato, Thomas Schmidt and Erik HJ Danen, Integrin expression profile modulates orientation and dynamics of force transmission at cell-matrix adhesions. , *J. Cell. Sci.*, **128**, 1316-26 (2015)

Abstract

Integrin adhesion receptors connect the extracellular matrix (ECM) to the cytoskeleton and serve as bidirectional mechanotransducers. During development, angiogenesis, wound healing, or cancer progression the relative abundance of fibronectin receptors, including α5β1 and αvβ3 changes, thus altering the integrin composition of cell-matrix adhesions. Here, we show that enhanced αvβ3 expression can fully compensate for loss of α5β1 and other β1 integrins to support outside-in and inside-out force transmission. α5β1 and αvβ3 each mediate actin cytoskeletal remodeling in response to stiffening or cyclic stretching of the ECM. Likewise, α5β1 and αvβ3 support cellular traction forces of comparable magnitudes and similarly increase these forces in response to ECM stiffening. However, cells using αvβ3 respond to lower stiffness ranges, more robustly reorganize their actin cytoskeleton in response to stretch, and traction forces are more randomly oriented in cells using αvβ3. Centripetal traction force orientation requires Rho kinase-Myosin II-mediated long stress fibers that are supported by α5β1. Thus, altering the relative abundance of fibronectin-binding integrins in cell-matrix adhesions affects spatiotemporal organization of force transmission.

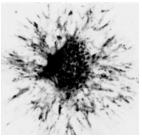

3.1 Introduction

Cells sense the mechanical properties of their surrounding environment and activate intracellular signaling cascades generating an elaborate response that plays a role in cell survival, proliferation, differentiation, and migration [1]. Cell-matrix adhesions are dynamic force responsive protein complexes that couple the extracellular matrix (ECM) to the cytoskeleton [2]. Within these adhesions, integrin α-β heterodimeric transmembrane receptors bind ECM proteins with their globular head domains and connect to the cytoskeleton via multi-protein interactions at their cytoplasmic tails [3]. Integrins transmit forces in a bi-directional manner: extracellular forces applied to the head domains enhance integrin activity and clustering, and trigger cell-matrix adhesion growth and cytoskeletal reorganization. Vice versa, actomyosin-mediated contractile forces cause strengthening of integrin-ECM binding [4–7].

Cell-matrix adhesions formed on fibronectin contain a mixture of different integrins, including α5β1 and αvβ3. When cells are stimulated to move or proliferate during development, angiogenesis, or tissue regeneration, shifts in the relative abundance of these fibronectin-binding integrins occur [8, 9]. Likewise, alterations in the abundance of α5β1 or αvβ3 take place during cancer progression [10]. Such changes will alter the integrin composition of cell-matrix adhesions and we and others have previously shown that this affects cytoskeletal organization, activity of Rho GTPases, and migratory behavior [11–13].

Using mouse embryonic stem (ES) cell-derived fibroblastic cells (GD25) and mouse embryo-derived neuroepithelial cells (GE11) lacking the common β1 subunit we have shown that re-expression of β1 (but not increased expression of β3 supporting a similar level of adhesion to fibronectin) stimulates RhoA-Rho kinase-mediated contractility and more random migration [11, 12]. Likewise, White et al. have shown that prevention of αvβ3 recycling in NIH3T3 cells thereby causing enhanced surface abundance of α5β1, stimulates Rho kinase-mediated contractility and random movement [14]. Conversely, Miao et al. demonstrated that expression of β3 integrins (but not increased expression of β1 integrins) in CHO cells that lack β3 causes enhanced RhoA-Rho kinase activity [13]. This may

suggest that the total amount of fibronectin-binding integrins is more relevant or that expression of both β1 and β3 integrins is needed for effective Rho-Rho kinase-mediated contractility. However, we showed that β3 knockout MEFs have no defect in RhoA-Rho kinase-mediated contractility and ectopic expression of β3 integrins does not further stimulate this pathway (whereas increased expression of β1 integrins does) [15]. Moreover, like expression of β1 integrins in β1 null cells; expression of α5 in α5 null mouse ES-derived fibroblastic cells also stimulates RhoA-Rho kinase-mediated contractility [15].

It has subsequently become clear that different integrins can mediate distinct signaling routes that support distinct aspects of mechanotransduction. Experiments using MEFs in which ligand-coated beads were used to pull on small integrin clusters have shown that α5β1 mediates adhesion strength whereas αvβ3 mediates cytoskeletal stiffening [16]. A recent study using pan-integrin knockout kidney fibroblasts reconstituted with αv, β1, or both subunits resulting in equimolar surface levels of α5β1 and/or αvβ3 and αvβ5 has provided further insight: α5β1-mediated adhesion indeed stimulates RhoA-Rho kinase signaling to activate Myosin II but αv integrins are required to support RhoA-mDia-mediated actin polymerization and these processes cooperate to regulate contractility [17]. Thus, the expression levels of α5β1, αvβ3, as well as other αv-integrins participating in fibronectin-binding (e.g. αvβ1 and αvβ6) in combination with the distinct signaling networks of integrin-associated proteins present in embryonic or ES-derived epithelial or fibroblastic cells, kidney cells, or CHO cells used in the above-mentioned studies ultimately determine the outcome of changes in the fibronectin-receptor repertoire for RhoA-mediated signaling and cytoarchitecture.

In this study we asked to what extent a shift from α5β1 to more αvβ3 expression, as often seen with angiogenesis, wound healing, or cancer progression, affects mechanotransduction. We used two independent cell systems in which adhesion to fibronectin is mediated mainly by α5β1 or by αvβ3 integrins resulting in comparable adhesion efficiency and compared the ability of such cells to i) sense and respond to extracellular forces (outside-in signaling), and ii) exert forces onto the ECM (inside-out signaling).

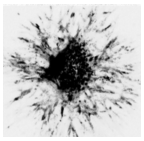

3.2 Results

3.2.1 Cells adhering through αvβ3 show more robust cytoskeletal reorganization in response to cyclic stretch as compared to cells using α5β1

To compare responses to extracellular forces we made use of GEβ1 and GEβ3 cells. These cells derived from β1 integrin chimeric mouse embryos lacked the common β1 subunit and were engineered to express human β1 or β3 subunits. Fluorescence-activated cell sorting (FACS) showed that ectopically expressed β1 and β3 led to high cell surface levels but these did not exceed endogenous levels observed in MDA-MB-435s human breast cancer cells (Figure S1C,D,G,I). GEβ1 and GEβ3 cells were previously shown to support adhesion to fibronectin-coated glass substrates with the same efficiency through either α5β1 or αvβ3, respectively [11]. The cells were transduced with mCherry-LifeAct for actin imaging (Figure S1E,F,I,J) and plated on a fibronectin-coated Poly (DiMethyl)Siloxane (PDMS) membrane and subjected to uniaxial, cyclic stretch first at 10% 1 Hz for 2 hours, then at 20% 1 Hz for 1 hour (Figure 3.1A). Incubation with integrin blocking antibodies confirmed that, like fibronectin-coated glass substrates, GEβ1 and GEβ3 adhered to fibronectin-coated PDMS substrates mainly through α5β1 and αvβ3, respectively (Figure S2H). Upon cyclic stretch, both GEβ1 and GEβ3 cells showed a gradual decrease in cell-spreading area with the two subsequent stretching regimes. The total actin filament length showed the same trend for GEβ1 but for GEβ3 cells the total filament length already approached a minimum value at 10% stretch and showed only a slight additional decrease after subsequent 20% stretching (Figure 3.1B-E).

PDMS membranes, coated with fluorescent beads or stamped with patterned fluorescently labeled fibronectin were used to characterize the strain field over the membrane, the dynamic strain in the imaging field, and to determine the angle of minimal strain (Figure 3.1A; Figure S2A-D). GEβ1 cells oriented their F-actin towards the minimal strain direction (∼60° to the macroscopic strain) following the 10% stretch regime but this response was lost during the subsequent, second regime of 20% stretch (Figure 3.1F,H). GEβ3 cells subjected to the first stretch regime showed a more prominent actin filament orientation towards the minimal strain direction and this response was maintained during the 20% stretch regime (Figure 3.1G,H).

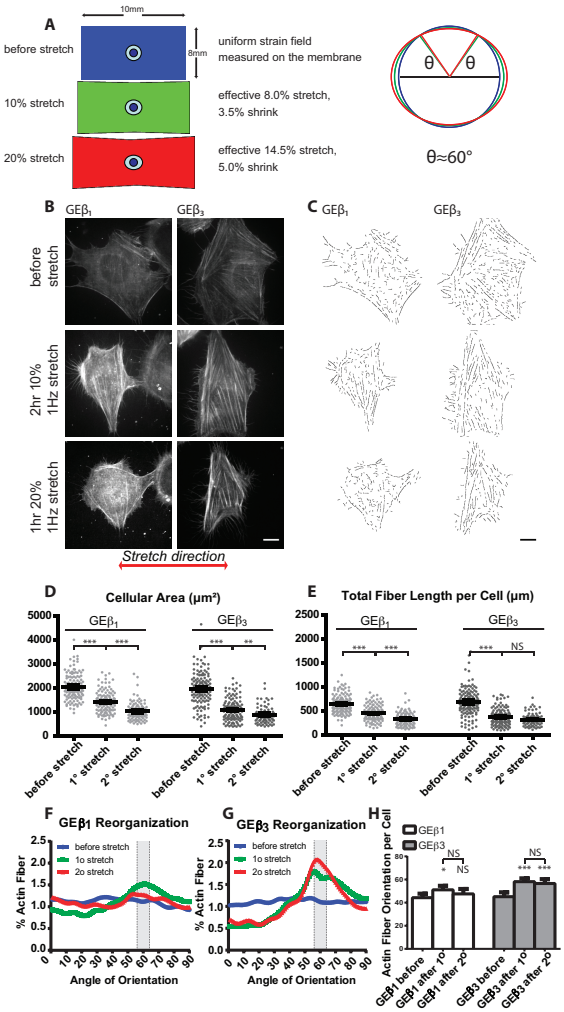

Figure 3.1

Cells expressing αvβ3 integrins more effectively reorganize their cytoskeleton upon cyclic stretch. *(A) Stretch regimes used during the experiment. Driving the piezo controllers with 10%/20% displacement resulted in 8%/14.5% stretch on the PDMS membrane in the direction of the displacement, and 3.5%/5% shrink in the perpendicular direction. This resulted in a minimal strain angle of ∼60°. (B) mCherry-LifeAct-transduced GEβ1 and GEβ3 cells respond to 2 step cyclic stretch. (C) Characterization of actin organization. (D,E) Quantification of cellular spread area (D) and total actin filament length (E). Mean 95% clearance level of >75 cells from 3 independent experiments. (F,G) Angular organization of actin filaments averaged over all GEβ1 (F) or GEβ3 (G) cells measured. Measured angle of orientation of actin filaments is relative to stretch direction. Grey bar indicates region of minimal strain. (H) Average actin filament orientation per cell, mean ± 95% clearance level of >75 cells from 3 independent experiments. NS, p>0.05; *,p<0.05; **, p<0.005; ***, p<0.0005 according to Mann-Whitney test. Scale bar is 10 μm.*

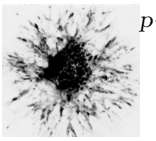

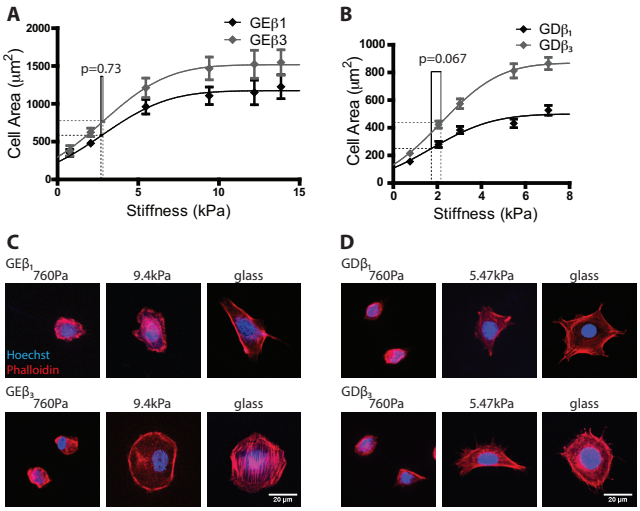

Figure 3.2
Cells respond to increased substrate stiffness by increased spreading irrespective of the integrin engaged. *(A,B) Quantification of cellular spread area of GEβ1 and GEβ3 cells (A) or GDβ1 and GDβ3 cells (B) over measured rigidities and cumulative Gaussian distribution model fitted. Mean ±95% clearance level is shown. >100 cells were measured from 3 different experiments (except at 760 Pa for GEβ1 and GEβ3 cells where more than 60 cells were measured from a single experiment). P values were calculated by comparing the halfway points of the cumulative Gaussian fits with an F-test. (C,D) Representative images for A and B. Scale bar is 20 µm.*

These findings indicate that cells adhering mainly through α5β1 or αvβ3 integrins can both sense cyclic ECM strain and trigger actin cytoskeleton remodeling. However, high expression of αvβ3 allows cells to more effectively reorient their cytoskeleton in the direction of minimal strain and maintain this orientation at high strain rates.

3.2.2 Cells expressing α5β1 or αvβ3 each support cell spreading in response to substrate stiffening

Next, we seeded GEβ1 and GEβ3 cells onto fibronectin-crosslinked polyacrylamide (PAA) gels with shear moduli varying between 760 Pa and 13.4 kPa (Figure S2F,G). Incubation with integrin blocking antibodies confirmed that, like fibronectin-coated glass and PDMS substrates, GEβ1 and GEβ3 adhered to fibronectin-crosslinked PAA substrates mainly

through α5β1 and αvβ3, respectively (Figure S2I). Both cell types showed a gradual increase in cell spreading area with increasing stiffness (Figure 3.2A,C). Similar findings were obtained using the GD25 cell line derived from β1 null ES cells where expression of human β1 or β3 subunits supports adhesion to fibronectin with the same efficiency through α5β1 or αvβ3, respectively [11] and had comparable surface expression levels of these integrins as MDA-MB-435s cells (Figure S1A,B,H,I). Parenthetically, for GD cells lower stiffness ranges were used as compared to those used for the GE cell lines since full cell spreading was already observed on softer substrates for this cell type. Again, cell-spreading area increased with increasing stiffness over the range of stiffnesses tested for cells adhering through either of these integrins (Figure 3.2B,D). Non-linear fitting using a cumulative Gaussian distribution (Figure S3A) showed that despite having significantly different response curves (Figure S3B-D) the estimated half response stiffness ($E_{1/2}$) was not integrin specific (Figure 3.2A,B).

3.2.3 Cells adhering through αvβ3 form cell-matrix adhesions at lower substrate stiffness compared to cells adhering through α5β1

Similar to cellular area, the number of peripheral cell-matrix adhesions increased with increasing stiffness for all cell lines. For GEβ3 and GDβ3 cells the number of peripheral cell-matrix adhesions reached its maximum at intermediate stiffness with an elastic modulus of 9.4 and 5.47 kPa, respectively (Figure 3.3A,B,D; Figure S3J). By contrast, the number of cell-matrix adhesions in GEβ1 and GDβ1 cells showed a more gradual increase over the entire range of stiffnesses tested (Figure 3.3A,B,C; Figure S3I). The half response stiffness ($E_{1/2}$) was also significantly lower for cells using αvβ3, as compared to that for cells using α5β1 (Figure 3.3A,B; Figure S3B,E,F). The average cell-matrix adhesion size did not show the same gradual response to rigidity: once adhesions were formed, they reached similar sizes irrespective of the ECM stiffness (Figure 3.3C,D; Figure S3G-J).

Taken together, these findings demonstrate that cells expressing α5β1 and αvβ3 can each sense - and respond to - variations in substrate stiffness but αvβ3 supports cell-matrix adhesion formation more readily at a lower stiffness.

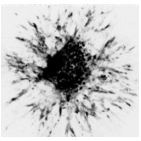

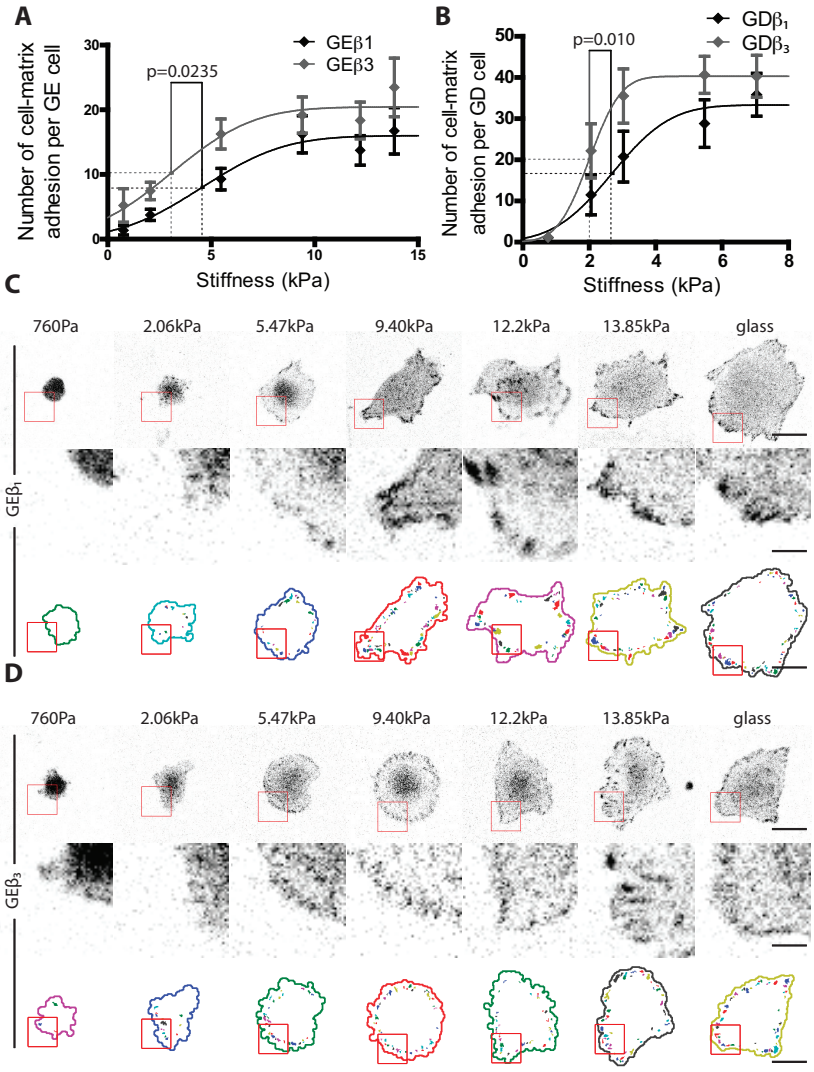

Figure 3.3

Number of cell-matrix adhesions increases with increasing stiffness in an integrin-controlled manner. *(A,B) Quantification of number of peripheral cell-matrix adhesions of GEβ1 and GEβ3 cells (A) or GDβ1 and GDβ3 cells (B) over measured rigidities and fitted cumulative Gaussian distribution function. In all graphs, mean ±95% clearance level is shown and at least 20 cells were measured over 3 different experiments (except for 760 Pa for GEβ1 and GEβ3 cells where results of one experimental replica is shown). P values were calculated by comparing the halfway points of the cumulative Gaussian fits (A,B) with F-test. (C,D) Representative images of Paxillin (top), zoomed in region of the boxed area (middle) and adhesions detected by the automated analysis algorithm (bottom). Scale bar is 20 µm (5 µm for zooms).*

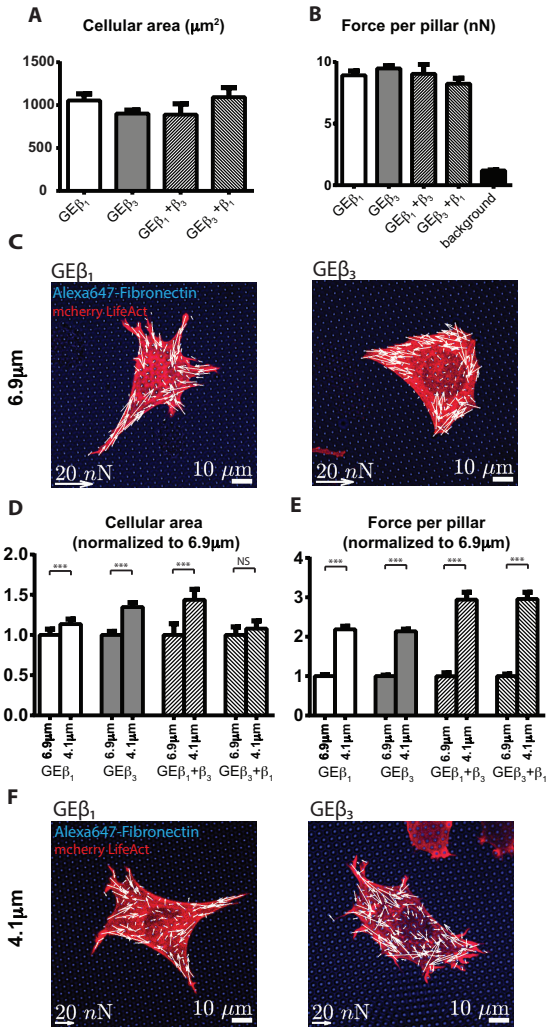

Figure 3.4

Cellular traction force generation is similar for cells using α5β1 or αvβ3 integrins. *(A-B) Bar plots of cellular spread area and force per pillar of the indicated cell lines seeded on 6.9 µm PDMS pillars. Background indicates forces measured in areas not covered by cells. (C) Representative images from A,B; white arrows indicate magnitude and direction of forces measured. Scale bar, 20 nN/10 µm. (D,E) Bar plots of cellular spread area and force per pillar of the indicated cell lines seeded on 4.1 µm PDMS pillars, relative to measurements on 6.9 µm pillars. In all graphs, mean ±95% clearance level is shown and at least 30 cells were measured over 3 different experiments. (F) Representative images from D,E. White arrows and scale bars as in C.*

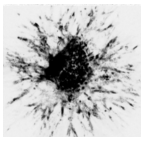

3.2.4 Cells adhering through α5β1 or αvβ3 each mediate traction forces that are regulated in response to altered substrate rigidity

Having examined the consequences of expression of either α5β1 or αvβ3 for outside-in cellular responses to extracellular forces, we next investigated whether these integrins differed in their ability to mediate inside-out cellular traction forces onto the ECM. Therefore, mCherry-LifeAct-expressing GEβ1 and GEβ3 cells were seeded on fibronectin-stamped PDMS micropillars of 6.9 µm height (bending stiffness of 16 nN/µm). Cell spreading on these micropillars as well as the average force per pillar was similar for both cell lines (Figure 3.4A-C). This indicated that β1 integrins were not required for the generation of traction forces in cells where αvβ3 levels are sufficiently high to compensate for adhesion, despite earlier reports pointing to a critical role for β1 integrins [16, 17]. To address whether expression of β1 integrins might further increase traction forces in GEβ3 cells we plated GEβ1+β3 and GEβ3+β1 cells on 6.9 µm fibronectin-stamped micropillars. However, comparable cell spreading and forces were measured for these cells as observed for GEβ1 and GEβ3 cells (Figure 3.4A,B). Together, these findings indicate that traction forces can be generated irrespective of the type of fibronectin-binding integrin expressed.

We next analyzed the ability of these cells to increase traction forces in response to increased substrate stiffness. Plating cells on shorter pillars (4.1 µm height; bending stiffness of 66 nN/µm) led to increased cell spreading and to ∼2-fold increase in traction forces, irrespective of the integrin used (Figure 3.4D-F). The increase in traction force was ∼3-fold for GEβ1+β3 and GEβ3+β1 cells indicating that the total amount of fibronectin-binding integrins may determine the magnitude of the response (Figure 3.4E). The 2-fold increase in response to substrate stiffening was maintained for GEβ1 and GEβ3 cells in post-fixation samples and GDβ1 and GDβ3 cells each showed a similar response although the magnitude of the response to stiffening was lower for GDβ3 cells (Figure S4A-C). In addition, a similar, albeit somewhat stronger increase in traction forces upon seeding on shorter pillars was observed for NIH3T3 cells that bind to fibronectin via both α5β1 and αvβ3 [18] (Figure S4A,B). Lastly, having established that initial adhesion to fibronectin-coated PDMS involved α5β1 for GEβ1 cells and αvβ3 for GEβ3 cells (Figure S2H), we analyzed the potential role of αv integrins in the traction forces exerted

by these cells. As expected, αv integrin-blocking antibodies decreased force application by GEβ3 cells but they did not affect traction forces in GEβ1 cells, indicating that α5β1 was the major integrin responsible for force application on fibronectin in GEβ1 (Figure S4D-F).

These results indicate that cells are able to exert traction forces and respond to increased ECM stiffness by enhanced force application, irrespective of the type of fibronectin receptor engaged. Notably, the approximated shear modulus of 3.87 and 15.7 kPa of these long and short pillars (see Materials and methods section), was within the outside-in sensing regimes tested using PAA substrates (Figures 3.2, 3.3).

3.2.5 Cells adhering through α5β1 preferentially support centripetal force application and long actin filaments in an actomyosin contractility-dependent manner

Cells expressing α5β1 or αvβ3 show distinct organization of the actin cytoskeleton and cell-matrix adhesions with α5β1 supporting predominantly concave cortical actin structures [11, 12] (Figure 3.2C-D). We hypothesized that the morphology supported by α5β1 was related to more centripetally oriented forces exerted at cell-matrix adhesions. In order to investigate this, we analyzed the centripetally oriented force fraction, i.e. forces directed towards the cell center compared to the total force. Live measurement of traction forces on 6.9 µm and on 4.1 µm pillars showed that the centripetal force fraction in GEβ1 cells was slightly but significantly higher than that observed in GEβ3 cells (Figure 3.5A, left panel). The centripetal force fraction in GEβ1+β3 and GEβ3+β1 cells was comparable to that in GEβ1 cells. The higher centripetal force fraction in β1-expressing cells was also observed in post-fixation samples of GDβ1, GDβ3, GEβ1, and GEβ3 cells on 4.1 µm pillars (Figure 3.5A, middle panel).

We measured cortical actin filament lengths in GEβ1 and GEβ3 cells on 4.1 µm pillars and noticed that higher centripetal force orientation in GEβ1 correlated with longer average cortical actin filament length (Figure 3.5B,C). This suggested that the longer actin filaments in α5β1 expressing cells, rather than shorter actin cables in αvβ3 expressing cells, supported the centripetal orientation of forces. We and others have previously observed that α5β1 supports Rho kinase-mediated actomyosin contractility [11, 12, 14, 17] and we tested whether Rho kinase signaling was involved in the centripetal orientation of applied forces. Indeed, inhi-

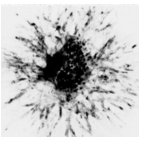

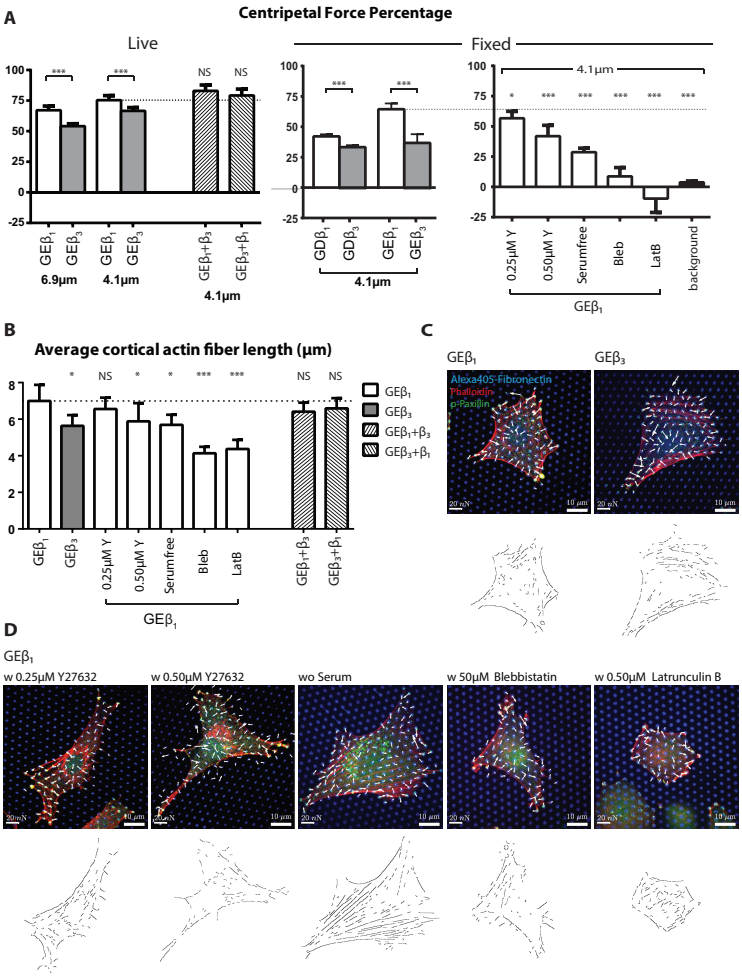

Figure 3.5

Higher centripetal force fraction in cells using α5β1 correlates with longer cortical actin filaments through Rho kinase-Myosin activity. *(A) Bar plots showing percentage centripetal force for the indicated cell lines on 6.9 µm and 4.1 µm PDMS pillars determined by live microscopy (left graph) or post-fixation analysis (middle and right graphs). Treatments in the right graph are 0.25 µM Y and 0.5 µM Y, Y27632 concentrations; bleb, 50 µM blebbistatin; LatB, 0.5 µM Latranculin B. Background indicates forces measured in areas not covered by cells. (B) Bar plots of average cortical actin filament length of the indicated cell lines on 4.1 µm PDMS pillars. Indicated treatments as in A, right graph. In all graphs mean ±95% clearance level is shown and at least 15 cells were measured over 3 different experiments. Indicated P values are compared to untreated β1 expressing cells (marked by dotted lines); NS, p>0.05; *, p<0.05; **, p<0.005; ***, p<0.0005 according to Mann-Whitney test. (C, D) Representative images (top) and extracted actin cytoskeleton (bottom) for control (C) and treatment conditions (D). White arrows indicate magnitude and direction of forces measured. Scale bar, 20 nN/10µm.*

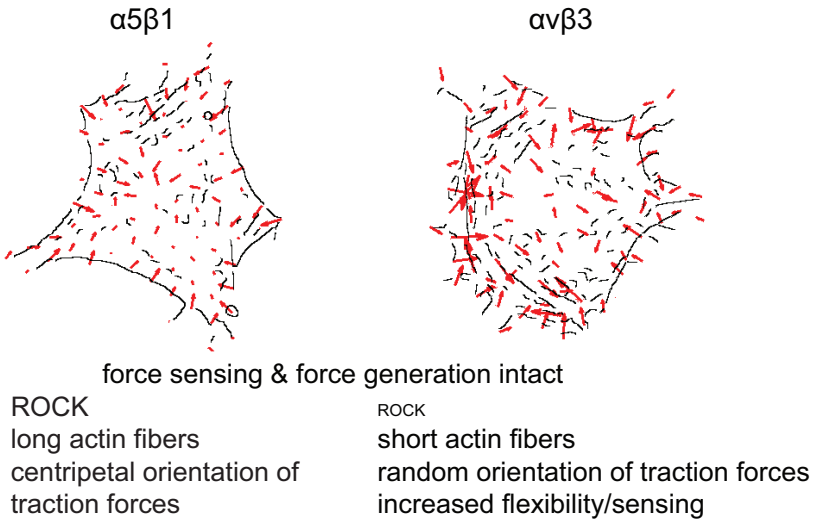

Figure 3.6
Model for integrin regulated mechanotransduction. *Both α5β1 and αvβ3 integrins are able to support sensing and responding to mechanical cues from the environment (outside-in signaling) and to mediate force generation onto the ECM (inside-out signaling). Rho kinase-Myosin-mediated long actin filaments are supported by α5β1 integrins and allow cells to apply centripetally oriented forces. Shorter actin filaments in αvβ3 expressing cells support more randomly oriented traction forces and may provide flexibility to reorganize the actin cytoskeleton in response to mechanical cues from the environment. Potential roles for alternative αv integrins (e.g. αvβ1 and αvβ6) are not tested here but may modulate the outcome of shifts in expression of α5β1 and αvβ3.*

bition of Rho kinase or withdrawal of serum (containing lysophosphatidic acid, a known stimulator of Rho-Rho kinase signaling [19]) reduced the centripetal orientation of force (Figure 3.5A right panel). These treatments also, though less effectively, reduced the average cortical actin filament length in GEβ1 to the level observed for GEβ3 (Figure 3.5B,D). Likewise, treatment of GEβ1 cells with the Myosin-II inhibitor blebbistatin or disruption of the actin cytoskeleton with latrunculin B left only short actin cables intact and abolished the centripetal force orientation (Figure 3.5B,D).

Together, these data show that even though traction forces mediated by α5β1 and αvβ3 (possibly supported by other fibronectin-binding αv integrins) are similar in magnitude; orientation of these forces is dif-

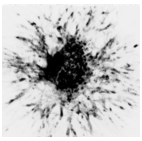

ferentially regulated. This difference is related to long-range cortical actomyosin fibers supported by Rho kinase and Myosin-II in the context of α5β1 versus shorter actin cables in the context of αvβ3 (Figure 3.6).

3.3 Discussion

Cell matrix adhesions couple the ECM to the F-actin network and are regions for force transmission, allowing cells to adapt to the mechanical properties of the environment and to exert forces needed to remodel their environment. Our findings demonstrate that cell matrix adhesions can function as bi-directional force transducers irrespective of whether they contain α5β1 (and very little αvβ3) or αvβ3 (in the absence of any β1 integrins). It should be noted that a contribution of alternative αv integrins such as αvβ5, αvβ6, αvβ8 or, in the case of cells expressing β1 integrins, αvβ1 cannot be fully ruled out in our study. Integrins α5β1 and αvβ3 have been shown to play distinct roles in adhesion strengthening and actin cytoskeletal stiffening in integrin clusters under force [16]. Our findings show that this does not translate into reduced force application by cell-matrix adhesions in the absence of α5β1 or ineffective F-actin reorganization when αvβ3 expression is low; provided there is compensation through enhanced expression of αvβ3 or α5β1, respectively. Cells expressing either α5β1 or αvβ3 each respond to cyclic substrate stretching and each can sense variations in substrate stiffness and accordingly trigger cell spreading and cell matrix adhesion formation. Likewise, both integrins allow cell matrix adhesions to apply traction forces onto the ECM and respond to increased stiffness with enhanced force application.

Nevertheless, the manner in which force transduction is dynamically organized in cells expressing either of these integrins does differ. Our findings indicate that cells expressing αvβ3 form cell matrix adhesions more effectively at lower substrate stiffnesses and more robustly reorganize their actin cytoskeleton to find the minimal strain in response to substrate stretching. It has been reported that substrate stretching triggers Phosphatidylinositol-4,5-bisphosphate 3-kinase-(PI3K)-mediated αvβ3 activation, which in turn stimulates cellular responses including c-Jun N-terminal kinase(JNK) activation [20]. It will be of interest to explore whether such a mechanism underlies the effective cytoskeletal reorganization observed in cells expressing high levels of αvβ3. The emergence of αvβ3, which is frequently observed during active processes such as an-

giogenesis or cancer invasion [10] may provide endothelial or tumor cells in these cases with enhanced flexibility to adapt their cytoarchitecture to ECM properties and activate cellular signaling in soft environments.

Our findings indicate that cells using α5β1 or αvβ3 respond to substrate stiffening by cell spreading, cell matrix adhesion formation, and by applying more force to the substrate. It has been demonstrated that αv-integrins support coupling of RhoA activity to mDia, which drives actin polymerization [17]. Unlike that study, our experiments do not test such a role for fibronectin-binding αv-integrins in mechanotransduction; αv-integrins are expressed in all cell variants tested in our study (αvβ1 and others in GEβ1 and GDβ1; αvβ3 and others in GEβ3 and GDβ3). Unlike earlier reports [16, 17], we do not observe a marked deficiency in traction force induction by cells lacking β1 integrins when αvβ3 is expressed at sufficient levels to fully rescue the adhesion defect. Notably, expression levels in our study are comparable to endogenous levels of β1 or β3 found in cancer cells. The role of fibronectin-binding integrins in traction force generation appears to differ for different cell types. Besides variations in the profile of αv integrins for which the distinct roles in cytoskeletal organization are poorly understood; the integrin-associated signaling complex including Rho GTPases and their upstream regulators and downstream effectors may differ considerably in the variety of cell types used in different studies. This makes a direct comparison of different studies exploring integrin-mediated control of cytoskeletal organization and mechanotransduction difficult.

It has been reported that extracellular stimuli leading to activation of α5β1 but not those causing activation of αvβ3 can trigger cell traction forces [21]. The authors measured total force per cell; a parameter that is sensitive to effects on cell spreading area. Instead, here we determined force per pillar, which is independent of cell spreading area, and show that the induction of traction forces in response to extracellular stiffening can occur through both α5β1 and αvβ3. The report from Lin et al. and our current study differ in the stimuli that are used (antibody-mediated integrin activation versus substrate stiffening through pillar shortening) and in the cell types that are tested, which may regulate force transmission differently. Our findings show that both integrins can be used by cells to sense alterations in the physical properties of the environment and to respond to such changes by modulation of traction forces exerted onto the ECM.

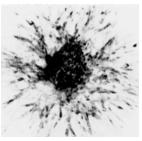

Rather than a role for α5β1 in force generation per se, which we show can be compensated for by enhanced expression of αvβ3 in complete absence of β1 integrins, we demonstrate that the orientation of forces is determined by the absence or presence of α5β1. This integrin allows cells to maintain contractile forces directed to the center of the cell and in its absence, forces become more randomly oriented. The ability of α5β1 to induce Rho kinase-Myosin-II-mediated signaling as demonstrated by us and others [11, 12, 14, 17] is important in this respect. We show that it allows cells to form long actin filaments that may support long-range force organization.

In conclusion, our findings show that both α5β1 and αvβ3 integrins support force sensing and force generation, but α5β1 predominantly mediates centripetally-oriented traction forces that are supported by Rho kinase and Myosin-II-mediated long actin filaments. By contrast, the shorter actin cables that are supported by αvβ3 allow more random force application and may provide cells with increased actin cytoskeletal flexibility, allowing them to more dynamically respond to mechanical cues (Figure 3.6). This may be particularly relevant in processes in which tissues go through extensive physical remodeling such as embryonic development, angiogenesis and cancer progression where emergence of αvβ3 has been documented.

3.4 Materials and methods

3.4.1 Fluorescence-activated cell sorting (FACS) analysis

For FACS, cells were detached using trypsin/EDTA and integrin surface expression levels were determined using primary antibodies (for human integrin β1, AIIB2, Developmental Studies Hybridoma Bank, Iowa City, IA, USA and for human integrin β3, 23CA, Santa Cruz Biotechnology, Inc., Dallas, TX, USA) and fluorescence-conjugated secondary antibodies (Alexa488-conjugated anti-rat or anti-rabbit, both from Invitrogen/Fisher Scientific, Breda, The Netherlands) and analyzing on a FACSCanto (Becton Dickinson, Breda, The Netherlands).

3.4.2 Cell culture

GD25 and GE11 cell lines expressing either α5β1 or αvβ3 or both integrins have been described previously [11, 12] and were selected for integrin ex-

pression using bulk FACS (Figure S1). Cells were cultured in medium (DMEM; Dulbecco's modified Eagle's Medium, Invitrogen/Fisher Scientific) supplemented with 10% fetal bovine serum (HyClone, Etten-Leur, The Netherlands), 25 U/ml penicillin and 25 µg/ml streptomycin (Invitrogen/Fisher Scientific cat. # 15070-063). For visualization of the actin cytoskeleton, cells were transduced using a lentiviral mCherry-LifeAct cDNA expression vector (provided by Dr. Olivier Pertz, University of Basel, Basel, Switzerland), selected in medium containing 2 µg/ml puromycin (Acros Organics/Fisher Scientific cat. # 227420500), and bulk sorted for mCherry expression using FACS (Figure S1C-F,J). MDA-MB-435s human breast cancer cells were cultured in RPMI medium 1640 (Invitrogen/Fisher Scientific) supplemented with 10% fetal bovine serum, 25 U/ml penicillin and 25 µg/ml streptomycin. NIH3T3 cells were cultured in DMEM supplemented with 10% newborn calf serum, 25 U/ml penicillin and 25 µg/ml streptomycin.

3.4.3 Cyclic cell stretching

An in-house made, piezo-driven, uniaxial stretcher was used to apply cyclic stretch with defined frequency, duration and displacement, on cells adhered to a fibronectin-coated PDMS membrane. Membranes were generated by pipetting well mixed PDMS (Sylgard 184, Dow Corning, Midland, MI, USA) at 1:10 (crosslinker:prepolymer) ratio inside a glass mold passivated with trichloro (1H,1H,2H,2H-perfluorooctyl)silane (Sigma Aldrich, Zwijndrecht, The Netherlands) and incubating for 20 hours at 110°C. This membrane was mounted on the stretcher, coated with 10 µg/mL fibronectin (Sigma Aldrich cat. # F1141) in phosphate buffered saline (PBS) and cells were seeded and incubated overnight in complete medium at 37°C and 5% CO_2 to allow full spreading. The stretcher was then mounted on a spinning-disk confocal microscope (see microscopy), and was kept at 37°C by a stand-alone single loop temperature controller (#3216, InvensysEuroterm, Alphen aan den Rijn, The Netherlands) connected to heaters and a thermo-coupler. LabVIEW (National Instruments, Austin, TX, USA) scripts developed by Wim Pomp (Physics of Life Processes, Kamerlingh Onnes-Huygens Laboratory, Leiden University, Leiden, the Netherlands) and provided by the manufacturer of the controller unit (MCS-3D, SmarAct, Oldenburg, Germany) were used to drive two independent piezo motors (SLC2430s, SmarAct) that allowed uniaxial stretching. Images were collected before

stretch application, after 2 hours of 10%, 1 Hz stretching and after a subsequent 1 hour of 20% 1 Hz stretching.

3.4.4 Characterization of stretcher strain field

The strain field was quantified with help from Donato Civita (Physics of Life Processes, Kamerlingh Onnes-Huygens Laboratory, Leiden University, Leiden, the Netherlands) by stretching a membrane with a microcontact printed hexagonal lattice of fluorescent dots (Alexa647, Invitrogen). Two-dimensional image cross-correlation provided a deformation field over the entire substrate (Figure S2A). Differentiation using the Lagrangian strain tensor yielded the strain on every position on the substrate. The strain was 0.43% in the x-direction and -0.18% in the y-direction for every 0.5% externally applied static strain. These results were homogeneous and reproducible over the entire substrate within a strain measurement error of 0.01%.

For characterizing strain at cyclic stretch conditions, a PDMS membrane with fluorescent beads dried on top was used and the piezo motors were run at 10% or 20% displacement at 0.01Hz and a stack of images was obtained every 2 or 3 seconds, respectively to get the in-focus image and calculate strain. A macroscopic strain of 10% and 20% resulted in 8.0% and 14.5% strain, respectively, on the central area of the membrane along the direction of global strain. The substrate showed 3.5% and 5.0% shrinkage, respectively, in the perpendicular direction (Figures 3.1A, S2A-D). Based on these measurements we calculated that the minimal strain was at 57° and 60°, respectively relative to direction of macroscopic strain.

3.4.5 PAA substrates

PAA gels on 12 mm coverslips were made according to specifications adapted from [22]. Briefly, autoclaved 12 mm coverslips (Thermo Fisher cat. #360302) were cleaned with 0.1 M NaOH, and then rendered hydrophilic by incubating with 0.5% 3-aminopropyltrimethoxysilane (Sigma-Aldrich cat. # 281778). The coverslips were then washed thoroughly with sterile distilled water and incubated in 0.5% glutaraldehyde (Sigma-Aldrich cat. # G6257). Upon removal of the glutaraldehyde, the coverslips were left overnight to dry in a laminar flow cabinet. Coverslips of 10 mm diameter (Thermo Fisher cat. #360301) were rendered hy-

drophobic by incubating with a solution of 10% Hydrocarbon-Soluble Siliconizing Fluid (Surfa Sil; Thermo Fisher, cat. # TS-42800) in chloroform. Surfa Sil-treated coverslips were washed in 100% chloroform and then washed twice with methanol before being left overnight in a laminar flow cabinet to dry. PAA solutions were made with compositions of 7.5% acrylamide (Biorad cat. # 161-0141, Veenendaal, The Netherlands) and varying concentrations (0.01%, 0.03%, 0.05, 0.1%, 0.15%, 0.2%, 0.3% and 0.5%) of bis-acrylamide (Biorad cat. # 161-0200) to a final volume of 1 mL. To this solution 1.5 µL of TEMED (Thermo Fisher cat. # 17-1312-01) and 5 µL of 10% ammonium persulfate were added to start polymerization. 10 µL of this final solution was applied to the middle of each 12 mm coverslip. The 10 mm coverslips were then placed on top of this solution to form a sandwich and left to polymerize for 30 minutes. 50 mM (4-(2-hydroxyethyl)-1-piperazineethanesulfonic acid) HEPES was added and after 15 minutes the top coverslips were removed and the gels were washed once with 50 mM HEPES. PAA gels were activated with an organic crosslinker by removing HEPES and submerging gels in a solution of 0.5 mM sulfosyccinimidyl-6-[4-azido-2-nitrophenylamino]hexanoate (Thermo Fisher, cat. # 22589) and 50 mM HEPES and placing under UV light (Philips HP3114, Eindhoven, The Netherlands). This step was repeated a second time after a wash with 50 mM HEPES. The gels were then washed twice with 50 mM HEPES and incubated overnight at 4°C in 10 µg/mL fibronectin (Sigma Aldrich cat. # F1141) in PBS. After washing with PBS, gels were allowed to equilibrate for one hour in complete culture medium at 37°C before seeding with 25,000 cells/well in complete medium. Cells were allowed to adhere and spread before fixation by incubating for two hours at 37°C and 5% CO_2.

3.4.6 Analysis of stiffness of PAA gels by rheology

Rheology experiments were performed with a stress-controlled rheometer (Physica MCR 501; Anton Paar, Graz, Austria) with assistance from Karin A. Jansen and Gijsje H. Koenderink (Biological Soft Matter Group, FOM Institute AMOLF, Amsterdam, The Netherlands) as previously described [23]. Briefly the PAA gel was polymerized at 21°C between a steel cone and plate (40 mm diameter, 1°) and shear storage modulus was recorded in real time during the polymerization (approximately 1 hour) by applying a small-amplitude oscillatory strain with

amplitude 0.5% and frequency 3.14 rad/s. After polymerization, PBS was added to the measuring chamber and the system was brought to 37°C while monitoring the shear storage modulus. The measured shear loss modulus was more than two orders of magnitude smaller than the storage component, hence was ignored.

3.4.7 PAA and PDMS adhesion assay

GEβ1 and GEβ3 cells were first incubated on ice with blocking antibodies targeting integrin mouse-α5 (cat# MAB1984, Millipore, CA, USA), mouse-αv (cat# 552299 Becton Dickinson, Breda, The Netherlands), human-β1 (AIIB2) and human-β3 (23CA) for 30 minutes and then seeded on PAA gels (stiffness of 12.2 kPa) for 1 hour or on PDMS blocks (1:10 crosslinker:prepolymer ratio) for 30 min at 37°C and 5% CO_2 fixed with formaldehyde and cells on 6-10 different fields of view per condition were counted.

3.4.8 Assays using PDMS micropillars

Micropillars were used for cellular traction force measurements according to methodology described previously [24, 25]. A negative silicon wafer master was made using a two-step Deep Reactive Ion Etching (DRIE) process. Two different etching depths were obtained by subsequently applying two masks to the same wafer. A mask with 10x10 mm arrays with circles of 2 µm diameter and 4 µm center-to-center distance in a hexagonal grid was used as a negative for the micropillar arrays and a mask with two rectangular spacers of 10x2 mm was aligned on the sides of the arrays. The etching depth was varied for the micropillar arrays to make short and long pillars, calculated to have a bending stiffness of 66 nN/µm and 16 nN/µm, respectively using finite element modeling [25]. Using a published elastic model [26], we calculated that these bending stiffnesses corresponded to a Young's modulus in continuous (e.g. PAA) substrates of approximately 47.2 and 11.6 kPa; corresponding to a shear modulus of 15.7 and 3.87 kPa, respectively. The etching depth of the spacers was set to 50 µm, to enable high-resolution microscopy with inverted micropillar arrays (see microscopy).

After passivation of the negative silicon master with trichloro silane (Sigma Aldrich), well-mixed PDMS at 1:10 (crosslinker:prepolymer) ratio was poured over the wafer. After 20 hours at 110°C, the PDMS was

fully cured at a stiffness of 2.5 MPa (as determined by tensile testing). The individual micropillar arrays were peeled off with two spacers on the sides. ECM stamping was performed using a flat piece of PDMS (1:30 ratio, cured 16 hours at 65°C). Per stamp, a 40 µL mix of 50 µg/mL unlabeled fibronectin (Sigma Aldrich) and 10 µg/mL Alexa405 or Alexa647 (both from Invitrogen)-conjugated fibronectin was used. After stamping, the micropillars were blocked with 0.2% Pluronic (F-127, Sigma Aldrich) in PBS for 1 hour at room temperature and washed with PBS.

Cells were seeded either in complete medium, serum-free medium or medium containing blocking antibodies targeting mouse integrin αv subunit and imaging of F-actin and labeled fibronectin was performed after cell spreading. For some analyses, after cell spreading the medium was exchanged for medium containing 0.25 or 0.5 µM Y27632 Rho kinase inhibitor (Tocris cat.#1254, Bristol, UK); 50 µM blebbistatin Myosin-II inhibitor (Calbiochem cat. #203389, Merck KGaA, Darmstadt, Germany); or 0.5 µM Latranculin B F-actin polymerization inhibitor (Calbiochem cat. #428020) and further incubated for 1 hour followed by 4% formaldehyde fixation and immunostaining.

3.4.9 Immunostaining

Cells were fixed in 4% formaldehyde and then permeabilized with 0.1% Triton-X and 0.5% BSA in PBS. Immunostaining was performed for (pY188) Paxillin (Biosource/Invitrogen cat. # 44-722G; Becton Dickinson cat# 610052) followed by secondary antibodies conjugated with Alexa488 (Invitrogen / Fisher Scientific cat# A11008) or Alexa647 (Jackson ImmunoResearch cat# 115-605-006). Rhodamine-Phalloidin (Sigma-Aldrich cat. # 77418-1EA) or Alexa 568-Phalloidin (Fisher Emergo B.V. cat. # A12380, Thermo Fisher) was used to stain F-actin. Hoechst 33258 was used to visualize nuclei.

3.4.10 Microscopy

High-resolution imaging was performed on an in-house constructed setup based on an Axiovert200 microscope body (Zeiss, Sliedrecht, The Netherlands). Confocal imaging was achieved by means of a spinning disk unit (CSU-X1, Yokogawa, Amersfoort, The Netherlands). The confocal image was connected to an emCCD camera (iXon 897, Andor, Belfast, UK). IQ-software (Andor) was used for basic setup-control and data acquisi-

tion. Three laser lines were coupled through a polarization-maintaining single-mode fiber, controlled using an Acousto-Optical Tunable Filter (AA Optoelectronics, Orsay, France): 405 nm (Crystalaser, Reno, NV, USA), 488 nm (Coherent, Santa Clara, CA, USA) and 561 nm (Cobolt, Stockholm, Sweden). Incorporated 50 µm spacers next to the micropillar arrays combined with a 100 µm thick coverslip enabled the use of a high numerical-aperture (1.4) objective with 100X magnification. For live cell imaging and imaging of 3T3 cells; Nikon Eclipse Ti microscope in scanning confocal mode was used together with 20x magnification 0.75NA dry air lens with internal 1.5x magnification and 4.184 scanner zoom to obtain a pixel size of 0.2 µm.

3.4.11 Image analysis

All image analysis was performed using specifically designed Matlab scripts (Mathworks, Natick, MA, USA). For cell area analysis scripts generated by Hans de Bont (Division of Toxicology, Leiden Academic Center for Drug Research, Leiden, the Netherlands) were adapted to apply a rolling ball filter to the image followed by a median filter and subsequently cell detection and image segmentation was performed manually per image to best obtain area per single cell.

For cell-matrix adhesion analysis a cell mask was generated by passing the image of the actin channel through a Gaussian low pass filter. Subsequently, the background intensity was subtracted and the image was run through a sobel and a log-edge detection algorithm followed by image dilation and hole filling each time. The outputs were checked and new masks were generated manually as described above when the mask did not correctly correspond to the cell. Subsequently, for cell-matrix adhesion detection, pY188 Paxillin signal that was assigned to a cell within 20 µm from the cell border was first passed through a Gaussian low pass filter, and signal that was 4 standard deviations larger than the average of the signal was assigned to cell-matrix adhesions. The binary adhesion images were then subjected to a hole-filling algorithm followed by watershed segmentation. The results were manually checked and images showing incorrect adhesion recognition due to low signal-to-noise ratio were excluded from analysis.

For the actin filament analysis, a rolling ball filter was applied to the actin signal inside the cell mask area. Then the signal one standard deviation above the mean was taken as foreground signal. To re-

move noise from the signal, the signal was shrunk, then singular pixels were removed and finally the image was dilated once. From this image, objects smaller than 0.2 µm^2 were removed and then the image was skeletonized followed by connecting diagonals to connect neighboring filaments and then removing all branching points to analyze filaments separately. When analyzing cortical actin, only filaments within 2 µm of the cell border were taken into account. For orientation analysis, all filaments were averaged over all cells and the output was convolved with a unit Gaussian to improve the visualization. This was then corrected for square imaging window by calculating the maximum measurable fiber length in a given angle and weighing this correction per stretch condition by the percentage of a cell of measured average size falling outside of the imaging window if it was circle (Figure S2E).

3.4.12 Pillar deflection analysis

Pillar deflections were determined with approximately 30 nm precision using a specifically designed Matlab script [25]. Briefly, the exact pillar locations were determined from the labeled fibronectin fluorescence image using a fit to the cross-correlation function between a perfect binary circle and the local fluorescence of one pillar. The undeflected hexagonal grid was determined and used as reference to the determined pillar locations. The precision of the forces was pillar bending stiffness dependent, where the high- and low stiffness pillars had a precision of 2 nN and 0.5 nN, respectively.

Cell masks were generated using the same algorithm as cell-matrix adhesion analysis that was then dilated. The pillars under this dilated image that had a deflection larger than 0.06 µm for fixed and integrin blocking assay and larger than 0.2 µm for all other live assays were taken for analysis. Total force was calculated by adding all the absolute deflections and multiplying it by the bending stiffness. The centripetal force percentage was obtained by dividing the radial components of the forces (the forces that point towards the center of the generated cell mask) by the total cellular force.

3.4.13 Statistical analysis

To calculate significance between two conditions, the Mann-Whitney U test was used. To quantify the PAA substrate responses, a cumulative

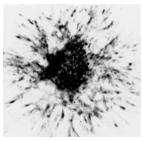

Gaussian distribution was fitted to the data and the half response point (the mean of the distribution) was compared between the conditions using the F-test in the GraphPad Prism 6 program (GraphPad Software, La Jolla, CA, USA).

3.5 Acknowledgements

We thank O. Pertz for providing the mCherry-LifeAct construct; W. Pomp and D. Civita for assistance in setting up cyclic stretcher; K.A. Jansen and G.H. Koenderink for their help in characterizing PAA gels; and H. De Bont for assistance with image analysis. **Funding:** Support for this work came from the Netherlands Organization for Scientific Research (FOM 09MMC03 and 09MMC01). **Author contributions:** H.E.B. performed the experiments. H.E.B., H.v.H., D.M.D., T.S., and E.H.J.D. designed the experiments and analyzed and interpreted data. H.E.B. and E.H.J.D wrote the manuscript. **Competing interests:** The authors declare no competing interests.

3.6 Supplemental figures

Figure S1

Integrin and mCherry-LifeAct expression measurements using FACS. *(A,B) Human integrin β1 and integrin β3 expression levels for GDβ1 (A) and GDβ3 cells (B). (C-F) Human integrin β1, human integrin β3 and mCherry-LifeAct expression levels for either wild type(C,D) or mCherry-LifeAct expressing (E,F) GEβ1 (C,E) and GEβ3 (D,F) cells. (G,H) Human integrin β1 (left) and human integrin β3 (right) expression levels in GEβ1 (blue), GEβ3 (red) (G) or GDβ1 (blue) and GDβ3 (red) (H) compared to expression of these integrins in the human breast cancer cell line MDA-MB-435s (green). (I,J) Quantification of percentage of cells that are integrin positive, i.e. falls in P2 gate indicated at A-F (I), or positive for mCherry-LifeAct expression, i.e. falls in P3 gate indicated at C-F (J). Mean and standard deviation are shown of three independent experiments for I and J.*

Figure S2

Strain field of cyclic stretcher, characterization of PAA gels with bulk rheology and integrin-mediated cell adhesion to PAA and PDMS substrates. *(A) Magnified homogeneous displacement field under static strain over the entire substrate of 8x10 mm (height x width). Global strain is applied over the x-axis and the net strain from differentiation over this field is homogeneous. (B) Positions of fluorescent beads at the minimal and maximal strain during 10% (top) or 20% (bottom) cyclic stretch measured manually and calculated strain (calculations of only point 0 reference is shown, mean and deviation are obtained by taking all points as reference one by one). (C) Representation of how the length "r" and orientation angle "A" of a filament would change under a horizontal and vertical strain of εx and εy, respectively to a length of r' and an angle of A'. (D) Analytical calculation of minimal strain direction, finding A where r'(A')=r(A), for measured strain values (B). (E) Correction factor for square imaging window where A is the angle, C is the cell size (obtained from Figure 1D) and L is the imaging window length (69 µm for this experiment). The cosine/sine term in the denominator is due to the variation in maximum measurable fiber length in a given angle and the nominator is the portion of a cell of measured size falling outside of the imaging window if the imaging window was a circle with diameter L. (F) Shear storage modulus of a PAA gel of 7.5% acrylamide and 0.2% bis-acrylamide during polymerization and its temperature dependence. (G) The final shear elastic modulus measured at 37°C for PAA gels with varying bis-acrylamide concentration. Each bar represents a separate experiment performed on different days and using two different rheometers. (H,I) Adhesion to 1:10 (crosslinker:prepolymer) ratio PDMS (H) and 12.2 kPa PAA (I) of GEβ1 and GEβ3 cells preincubated with- and seeded in the absence or presence of integrin blocking antibodies targeting mouse-αv, mouse-α5, human-β1 or human-β3.*

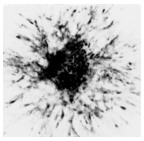

Figure S3

Average cell-matrix adhesion area remains constant with increasing stiffness. *(A) Cumulative Gaussian distribution and Gaussian distribution functions used to obtain the fit parameters for cell spreading and cell matrix adhesion formation. (B) The fit parameters obtained by fitting cumulative Gaussian distribution model and the p values obtained by comparing the indicated fit parameters between β1 and β3 expressing cells using the F-test. (C-F) Slopes of the fits shown in figures 2A,B and 3A,B describing stiffness-dependent induction of cell spreading (C,D) and peripheral cell matrix adhesion formation (E,F) as a function of substrate rigidity at the stiffness range tested. (G,H) Quantification of average size of peripheral cell-matrix adhesions of GEβ1 and GEβ3 cells (G) or GDβ1 and GDβ3 (H) for cells with at least 10 adhesions. In all graphs, mean ±95% clearance level is shown and at least 20 cells were measured over 3 different experiments (except for 760 Pa for GEβ1 and GEβ3 cells where results of one experimental replica is shown). P values were calculated by comparing the slope of the linear fits with F-test. (I,J) Representative images of Paxillin staining for GDβ1 (I) and GDβ3 cells (J). Upper row shows raw immunofluorescence staining, middle row shows zoomed in region of the boxed area, and bottom row shows adhesions detected by the automated analysis algorithm. Scale bar is 20 µm (5 µm for zooms).*

Figure S4

Increased cellular traction force in response to substrate stiffening is maintained in post-fixation samples and antibody blocking confirms role for αv integrins in force exertion by GEβ3 but not by GEβ1 cells. *(A,B) Bar plots of cellular spread area (A) and force per pillar (B) measured in fixed GEβ1, GEβ3, GDβ1, GDβ3 and NIH-3T3 cells on 6.9 and 4.1 µm pillars. In A,B mean ±95% clearance level is shown and at least 15 cells were measured from three independent experiments. (C) Representative images from A,B. (D,E) Bar plots of cellular spread area (D) and force per pillar (E) analyzed by live cell imaging of mCherry-LifeAct-expressing GEβ1 and GEβ3 cells seeded on 4.1 µm pillars for 5 hours in the presence or absence of blocking antibody against mouse integrin αv. In D,E mean ±95% clearance level is shown and at least 50 cells were measured from a single experiment. NS, $p>0.05$; **, $p<0.005$; ***, $p<0.0005$ compared to control according to Mann-Whitney test. (F) Representative images of D,E. White arrows indicate magnitude and direction of forces measured. Scale bar, 20 nN/10 µm.*

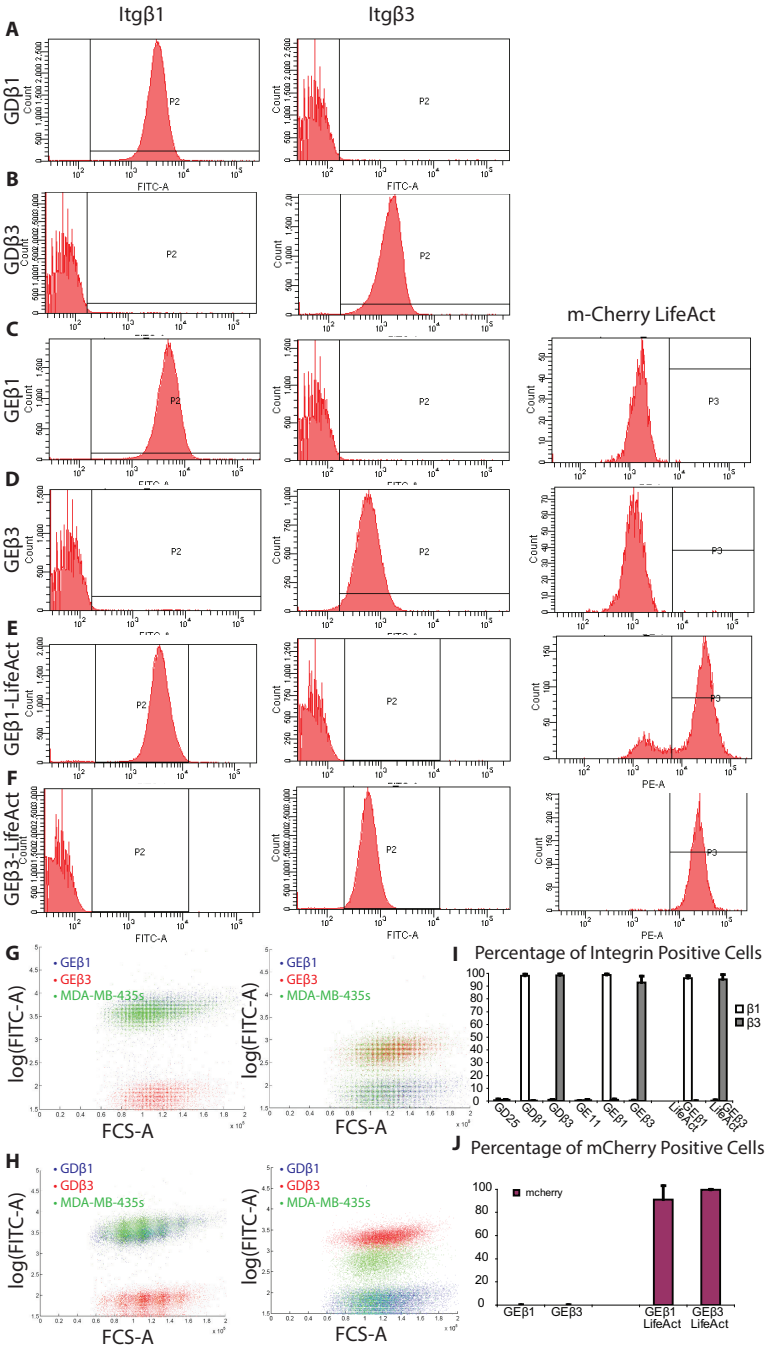

Figure S1
Integrin and mCherry-LifeAct expression measurements using FACS.

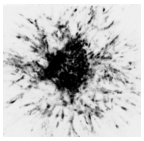

A

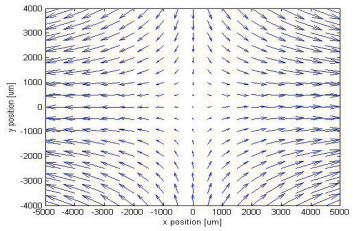

B

10% stretch	absolute positions before stretch x	y	after stretch x	y	reference from point 0 before stretch dx	dy	after stretch dx	dy	strain when dx(or dy)>100 dcx	dcy
point 0	208	372	183	382	0	0	0	0		
point 1	131	439	100	445	-77	67	-83	63		
point 2	392	285	380	298	184	-87	197	-84	1.0707	
point 3	163	144	133	160	-45	-228	-50	-222		0.9737
point 4	431	437	424	445	223	65	241	63	1.0807	
point 5	494	332	491	342	286	-40	308	-40	1.0769	
point 6	185	99	159	119	-23	-273	-24	-263		0.9634
point 7	313	86	299	105	105	-286	116	-277	1.1048	0.9685
point 8	174	31	146	52	-34	-341	-37	-330		0.9677
point 9	400	67	390	87	192	-305	207	-295	1.0781	0.9672
point 10	66	215	31	230	-142	-157	-152	-152	1.0704	0.9682
point 11	415	494	409	499	207	122	226	117	1.0918	0.959
								mean	**1.0806**	**0.9654**
								std	**0.0105**	**0.0053**

20% stretch	absolute positions before stretch x	y	after stretch x	y	reference from point 0 before stretch dx	dy	after stretch dx	dy	strain when dx(or dy)>100 dcx	dcy
point 0	401	64	316	190	0	0	0	0		
point 1	214	123	102	246	-187	59	-214	56	1.1444	
point 2	265	314	158	424	-136	250	-158	234	1.1618	0.936
point 3	400	365	314	475	-1	301	-2	285		0.9468
point 4	232	246	127	363	-169	182	-189	173	1.1183	0.9505
point 5	163	259	43	374	-238	195	-273	184	1.1471	0.9436
point 6	465	345	385	453	64	281	69	263		0.9359
point 7	242	18	133	144	-159	-46	-183	-46	1.1509	
point 8	317	314	217	427	-84	250	-99	237		0.948
point 9	315	202	218	321	-86	138	-98	131		0.9493
point 10	495	312	429	428	94	248	113	238		0.9597
point 11	370	156	280	275	-31	92	-36	85		
								mean	**1.1445**	**0.9499**
								std	**0.022**	**0.0129**

C

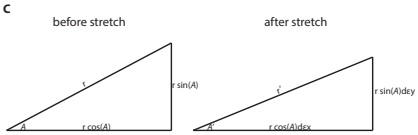

D

$$r' = \sqrt{(r\cos(A)\mathrm{d}ex)^2 + (r\sin(A)dey)^2} = r^2\sqrt{\cos^2(A)dex^2 + \sin^2(A)dey^2}$$

For minimal strain $\frac{r'}{r} = 1$ hence $\sqrt{\cos^2(A)dex^2 + \sin^2(A)dey^2} = 1$

For 10% stretch we measured $dex = 1.08 \pm 0.01$ and $dey = 0.965 \pm 0.005$

$$\sqrt{\cos^2(A)(1.08)^2 + \sin^2(A)(0.965)^2} = 1$$
$$1.166\cos^2(A) + 0.931\sin^2(A) = 1$$
$$0.166\cos^2(A) - 0.069\sin^2(A) = 0 \quad \Rightarrow \quad \tan^2(A) = 2.406$$
$$A = 57.2^0$$

And for 20% stretch we measured $dx = 1.14 \pm 0.02$ and $dy = 0.95 \pm 0.01$

$$\sqrt{\cos^2(A)(1.14)^2 + \sin^2(A)(0.95)^2} = 1$$
$$1.300\cos^2(A) + 0.903\sin^2(A) = 1$$
$$0.300\cos^2(A) - 0.097\sin^2(A) = 0 \quad \Rightarrow \quad \tan^2(A) = 3.093$$
$$A = 60.4^0$$

E

$$f(A,C) = \frac{\left(1 + \frac{2}{L}\sqrt{\frac{C}{\pi}}\right)^2 - 1}{\cos(A)} + 1 \quad for\ A < 45^\circ\ and \quad f(A,C) = \frac{\left(1 + \frac{2}{L}\sqrt{\frac{C}{\pi}}\right)^2 - 1}{\sin(A)} + 1 \quad for\ A > 45^\circ$$

F

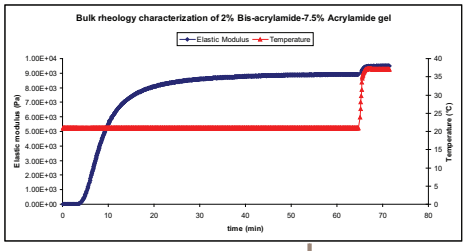

H

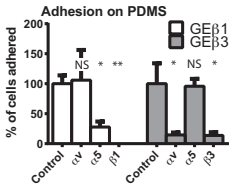

G

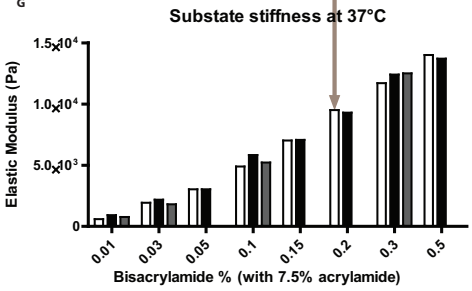

I

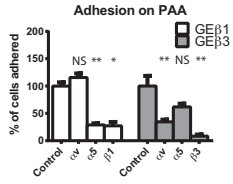

Figure S2

Strain field of cyclic stretcher, characterization of PAA gels with bulk rheology and integrin-mediated cell adhesion to PAA and PDMS substrates.

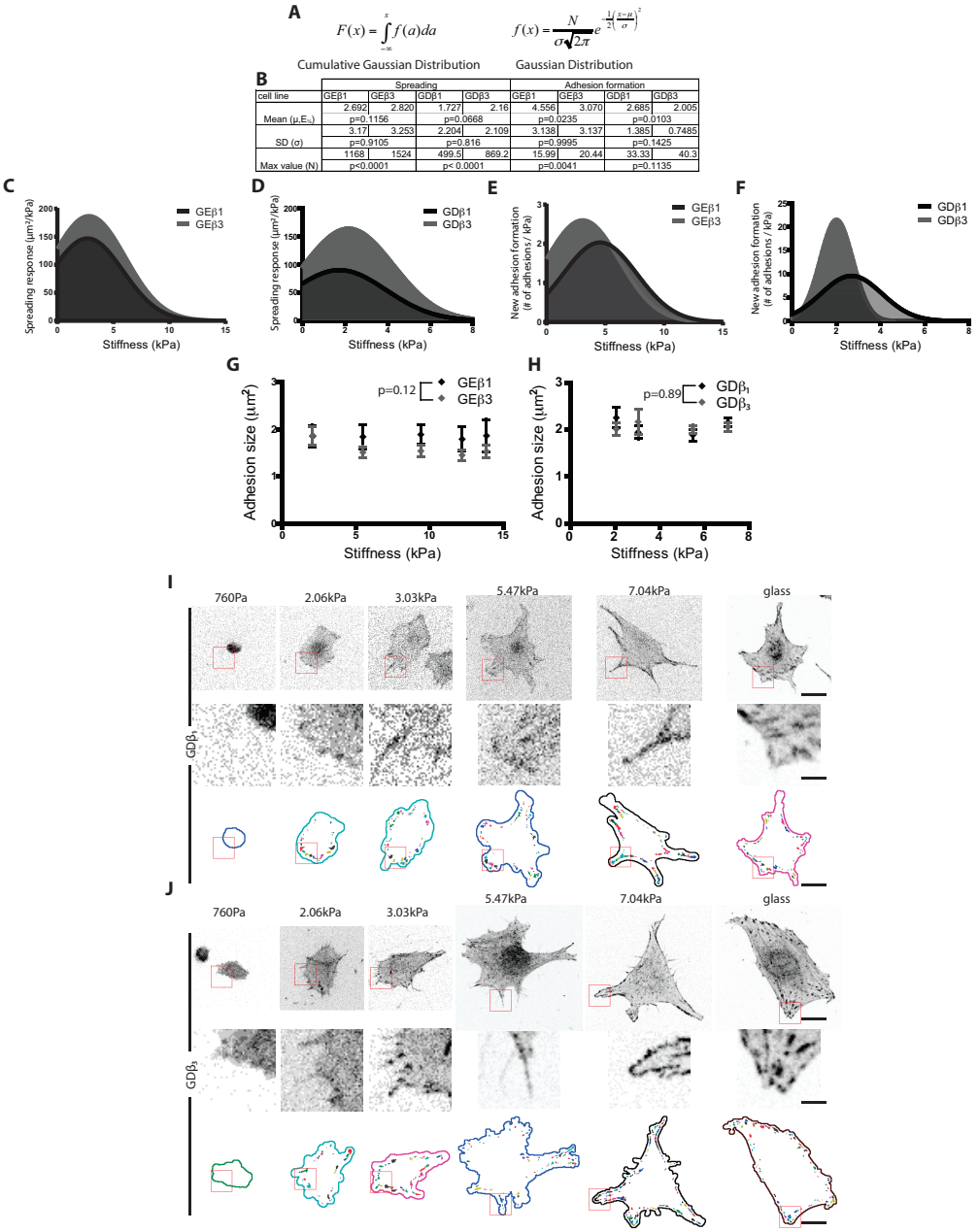

	Spreading				Adhesion formation			
cell line	GEβ1	GEβ3	GDβ1	GDβ3	GEβ1	GEβ3	GDβ1	GDβ3
Mean (μE_{50})	2.692	2.820	1.727	2.16	4.556	3.070	2.685	2.005
	p=0.1156		p=0.0668		p=0.0235		p=0.0103	
SD (σ)	3.17	3.253	2.204	2.109	3.138	3.137	1.385	0.7485
	p=0.9105		p=0.816		p=0.9995		p=0.1425	
Max value (N)	1168	1524	499.5	869.2	15.99	20.44	33.33	40.3
	p<0.0001		p< 0.0001		p=0.0041		p=0.1135	

Figure S3

Average cell-matrix adhesion area remains constant with increasing stiffness.

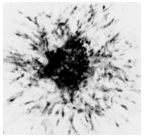

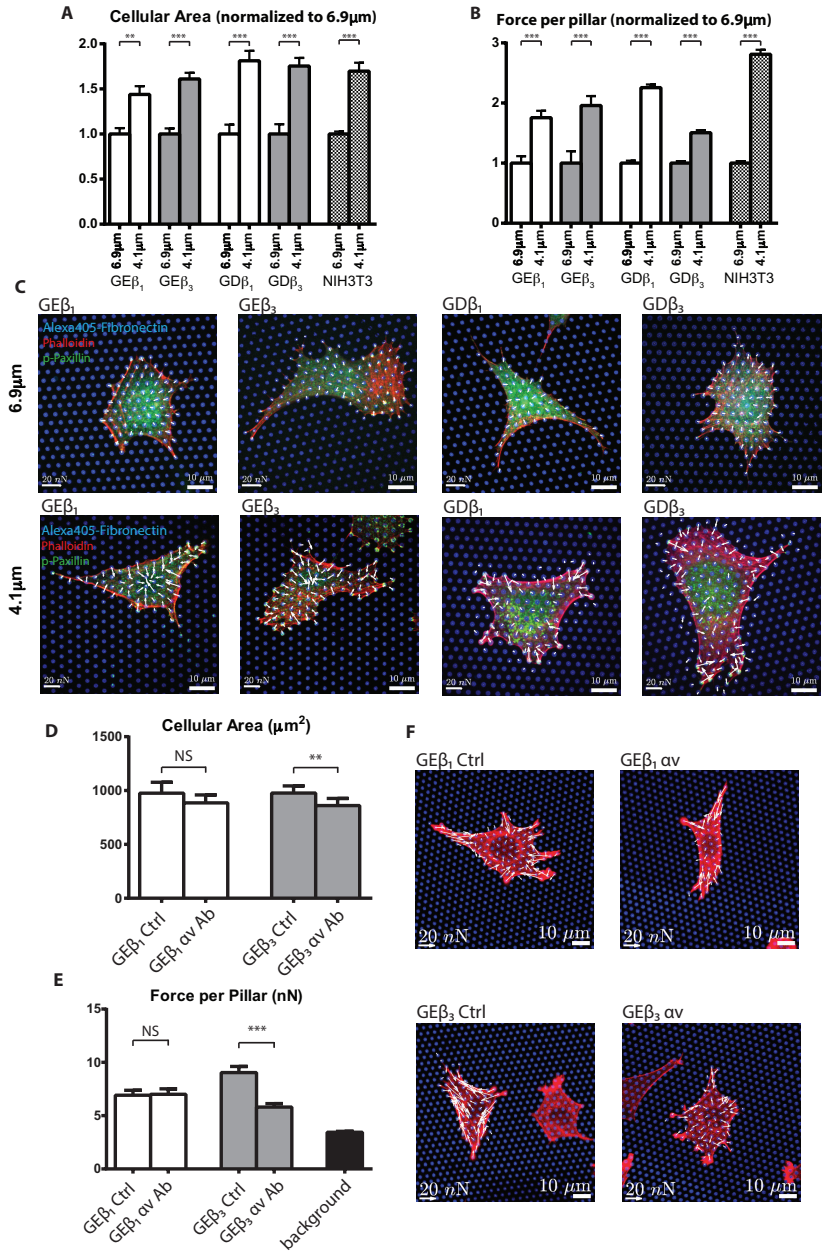

Figure S4

Increased cellular traction force in response to substrate stiffening is maintained in post-fixation samples and antibody blocking confirms role for αv integrins in force exertion by GEβ3 but not by GEβ1 cells.

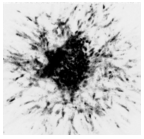

Bibliography

[1] Brenton D Hoffman, Carsten Grashoff, and Martin A Schwartz. "Dynamic molecular processes mediate cellular mechanotransduction". In: *Nature* 475.7356 (2011).

[2] Herbert B Schiller and Reinhard Fässler. "Mechanosensitivity and compositional dynamics of cell-matrix adhesions". In: *EMBO Reports* 14.6 (2013).

[3] Richard O Hynes. "Integrins: Bidirectional, allosteric signaling machines". In: *Cell* 110.6 (2002).

[4] Daniel Choquet, Dan P Felsenfeld, and Michael P Sheetz. "Extracellular matrix rigidity causes strengthening of integrin-cytoskeleton linkages". In: *Cell* 88.1 (1997).

[5] Julie C Friedland, Mark H Lee, and David Boettiger. "Mechanically Activated Integrin Switch Controls alpha(5)beta(1) Function". In: *Science (New York, N.Y.)* 323.5914 (2009).

[6] Christophe Guilluy et al. "The Rho GEFs LARG and GEF-H1 regulate the mechanical response to force on integrins". In: *Nature Cell Biology* 13.6 (2011).

[7] Pere Roca-Cusachs, Thomas Iskratsch, and Michael P. Sheetz. "Finding the weakest link - exploring integrin-mediated mechanical molecular pathways". In: *Journal of Cell Science* 125.13 (2012).

[8] Daniel Bouvard et al. "Integrin inactivators: balancing cellular functions in vitro and in vivo". In: *Nature Reviews Molecular Cell Biology* 14.7 (2013).

[9] Haguy Wolfenson, Irena Lavelin, and Benjamin Geiger. "Dynamic Regulation of the Structure and Functions of Integrin Adhesions". In: *Developmental Cell* 24.5 (2013).

[10] Jay S Desgrosellier and David A Cheresh. "Integrins in cancer: biological implications and therapeutic opportunities". In: *Nature Reviews Cancer* 10.1 (2010).

[11] Erik HJ Danen et al. "The fibronectin-binding integrins alpha5beta1 and alphavbeta3 differentially modulate RhoA-GTP loading, organization of cell matrix adhesions, and fibronectin fibrillogenesis". In: *Journal of Cell Biology* 159.6 (2002).

[12] Erik HJ Danen et al. "Integrins control motile strategy through a Rho-cofilin pathway". In: *Journal of Cell Biology* 169.3 (2005).

[13] Hui Miao et al. "Differential regulation of Rho GTPases by beta 1 and beta 3 integrins: the role of an extracellular domain of integrin in intracellular signaling". In: *Journal of Cell Science* 115.10 (2002).

[14] Dominic P White, Patrick T Caswell, and Jim C Norman. "alpha-v beta-3 and alpha-5 beta-1 integrin recycling pathways dictate downstream Rho kinase signaling to regulate persistent cell migration". In: *Journal of Cell Biology* 177.3 (2007).

[15] Stephan Huveneers et al. "Binding of soluble fibronectin to integrin alpha 5 beta 1 - link to focal adhesion redistribution and contractile shape". In: *Journal of Cell Science* 121.15 (2008).

[16] Pere Roca-Cusachs et al. "Clustering of alpha(5)beta(1) integrins determines adhesion strength whereas alpha(v)beta(3) and talin enable mechanotransduction". In: *Proceedings of the National Academy of Sciences of the United States of America* 106.38 (2009).

[17] Herbert B Schiller et al. "beta(1)- and alpha(v)-class integrins cooperate to regulate myosin II during rigidity sensing of fibronectin-based microenvironments". In: *Nature Cell Biology* 15.6 (2013).

[18] Douglas Woods et al. "Induction of beta 3-integrin gene expression by sustained activation of the Ras-regulated Raf-MEK-extracellular signal-regulated kinase signaling pathway". In: *Molecular and Cellular Biology* 21.9 (2001).

[19] Gordon B Mills and Wouter H Moolenaar. "The emerging role of lysophosphatidic acid in cancer". In: *Nature Reviews Cancer* 3.8 (2003).

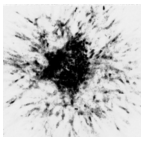

[20] Akira Katsumi et al. "Integrin activation and matrix binding mediate cellular responses to mechanical stretch". In: *Journal of Biological Chemistry* 280.17 (2005).

[21] Grace L Lin et al. "Activation of beta 1 but not beta 3 integrin increases cell traction forces". In: *FEBS Letters* 587.6 (2013).

[22] Tony Yeung et al. "Effects of substrate stiffness on cell morphology, cytoskeletal structure, and adhesion". In: *Cell Motility and the Cytoskeleton* 60.1 (2005).

[23] Karin A Jansen et al. "Cells Actively Stiffen Fibrin Networks by Generating Contractile Stress". In: *Biophysical Journal* 105.10 (2013).

[24] Lea Trichet et al. "Evidence of a large-scale mechanosensing mechanism for cellular adaptation to substrate stiffness". In: *Proceedings of the National Academy of Sciences of the United States of America* 109.18 (2012).

[25] Hedde van Hoorn et al. "The Nanoscale Architecture of Force-Bearing Focal Adhesions". In: *Nano Letters* 14.8 (2014).

[26] Marion Ghibaudo et al. "Traction forces and rigidity sensing regulate cell functions". In: *Soft Matter* 4.9 (2008).

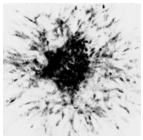

Chapter 4

Substrate rigidity modulates the association between traction forces and molecular composition of cell-matrix adhesions [1]

[1] This chapter is based on: Hayri E Balcıoğlu*, Rolf Harkes*, Thomas Schmidt#, Erik HJ Danen#, Substrate rigidity modulates the association between traction forces and molecular composition of cell matrix adhesions *In Preparation; *:These authors contributed equally to this work. #Shared corresponding authors.*

Abstract

In cell matrix adhesions, integrin receptors and associated proteins provide a dynamic coupling of the extracellular matrix (ECM) to the cytoskeleton. This allows bidirectional transmission of forces between the ECM and the cytoskeleton, which tunes intracellular signaling cascades that control survival, proliferation, differentiation, and motility. The quantitative relationships between recruitment of distinct cell matrix adhesion proteins and local cellular traction forces are not known. Here, we applied dSTORM to cell matrix adhesions formed on fibronectin-stamped PDMS pillars and developed a mathematical approach to relate the number of talin, vinculin, paxillin, and focal adhesion kinase (FAK) molecules to local cellular traction force. We find that FAK recruitment does not show an association with traction force application whereas a ∼60 pN force increase is associated with the recruitment of one talin, two vinculin, and two paxillin molecules on a substrate with an effective stiffness of 47 kPa. On a substrate with a four-fold lower stiffness the stoichiometry of talin:vinculin:paxillin changes from 1:2:2 to 2:12:6 for the same ∼60 pN traction force. The marked relative change in force-related vinculin recruitment indicates a stiffness-dependent switch in vinculin function in cell matrix adhesions. Taken together, application of a novel mathematical approach to super resolution microscopy data reveals substrate stiffness-dependent modulation of the relation between traction force and molecular composition of cell matrix adhesions.

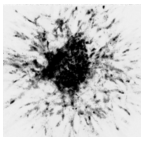

4.1 Introduction

Cell matrix adhesions couple the intracellular cytoskeletal network to the extracellular matrix (ECM) and are key sites for bidirectional mechanotransduction. First, they are the sites where cells apply myosin-driven contractile forces to their environment, for instance during cell migration or tissue remodeling [1]. Second, they allow cells to sense and respond to changes in stiffness of their environment, which is an important mechanical cue regulating stem cell differentiation, cancer progression, and other processes [2, 3].

Cell matrix adhesions contain integrin transmembrane receptors that bind ECM components with their globular head domains, and connect to a large complex of associated proteins with their intracellular tail domains. Integrins and integrin-associated proteins in cell matrix adhesions have been demonstrated to change conformation and/or expose new protein-binding sites when stretched by force [4]. Several of the associated proteins, including talin and vinculin connect the integrin cytoplasmic tails to the F-actin network [5]. Others, such as paxillin and focal adhesion kinase (FAK) are involved in local signaling platforms that regulate actin cytoskeletal dynamics for instance through Rho GTPases [6]. This allows cell matrix adhesions to adjust their molecular architecture in response to force, thereby ensuring a balance between extracellular (ECM) and intracellular (cytoskeletal) forces.

Cell matrix adhesions are highly dynamic structures [7]. Super resolution microscopy techniques have been applied to reveal the 3D multimolecular architecture of cell matrix adhesions [8, 9]. It is well known that larger cell matrix adhesions support higher forces [10–12] but quantitative relationships between recruitment of individual cell matrix adhesion proteins and local traction force application have not been reported. Here, we developed a novel mathematical method for the analysis of antibody-mediated direct stochastic optical reconstruction microscopy (dSTORM) [13] images. For transformation of dSTORM data into molecular counts, we made use of a real space approach, which has similarities to the Fourier ring-correction analysis method [14] and relies on high positional accuracy characteristic of super-resolution imaging. We applied this method to four distinct cell matrix adhesion components, talin, vinculin, paxillin, and FAK, and combined dSTORM with traction force microscopy to determine quantitative relationships between their recruitment to cell matrix adhesions and local traction forces.

For cells plated on a substrate with an effective Young's modulus of 47.2 kPa, we determine that each additional talin, vinculin, and paxillin molecule is accompanied by a 66, 30, and 32 pN increase in traction force, respectively. On an 11.6 kPa substrate the stoichiometry for talin:vinculin:paxillin changes from ∼1:2:2 per ∼60 nN force increment to ∼2:12:6 for the same amount of traction force. Instead, FAK recruitment does not significantly correlate with traction force increases, irrespective of substrate rigidity. These findings provide a first quantitative relationship between recruitment of distinct cell matrix adhesion proteins and local traction forces and reveals remarkable regulation of this relationship by substrate stiffness.

4.2 Results

4.2.1 dSTORM on cell matrix adhesion proteins

We used vinculin knockout MEFs transiently expressing GFP-vinculin to compare signals derived from an Alexa-532-conjugated GFP nanobody to those from a vinculin monoclonal antibody and an Alexa-647-conjugated secondary antibody. Confocal microscopy confirmed that Alexa-532 and Alexa-647 signals co-localized only in GFP positive cell matrix adhesions as expected (Figure 4.1A, top, red arrows; i,ii). As a control, cell matrix adhesions in vinculin null MEFs lacking GFP-vinculin were readily identified using a paxillin antibody (Figure 4.1A, bottom, green arrows; iii) while such adhesions did not stain when the vinculin antibody was used (Figure 4.1A, top).

Next, stainings of Alexa-532-conjugated GFP nanobody and vinculin monoclonal antibody followed by Alexa-647-conjugated secondary antibody in vinculin null/GFP-vinculin cells were processed for dSTORM. dSTORM images showed overlap between Alexa-532 and Alexa-647 localizations (Figure 4.1B). Indeed localizations obtained from the two different fluorophores across 105 adhesions in 11 different cells as determined by dSTORM showed a strong linear dependence (Figure 4.1C).

4.2.2 Combination of dSTORM and cellular traction force measurements

Talin staining followed by confocal imaging identified cell matrix adhesions coupled to fibronectin-stamped µpillars (Figure S1A). The average

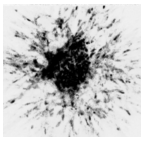

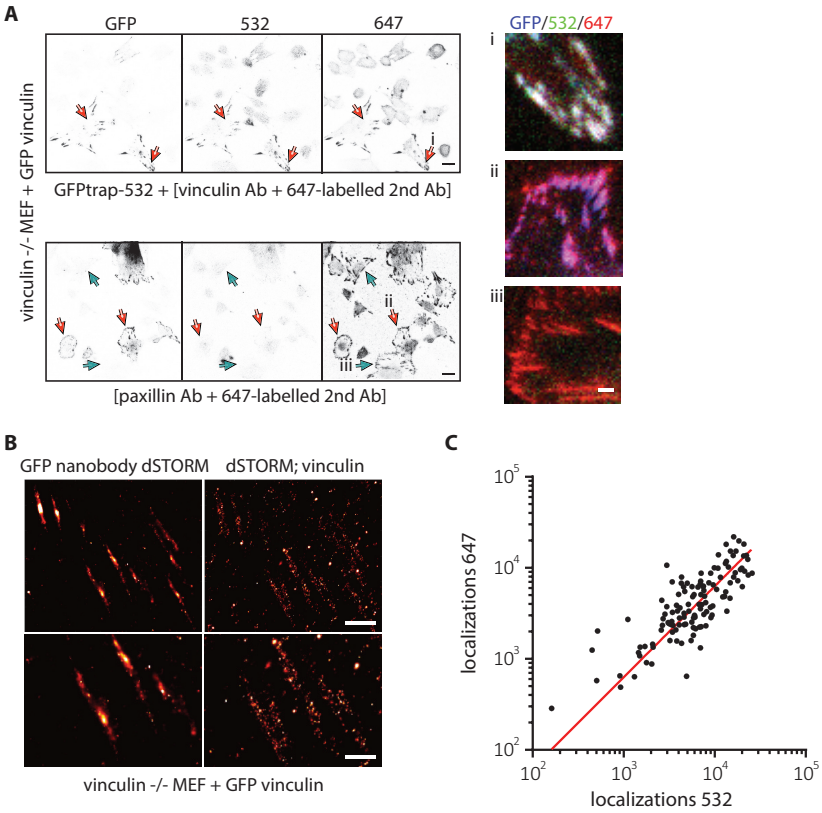

Figure 4.1

dSTORM on cell matrix adhesions. *A, confocal images of vinculin -/- MEFs transiently expressing GFP vinculin, immunostained with the indicated antibodies. Red arrows indicate cells that are GFP (and vinculin) positive, green arrows indicate cells that are GFP (and vinculin) negative. In i, ii and iii merged images for zoom-ins of the indicated adhesions are shown. B, representative dSTORM images of cells immunostained with GFP nanobody conjugated with Alexa 532 obtained with 532 nm laser (left) and [vinculin antibody plus secondary antibody conjugated with Alexa 647] obtained with 647 nm laser (right). C, comparison of number of localizations obtained from individual adhesions by applying dSTORM to first Alexa647 and then to Alexa532. Red line indicates the linear fit (R^2=0.47). Scale bars are 20 µm (A, left panels), 3 µm (A, right panels i-iii), 100 nm (B, top) and 50 nm (B, bottom).*

background deflection, corresponding to the displacement resolution, was 47±23 nm as determined by epi-fluorescence imaging in a cell free region in the field of view of dSTORM imaging (Figure S1B,C). For µpillar arrays with effective Young's moduli of 11.6 kPa or 47.2 kPa (spring constants of 16 nN/µm or 66 nN/µm, respectively), the displacement resolution of ∼50 nm corresponded to a force precision of 0.8 nN and 3 nN, respectively. Combining epi-fluorescence (displacements) and dSTORM, provided visualization of traction force and localizations in cell matrix adhesions (Figure 4.2A).

We established that forces measured in samples fixed for dSTORM application were slightly lower than forces measured by live confocal imaging of pillar deflections in mcherry-lifeact-labelled NIH3T3 cells (Figure 4.2B,C). Nevertheless, the increase in force, induced by seeding cells on a substrate with higher effective Young's modulus as measured post-fixation completely recapitulated the increase measured in live cells, as established previously for fixation for standard immunofluorescence [15]. In accordance with the results obtained by confocal imaging, forces determined by epi-fluorescence microscopy in combination with dSTORM imaging of NIH3T3 cells immunostained for talin showed a ∼3-fold increase for cells seeded on 47.2 kPa as compared to forces applied by cells seeded on 11.6 kPa (Figure 4.2B-D).

4.2.3 From dSTORM localizations to molecule counts

Following dSTORM on µpillar arrays, 2D Gaussian intensity profiles were obtained with an average of 521±404 photons, providing a localization precision of 14±5 nm (Figure 4.3A,B). To estimate the number of talin molecules in an adhesion coupled to one pillar (Figure 4.2B, red box; Figure 4.3C,D), we developed a method that uses the inherent high localization precision in super-resolution microscopy. We based our methodology on analysis of the inter-localization distance distribution in the images, which in turn was used to distinguish between spatially correlated and uncorrelated localizations. This method makes use of the fact that statistics associated with fluorescence labeling and photophysics, although partly unknown, are equivalent for the spatially correlated and uncorrelated localizations.

First, we determined statistics for the cumulative distribution function (cdf) of inter-localization distances within the adhesion shown in Figure 4.3D. For each distance "r" between 2 localizations, the number

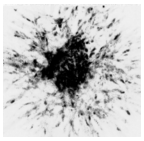

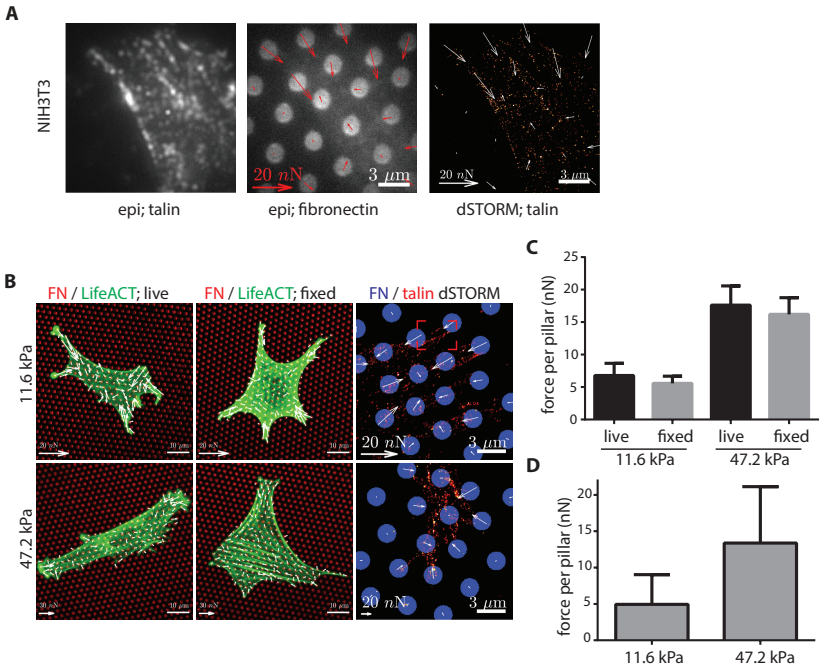

Figure 4.2

Combination of dSTORM with micropillars. *A, NIH3T3 cell imaged with the dSTORM setup using epi-fluorescence with 647 (left) and 405 (middle) or dSTORM with 647 channel (right) together with accompanying force measurements (arrows in middle and right image). B, images of live (left) and fixed (middle and right) NIH3T3 cells on pillars of effective Young's modulus of 11.6 kPa (top) or 47.2 kPa (bottom) stamped with fibronectin conjugated to Alexa647 (left and middle) or to Alexa405 (right). mCherry-LifeACT (left and middle) or talin immunostaining (secondary antibody conjugated with Alexa647) was imaged using confocal imaging (left and middle) or dSTORM setup (right) with calculated forces (arrows). C,D, bar graphs showing mean ± standard deviation of cellular forces applied per pillar calculated from confocal images (C) or images obtained with dSTORM setup (D) for cells on pillars with indicated stiffnesses. Scale bars are 3 µm (A, B-right), 10 µm (B, left and middle); deflection arrow scales are 20 nN (A, B, top-right and bottom) and 30 nN (B, top-left and top-middle).*

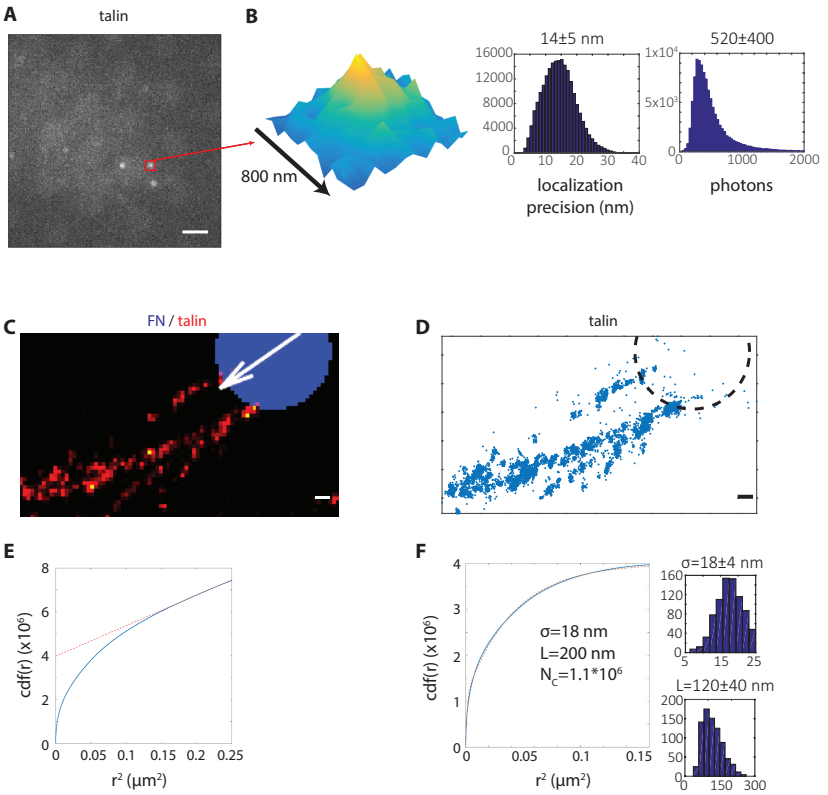

Figure 4.3

Distribution analysis of talin dSTORM localizations in a single adhesion. *A, example image frame from dSTORM acquisition with several Alexa647 molecules fluorescing. B, zoom in of the red square in A (left) and histograms showing the positional accuracy of localizations from this dSTORM acquisition (left) and for the intensity of localizations (right). C, zoom in of the red square from Figure 4.2B. D, image derived from C showing 6700 localizations of Alexa647 targeted to talin associated with one pillar (dashed circle). E, cumulative distance function (cdf) of interlocalization distances from the localizations in D with a linear line fit (red dashed line) from 0.16 µm² to 0.25 µm². F, cdf from E, with linear fit subtracted and accompanying double exponential fit* $cdf(r) = N_c(1-e^{-r^2/4\sigma^2})+N_L(1-e^{-r^2/L^2})$ *with* σ*=18 nm, L=200 nm,* N_c*=1.10x10⁶ and* N_L*=2.9x10⁶. Histograms of fit parameters* σ *(right-top) and L (right-bottom) obtained across all experiments are shown. Scale bars are 2 µm (A) and 250 nm (C, D).*

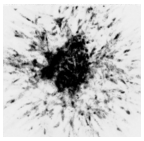

of distances smaller than r as a function of r^2 was obtained. For a spatial random distribution this function would exhibit linear dependence on r^2 since the distances are uncorrelated. However, the relationship between the cdf of inter-localization distances and r^2 showed a two-regime function. A linear regime was observed for high values of r^2, reflecting localizations belonging to different talin molecules (Figure 4.3E). When this linear relationship was subtracted from the distribution, a non-linear regime remained for lower r^2 values (Figure 4.3F). This reflected correlated detections belonging to a single talin molecule or a cluster of talin molecules. A good fit to this non-linear regime was obtained with a double exponential:

$$cdf(r)=N_c\ (1-e^{-r^2/4\sigma^2})\ +N_L\ (1-e^{-r^2/L^2})\ .$$

Here r denotes the distance between fluorophores, σ denotes the distribution of detections from a single talin molecule and N_c is the corresponding number of correlated distances. In the second part of the exponential, L is the structure parameter, and N_L is the contribution of spatial structures in the data, i.e. talin molecules in close proximity. The structural length scale, L (120±40 nm), was significantly larger than the positional accuracy, σ(18±4 nm), indicating the two components of the exponential fit to be well separable. From these fits the number of talin molecules in the adhesion (Figure 4.3D) was calculated with the equation $N_m=N^2/(N+N_c)$ (See Materials and methods); where N_m denotes the number of talin molecules and N is the number of detections. Simulations indicated good agreement between the estimated number of molecules and the input: the accuracy was >10% even at high overlap conditions (Figure S1D-F). Using this method, 40 talin molecules were detected in the adhesion shown (Figure 4.3C,D).

4.2.4 Relating the abundance of cell matrix adhesion proteins to traction forces

Next, we generated dSTORM-based localization maps for four different cell matrix adhesion proteins in cells seeded on pillars of two different effective Young's moduli. Cell matrix adhesion areas were selected and corresponding talin, vinculin, paxillin, and FAK molecules were calculated (see Figure S2 for histograms for all measurements and calculations). In order to relate force application to abundance of adhesion molecules, we examined the cross correlation between the determined number of molecules in an adhesion and the measured local traction force. We

then approximated the force induced by recruitment of a single molecule assuming a linear relationship. In >100 cell matrix adhesions from 30 NIH3T3 cells analyzed in 3 independent experiments on µpillars with an effective Young's modulus of 47.2 kPa, the force corresponding to the adhesion showed a strong correlation to the number of talin molecules in the adhesion (Figure 4.4A, Figure S3). This was accompanied by an increase in cell matrix adhesion area (Figure S3). Highly similar talin-force relations were identified across the different experiments. Likewise, experiments performed on µpillar arrays with lower effective Young's modulus (11.6 kPa) provided linear talin-force relations that were similar across different experiments but here, forces applied by the adhesion per talin molecule were generally lower (Figure 4.4B,C, Figure S3).

As was done for talin, dSTORM was used to relate the abundance of vinculin, paxillin, and FAK to force applied by a cell matrix adhesion. Similar to talin, the number of vinculin and paxillin molecules in a cell matrix adhesion positively correlated with force application on both 47.2 kPa and 11.6 kPa substrates (Figure S3). By contrast, the number of FAK molecules in an adhesion and force application were uncorrelated on both of the substrates (Figure S3). Using a linear fit, quantitative relations were determined between the number of talin, vinculin, and paxillin molecules in a cell matrix adhesion and the traction force applied by that adhesion. On a substrate with an effective Young's modulus of 47.2 kPa, for each additional talin molecule an increase in the traction force of 66 pN was determined (Figure 4.4C). Vinculin and paxillin molecules were associated with ∼50% of this force: for each additional vinculin and paxillin molecule, an increase in force of 30 pN and 32 pN was determined, respectively (Figure 4.4C). On a substrate with an effective Young's modulus of 11.6 kPa, force increments were less steep and a particularly strong decrease in force associated with vinculin was observed: 27 pN/talin, 4.9 pN/vinculin, and 10 pN/paxillin (Figure 4.4C).

Together these findings indicate that i) talin, vinculin, and paxillin recruitment to cell matrix adhesions is associated with distinct increments in force; ii) on a substrate of ∼50 kPa an increase in local traction force of ∼60 pN is accompanied by recruitment of 1:2:2 talin:vinculin:paxillin molecules; iii) on a ∼4 times softer substrate force increments per molecule are less pronounced and vinculin-related force decreases dramatically; iv) FAK recruitment is not significantly associ-

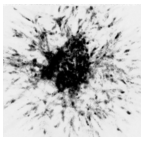

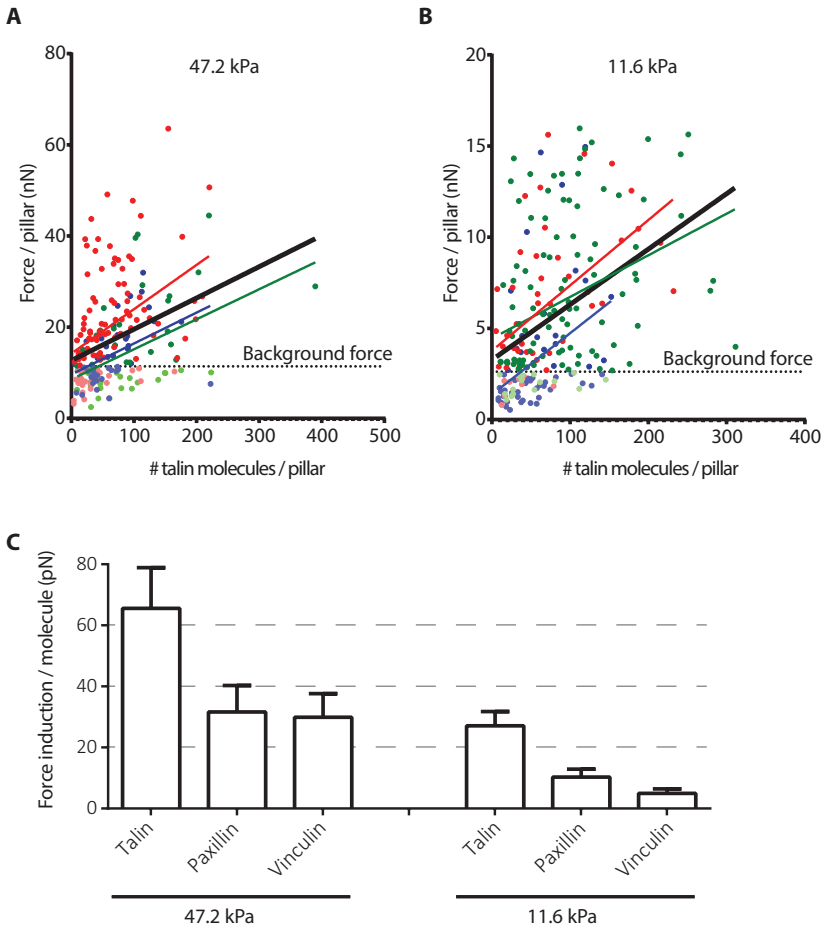

Figure 4.4

Recruitment of talin, vinculin, and paxillin to cell matrix adhesions is associated with distinct increments in force that depend on substrate stiffness. *A, B, measured force per cell matrix adhesion plotted against calculated number of talin molecules per adhesion for cells seeded on substrates with effective Young's modulus 47.2 kPa (A) and 11.6 kPa (B). Dots indicate individual adhesions; lines indicate linear fits. Red, green and blue colors represent data from three independent experiments. Solid black line represents linear fit for all data points from all three experiments. Dashed horizontal black line denotes the background forces measured. C, bar graphs showing linear fit slope values for relation between local traction force and number of talin, paxillin and vinculin molecules for cells seeded on substrates with effective Young's modulus 47.2 kPa and 11.6 kPa.*

ated with the amount of local traction force.

4.3 Discussion

Cell matrix adhesions are highly dynamic multiprotein complexes that allow cells to sense and respond to physical cues from their surrounding ECM. We combined micropillar based traction force microscopy with super resolution microscopy to obtain quantitative relationships between cell matrix adhesion composition and local traction force. In order to obtain the molecular composition from dSTORM data we developed a novel mathematical method that makes use of the high localization precision inherent in super resolution methods. We find distinct force relationships for talin, vinculin, and paxillin that are modulated by environmental stiffness, whereas recruitment of FAK molecules is not related to the amount of local traction force (Figure 4.5).

Similar to previous findings [10–12], we observe that larger adhesions support higher traction forces. Importantly, the increase in force associated with an additional talin, vinculin, or paxillin molecule does not represent the force exerted on these molecules but the overall force on the adhesion. Several additional cell matrix adhesion proteins (that are not analyzed in our current study) are likely to be recruited to the growing adhesion as it applies more traction force. These include proteins that couple integrins to the cytoskeleton, such as α-actinin and filamin [16] and their contribution has not been addressed here. As a single talin molecule interacts with a single integrin molecule, our finding that 1 additional talin molecule is associated with an additional 60 pN traction force on a ∼50 kPa substrate may point to an additional integrin being recruited to the adhesion with this increase in force. Alternatively, integrins may switch from interaction with filamins or α-actinin to interaction with additional recruited talin molecules under increased force.

It has been reported that FAK is necessary for cellular traction force generation [17] and blocking myosin II activity impairs FAK recruitment to cell matrix adhesions [18]. In that study myosin activity was blocked with blebbistatin (20 µM) resulting in very small adhesions (0.17 μm^2). We show that FAK recruitment to cell matrix adhesions does not correlate with increased traction forces on short or long pillars. This does not imply that FAK is not implicated in force generation. It has been shown that FAK activation through phosphorylation is force dependent

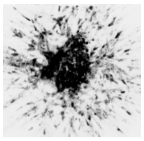

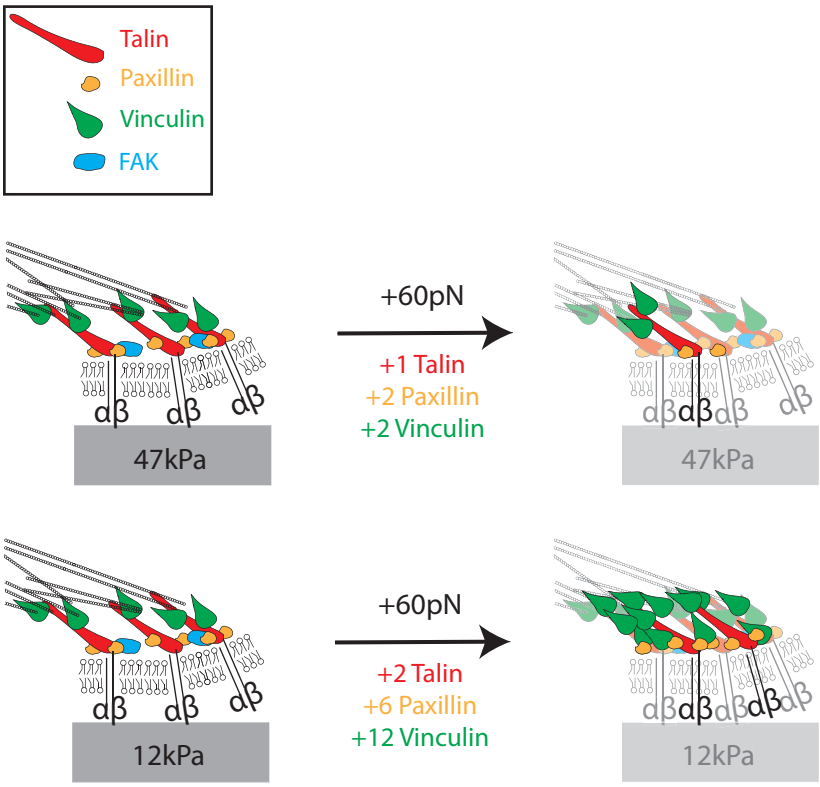

Figure 4.5
Molecular composition of force responsive cell matrix adhesions. *Cartoons depicting recruitment of talin, paxillin and vinculin molecules associated with a ∼60 pN increase in force on stiff and soft substrates with indicated effective Young's moduli.*

[19] and, in turn influences force dependent phosphorylation of paxillin and recruitment of vinculin [18]. Our findings, together with studies showing that FAK residence times are low and increase with increasing cell matrix adhesion size [18, 20] suggest that changes in FAK activity rather than its recruitment are coupled to force.

We find that the abundance of talin molecules is associated with the highest traction forces in cell matrix adhesions on stiff as well as softer substrates as compared to vinculin and paxillin. On a stiff substrate an increase in traction force of ∼60 pN is associated with one additional talin molecule, whereas two additional vinculin or paxillin molecules are associated with the same force increase (Figure 4.5). Talin connects the integrin to actin and acts as a scaffold for vinculin binding [21]. Binding of talin to the integrin cytoplasmic tail activates the integrin and enhances ECM binding, and interaction of talin with integrin αvβ3 is important for adhesion strengthening [22]. Forces on talin molecules open cryptic binding sites for vinculin [23]. It has been shown that induction of myosin contractility triggers this unfolding, which is also correlated with more actin proximal localization of vinculin and adhesion maturation [8]. This suggests that recruitment of talin and vinculin as well as their interaction is important for force related adhesion maturation. As described above, vinculin can also be recruited to cell matrix adhesions through FAK-mediated phosphorylation of paxillin, a process that depends on myosin-mediated contractility [8, 18].

Experiments with isolated talin molecules have shown that cryptic vinculin binding sites become available when talin is under 5-25 pN tension [24]. The 66 pN or 27 pN increase in traction force measured for a cell matrix adhesion on a stiff or soft substrate, respectively, per additional talin molecule is above the threshold for opening vinculin binding sites and below the 100 pN forces that can be supported by single actin molecules [25]. Notably, vinculin molecules that are recruited to the adhesion via talin, phospho-paxillin or other interactions such as force dependent p130Cas-vinculin binding [26], may partially remain in an inactive confirmation, especially on a soft substrate, which may explain the lower force induction measured for each recruited vinculin molecule as compared to talin.

Interestingly, it has been reported that as adhesions enlarge, forces on individual vinculin molecules decrease [27]. A recent publication shed more light on this by demonstrating a switch behavior for vinculin: for

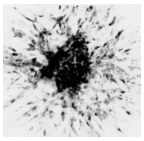

very small and very large adhesions tension on vinculin molecules negatively correlated with adhesion growth while for adhesions of intermediate size, a positive correlation of vinculin tension with adhesion growth was found [28]. The fact that vinculin has comparatively slow turnover in cell matrix adhesions on glass and that inhibition of myosin contractility raises its turnover to that observed for other cell matrix adhesion proteins further suggests that vinculin changes function with force [18, 29]. Our findings extend these observations showing that a decrease in substrate rigidity leads to a major decrease in vinculin-associated force on softer substrates: i.e. for the same amount of force increase many more vinculin molecules are recruited on a soft versus a stiff substrate (Figure 4.5). Vinculin activation is proposed to occur through its interaction with talin [8]. Larger forces applied on stiff substrates in our experiments may enhance talin-vinculin interaction, thereby more effectively supporting vinculin activation and subsequent coupling of vinculin to the actin cytoskeleton.

Taken together, we have combined dSTORM and traction force microscopy to obtain quantitative information on the relationship between the molecular composition of cell matrix adhesions and their force application. We report that an increase in force of ∼60 pN is accompanied by recruitment of 1:2:2 talin:vinculin:paxillin molecules on a substrate of ∼50 kPa (Figure 4.5). This stoichiometry changes on softer substrates, in particular due to a strong reduction of vinculin-associated force. Our novel mathematical method for extraction of molecular information from super resolution images is readily applicable to other cellular structures given that there is enough signal amplification, i.e. there are multiple fluorophores attached to the protein of interest and/or multiple blinking events observed per fluorophore.

4.4 Materials and methods

4.4.1 Cell culture and transduction

Vinculin KO MEFs (kindly provided by Dr. Johan de Rooij, Utrecht University, NL) and NIH-3T3 fibroblasts were cultured in medium (DMEM; Dulbecco's modified Eagle's Medium, Invitrogen/Fisher Scientific) supplemented with 10% new born calf serum, 25 U/ml penicillin and 25 µg/ml streptomycin (Invitrogen/Fisher Scientific cat. # 15070-063).

Vinculin KO MEFs were transduced with a GFP-vinculin retroviral construct as previously described [30].

4.4.2 Micropillar preparation and cell seeding

Micropillars were used for cellular traction force measurements according to methodology described previously [11]. A negative silicon master was made with 10x10 mm arrays of circular holes of 4.1 or 6.9 µm depth, 2 µm diameter and 4 µm center-to-center distance in a hexagonal grid with two rectangular spacers of 10x2 mm aligned on the sides of the arrays using a two-step Deep Reactive Ion Etching (DRIE) process. Negative silicon master was passivated with trichloro silane (Sigma Aldrich) and well-mixed PDMS at 1:10 ratio (crosslinker:prepolymer) was poured over the wafer and cured for 20 hours at 110°C. Pillar arrays of 4.1 and 6.9 µm height had a bending stiffness of 66 nN/µm and 16 nN/µm respectively corresponding to an effective Young's modulus, E_{eff}, of 47.2 and 11.6 kPa respectively [15]. Stamping of fibronectin was performed using a flat piece of PDMS (1:30 ratio, cured 16 hours at 65°C) previously incubated with 40 µL mix of 50 µg/mL unlabeled fibronectin (Sigma Aldrich) and 10 µg/mL Alexa405 or Alexa647 (both from Invitrogen)-conjugated fibronectin. Subsequently the micropillars were blocked with 0.2% Pluronic (F-127, Sigma Aldrich) and cells were seeded in single cell density in complete medium and incubated for 5 hours at 37°C and 5% CO_2.

4.4.3 Fixation and immunostaining

Samples were washed once with cytoskeleton buffer (CB) (10 mM MES, 150 mM NaCl, 5 mM EGTA, 5 mM $MgCl_2$, and 5mM glucose) [31], briefly permeabilized during fixation for 10 seconds with 0.1-0.25% Triton-X, 0.4% paraformaldehyde and 1 µg/mL phalloidin in CB. The triton concentration was adjusted per batch of CB to minimize the background signal without causing additional reduction to the force application. Samples were finally fixed for 10' with 4% formaldehyde in CB, permeabilized for 10' with 0.5% Triton-X and blocked for 30' with 0.5% BSA in PBS. Immunostaining was performed either with an Alexa-532-conjugated GFP nanobody (Chromotek, Germany) or with a primary mouse monoclonal antibody against talin (Sigma, T-3287), FAK (BD Transduction, 610087), paxillin (BD Transduction, 610052) or vinculin

(Sigma, V-9131), followed by an Alexa647 conjugated secondary antibody against mouse IgG (Jackson, 115-605-006) following the protocol suggested by [13].

4.4.4 Imaging and analysis

dSTORM imaging

Super-resolution imaging was performed on a home-built wide-field single-molecule setup, based on an Axiovert S100 (Zeiss) inverted microscope equipped with a 100x 1.4NA oil-immersion objective (Zeiss, Germany). Micropillar arrays were inverted onto #0, 25 mm diameter, round coverslips (Menzel Glaser). Imaging was performed in 100 mM mercaptoethylamine (MEA, Sigma Aldrich) in PBS. A 405 nm laser (CrystaLaser, USA) was used for imaging the pillars and photoswitching of the Alexa647 dye to adjust the density of visible fluorophores. The light was reflected into the objective by a dichroic mirror (ZT405/532/635rpc, Chroma, USA). The fluorescence light in the detection path was filtered using the emission filter ZET532/633m (Chroma, USA). Conversion intensities were between 0 and 250 W/cm^2 at 405 nm, and the excitation intensity was 5 kW/cm^2 at 647 nm. For each sample, we acquired 20000 images with an acquisition time of 10 ms per frame and a frame rate of 69 Hz. The signal of individual dye molecules was captured on a sCMOS Orca Flash 4.0V2 camera (Hamamatsu, Japan). The average integrated signal of a single dye molecule was 608 detected photons, spatially distributed by the 2 dimensional point-spread-function of the microscope of 440 nm FWHM, resulting in a sigma of 187 nm in a Gaussian approximation.

The signal from individual fluorophores was fitted with a 2-dimensional Gaussian using a custom least-squares algorithm in Matlab [32]. From the fit we determined the location of each fluorophore to an accuracy of 14±5 nm on average (Figure 4.3B). The localization accuracy is above the theoretical minimum predicted from the width of the point-spread-function and the detected signal, $187nm/\sqrt{520} = 8.2$ nm.

Obtaining and fitting the cumulative distribution function

From the position data of the adhesion, the two-point spatial correlation function g(r) and subsequently the cumulative distance function (cdf) could be calculated as

$$cdf(r) = \int_0^r g(r')dr'.$$

For discrete 2D position data $r_i = x_i, y_i$, as obtained in super-resolution microscopy, the cdf was constructed from

$$cdf(r) = 2 \sum_{i=1}^{N} \sum_{j=i+1}^{N} (x_i - x_j)^2 + (y_i - y_j)^2 < r^2.$$

The cdf describes the number of distances that are smaller than r, in a sample of N localizations. We assumed a Gaussian distribution in space leading to a cdf,

$$\mathrm{cdf(r)} = \mathrm{N_c}(1\text{-}e^{-r^2/4\sigma^2}),$$

as the correlation length, σ_i, is given by a combination of the localization uncertainty for an individual fluorophore, Δr_i, and the size of a primary and secondary antibody complex used to label the protein of interest and typically, both detection and labeling originate from statistical processes. Here N_c is the total number of correlated distances and σ the mean positional uncertainty for all localizations. This equation is valid for $r \sim \sigma$. On length scales longer than the correlation length the cdf was characterized by a distance distribution for uncorrelated molecules. Assuming a homogeneous, random organization of molecules within a given field-of-view of area, A, the cdf of uncorrelated localizations gave a quadratic dependence on distance as:

$$\mathrm{cdf(r)} = \mathrm{N_u}(\pi r^2)/A,$$

where N_u is the number of uncorrelated distances. Thus, the general form for the spatial correlation function was a linear combination of the correlated and the uncorrelated part:

$$\mathrm{cdf(r)} = \mathrm{N_c}(1\text{-}e^{-r^2/4\sigma^2}) + \mathrm{N_u}(\pi r^2)/A.$$

Running a simulation with 2048 individual molecules randomly positioned in a box of 2×2 µm^2 and each molecule reappearing 100 times with a positional accuracy of 20 nm (Figure S1D) the distance distribution was calculated and its dependence on the squared distance, r^2, is shown (Figure S1E). For squared distances beyond 4×10^{-3} µm^2 the cdf(r) became linearly dependent on r^2 with the slope of $\pi N_u/A$ and y-intersect at $N_c(2\times10^7)$ as predicted.

Calculation of number of molecules from the fit

From N_c the number of molecules was calculated as following. The number of localizations, N, originating from N_m molecules each being observed n_i times is given by

$$N = \sum_{i=1}^{N_m} n_i = N_m < n >,$$

where <n> is the average number of observations per molecule. Hence

$$N^2 = (N_m < n >)^2.$$

Likewise, the total number of correlated distances, N_c per molecule is given by $n_i \times (n_i\text{-}1)$. For all molecules this yields:

$$N_c = \sum_{i=1}^{N_m} (n_i^2 - n_i) = (N_m) < n^2 > -N.$$

Therefore

$$N^2/(N_c + N) = (N_m < n >)^2/((N_m) < n^2 >).$$

Rearranging these equations gives

$$N_m = N^2/(N_c + N)(1 + (var(n))/ < n >^2),$$

where $var(n) =< n^2 > - < n >^2$, is the variance in the number of detections per molecule. The second term, $(1 + (var(n))/ < n >^2)$, summarizes the properties of the joined statistics of labeling and photophysics of the fluorophores and its value varies between 1 and 2 depending on which of the various processes dominates the joined statistics and for a typical dSTORM experiment is close to one (see the Supplemental materials for a more detailed analysis). Simulations were performed for densities between 40 and 4000 randomly distributed molecules on an area of 2×2 µm^2. One hundred localizations per molecule were simulated with a mean positional accuracy $\sigma = 20$ nm. At high densities there was significant overlap of molecules within the image (Figure S1D). The number of estimated molecules faithfully followed the input within an accuracy of 10% (Figure S1F)

Estimation of number of molecules in an adhesion

In the quantification of the number of correlated distances it was assumed that all molecules were randomly organized, which is not the case for molecule clusters that are observed in a cell-matrix adhesion. This restriction is readily lifted by the addition of a second exponential term with weight, N_L that accounts for a length scale, L that characterizes any spatial structures in real data. Hence the cdf for a nonlinear regime becomes

$$cdf(r) = N_c(1 - e^{-r^2/4\sigma^2}) + N_L(1 - e^{-r^2/L^2}).$$

For the distinction of the two components, the typical structural length scale should be significantly larger than the positional accuracy, L > 4σ, typically 40 nm for a positional accuracy of 10 nm and holds true for many cellular structures, like large membrane compartments, adhesion clusters, chromosome territories. Hence the method described above provides a very general solution for molecule counting in super-resolution microscopy where

$$N_m = N^2/(N_c + N) \times (1 + (var(n))/ < n >^2).$$

Deflection analysis

Pillar deflections were determined with approximately 50 nm precision using a specifically designed Matlab script. The pillar locations were determined from the labeled fibronectin fluorescence image using a fit to the cross-correlation function between a perfect binary circle and the local fluorescence of one pillar. Those positions were compared to those of a perfect hexagonal grid used as reference. From an undeflected array image the accuracy was found to be 47.1 nm (Figure S1B,C), this corresponds to a force accuracy of 780 pN and 3.1 nN on the pillar array of E_{eff} = 11.6 kPa and 47.2 kPa, respectively. Masks for adhesions corresponding to individual pillars of interest were manually drawn for each case.

4.4.5 Statistic analysis

p-values were calculated using F-test for linear regression analysis using GraphPad Prism 6.0.

4.5 Acknowledgements

We thank Dr. Johan de Rooij (Utrecht University, NL) for kindly providing cells and Dr. Hedde van Hoorn (VU University, NL) for his assistance with pillar deflection analysis. Financial support for this work came from the Netherlands Organization for Scientific Research (FOM 09MMC03).

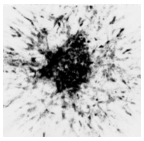

4.6 Supplemental materials

4.6.1 Obtaining the cdf

For N localizations, the total number of distances between localizations is given by N^2-N. For a typical dSTORM experiment with 10^6 localizations this would mean 10^{12} distances. If stored as double precision values this would require 8TB of memory, well beyond the limits of modern day PC's. Therefore our algorithm only takes distances into account that are smaller than a set value r_{max}. When 10^6 distances are found it terminates.

4.6.2 Relation between variance and squared mean

The factor $1+(var(n))/<n>^2$ in the equation giving the number of molecules, characterizes the joined statistics of the photophysics of the fluorophore and the statistics of labeling of the primary antibody by the secondary antibodies.

$$F = 1 + (var(n))/ < n >^2 = 1 + c_v^2$$

It is related to the coefficient of variation c_v of $n = \sigma_n/<n>$ in statistics. Values for F vary between 1 and 2 depending on the underlying and dominant statistics.

Distribution	Mean	Variance	F
Binomial	n p	n p (1-p)	1 + 1/np - 1/n
Poissonian	λ	λ	$1+1/\lambda$
Exponential	$1/\lambda$	$1/\lambda^2$	2
Gaussian	μ	σ^2	$1+\sigma^2/\mu^2$

4.6.3 Simulation for a combined statistics with secondary antibody labeling

A typical dSTORM experiment involves a dual labeling step where the molecule of interest is first labeled by a specific primary antibody that is subsequently labeled by multiple secondary antibodies, each conjugated to multiple fluorophores. To assess the distribution in this experiment we performed simulations. In those simulations we assumed:

1) The number of secondary antibodies bound to a primary antibody is constant, given that the excess of secondary antibody occupies all binding sites on the primary antibody.

2) The number of fluorophores bound to a secondary antibody has a Poissonian distribution with a mean of 4.7 (typical mean value provided by the manufacturer, Jackson Immunology).

3) The number of detections per fluorophore follows a single-exponential distribution, typical for photobleaching. The number of detections when a fluorophore is in the on-state equals $t_{on} \times$framerate. Alexa647, as used in the current study is generally assumed to behave according to a four-state molecule characterized by a ground, a fluorescent excited, a non-fluorescent triplet and a long-lived dark state. The latter populated via the excited triplet state [33]. The distribution in such a case is described in terms of a static trap model [34], with on-times following a single exponential distribution.

Figure S4 summarizes the result of this simulation. The factor $F=1+(var(n))/<n>^2$, is dominated by the number of secondary antibodies. For typical values found in literature as the secondary to primary ratio (4), F is found to be below 1.1. Even in the case of only a single secondary per primary F equals 1.5, which is still below its maximal value of 2. This is caused by the multiple fluorophores per secondary antibody.

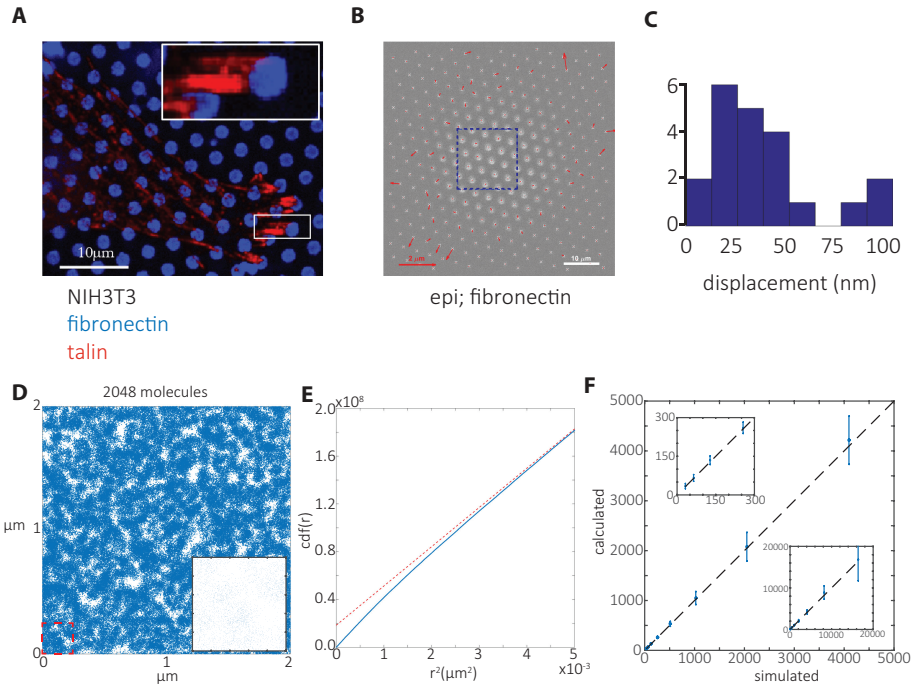

Figure S1

Pillar localization precision and analyses on simulations of molecules. *A, confocal image of a NIH3T3 cell on fibronectin (conjugated with Alexa 405) stamped PDMS pillars immunostained for talin (secondary antibody Alexa647). B, epi-fluorescence image of cell-free (force-free) PDMS pillar array obtained from dSTORM microscope with calculated pillar deflections (1024x1024 pixels). Blue box indicates area in which dSTORM measurements were performed (256x256 pixels). C, the histogram of pillar deflections measured in the boxed area (B) indicating the localization precision of pillar centers. D,E, detections from a simulation of random placement of 2048 molecules in a region of 4 µm^2 with 100 localizations per molecule (N=2048x100) with a positional accuracy of 20 nm (D), and cumulative distance function (cdf) of the inter-localization distances with a linear fit (red dashed line) with y-intercept at N_c=2x10^7, resulting in calculated N_m=$N^2/(N+N_c)$=2076 (E). F, calculated number of molecules N_m with standard deviation plotted against simulated number of molecules and dashed line of slope 1 with insets showing same graph with different zoom areas. Scale bars are 10 µm (A, B); deflection arrow scales are 2 µm (B).*

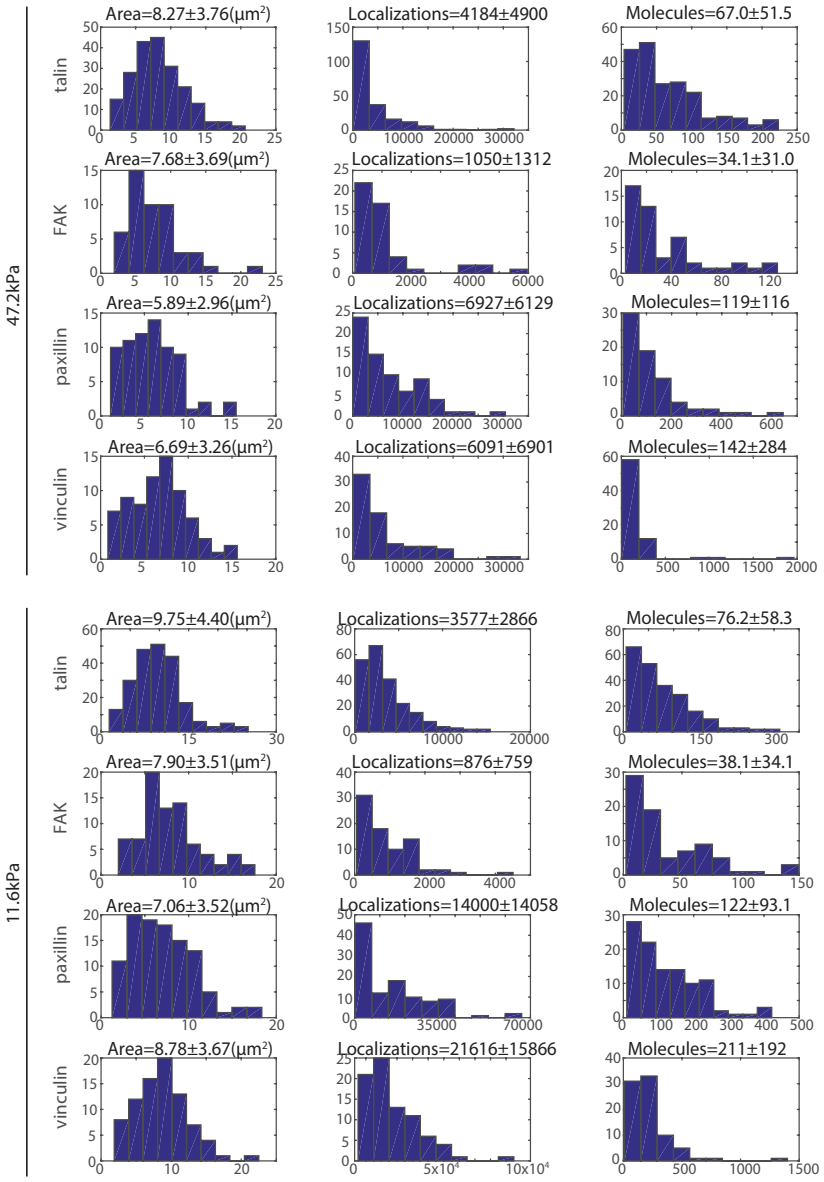

Figure S2

Histograms of adhesion area, localizations detected and molecules calculated per adhesion. *Histograms of areas of manually selected cell-matrix adhesions associated with pillars showing distribution of total cell matrix adhesion area (first column), detected localizations (second column), and calculated number of molecules (third column). Top four rows show data for adhesions coupled to pillars with effective Young's modulus of 47.2 kPa. Bottom four rows show data for adhesions coupled to pillars with effective Young's modulus of 11.6 kPa. Data for dSTORM experiments on talin (1st and 5th rows), FAK (2nd and 6th rows), paxillin (3rd and 7th rows) and vinculin (4th and 8th rows) are shown. Means and standard deviations are given above each histogram.*

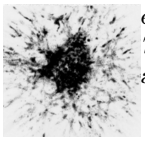

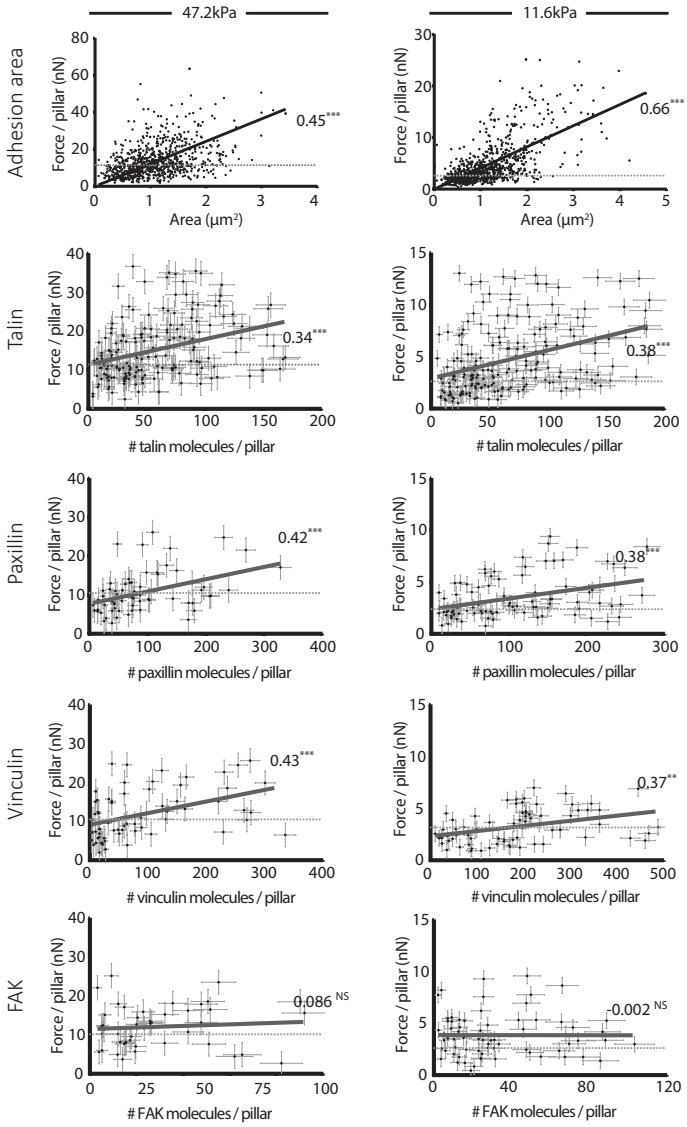

Figure S3

Total adhesion area and number of talin, vinculin, and paxillin molecules but not of FAK molecules correlates with local traction force. *Force per adhesion measured plotted against adhesion area and number of calculated talin, paxillin, vinculin and FAK molecules associated with the adhesion from three different experiments plotted with standard deviations; black solid line is the accompanying linear fit denoted with the calculated Pearson's correlation and dashed line is the measured background deflections for cells seeded on substrates with effective Young's modulus 47.2 kPa (left) and 11.6 kPa (right). ***, $p<0.0001$; **, $p<0.005$; NS: $p>0.05$: p values denote how significantly the slope is different from zero as calculated with F-test.*

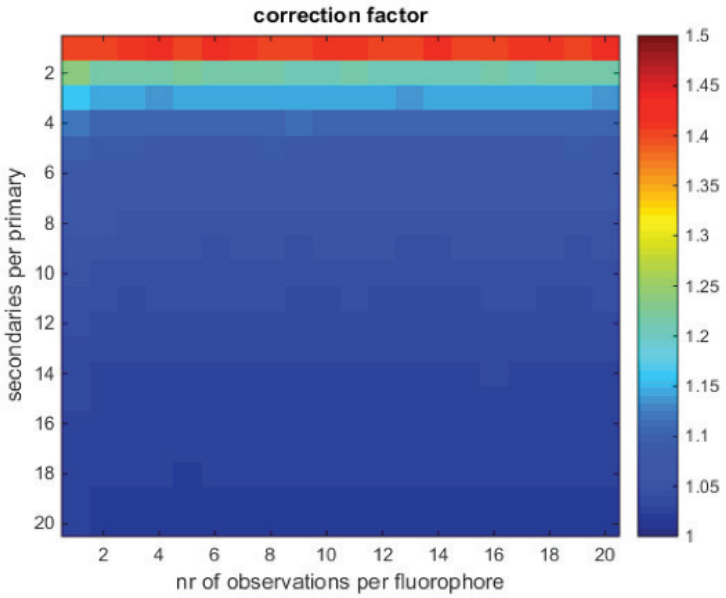

Figure S4

Simulations on correction factor, F. *Correction factor F as described in formula* $F=1+var(n)/<n>^2$ *for several simulations where the number of observations per fluorophore and the number of secondary antibodies per primary antibody were varied. The number of secondary antibodies per primary dominates the factor F.*

Bibliography

[1] Ekaterina Papusheva and Carl-Philipp Heisenberg. "Spatial organization of adhesion: force-dependent regulation and function in tissue morphogenesis". In: *The EMBO Journal* 29.16 (2010).

[2] Amnon Buxboim, Irena L Ivanovska, and Dennis E Discher. "Matrix elasticity, cytoskeletal forces and physics of the nucleus: how deeply do cells 'feel' outside and in?" In: *Journal of Cell Science* 123.3 (2010).

[3] Sanjay Kumar and Valerie M Weaver. "Mechanics, malignancy, and metastasis: The force journey of a tumor cell". In: *Cancer and Metastasis Reviews* 28.1-2 (2009).

[4] Simon W Moore, Pere Roca-Cusachs, and Michael P Sheetz. "Stretchy proteins on stretchy substrates: the important elements of integrin-mediated rigidity sensing." In: *Developmental Cell* 19.2 (2010).

[5] Cord Brakebusch and Reinhard Fässler. "The integrin-actin connection, an eternal love affair". In: *The EMBO Journal* 22.10 (2003).

[6] Stephan Huveneers and Erik HJ Danen. "Adhesion signaling – crosstalk between integrins, Src and Rho". In: *Journal of Cell Science* 122.8 (2009).

[7] J Thomas Parsons, Alan R Horwitz, and Martin A Schwartz. "Cell adhesion: integrating cytoskeletal dynamics and cellular tension." In: *Nature Reviews. Molecular Cell Biology* 11.9 (2010).

[8] Lindsay B Case et al. "Molecular mechanism of vinculin activation and nanoscale spatial organization in focal adhesions." In: *Nature Cell Biology* 17.7 (2015).

[9] Pakorn Kanchanawong et al. "Nanoscale architecture of integrin-based cell adhesions." In: *Nature* 468.7323 (2010).

[10] Nathalie Q Balaban et al. "Force and focal adhesion assembly: a close relationship studied using elastic micropatterned substrates". In: *Nature Cell Biology* 3.5 (2001).

[11] Hedde van Hoorn et al. "The Nanoscale Architecture of Force-Bearing Focal Adhesions". In: *Nano Letters* 14.8 (2014).

[12] Léa Trichet et al. "Evidence of a large-scale mechanosensing mechanism for cellular adaptation to substrate stiffness". In: *Proceedings of the National Academy of Sciences of the United States of America* 109.18 (2012).

[13] Sebastian van de Linde et al. "Direct stochastic optical reconstruction microscopy with standard fluorescent probes". In: *Nature Protocols* 6.7 (2011).

[14] Robert P Nieuwenhuizen et al. "Quantitative localization microscopy: effects of photophysics and labeling stoichiometry." In: *PLoS One* 10.5 (2015).

[15] Hayri E Balcıoğlu et al. "The integrin expression profile modulates orientation and dynamics of force transmission at cell-matrix adhesions." In: *Journal of Cell Science* 128.7 (2015).

[16] Alex-Xianghua X Zhou, John H Hartwig, and Levent M Akyürek. "Filamins in cell signaling, transcription and organ development." In: *Trends in Cell Biology* 20.2 (2010).

[17] Ben Fabry et al. "Focal Adhesion Kinase Stabilizes the Cytoskeleton". In: *Biophysical Journal* 101.9 (2011).

[18] Ana M Pasapera et al. "Myosin II activity regulates vinculin recruitment to focal adhesions through FAK-mediated paxillin phosphorylation." In: *The Journal of Cell Biology* 188.6 (2010).

[19] Jihye Seong et al. "Distinct biophysical mechanisms of focal adhesion kinase mechanoactivation by different extracellular matrix proteins." In: *Proceedings of the National Academy of Sciences of the United States of America* 110.48 (2013).

[20] Sylvia E Le Dévédec et al. "The residence time of focal adhesion kinase (FAK) and paxillin at focal adhesions in renal epithelial cells is determined by adhesion size, strength and life cycle status." In: *Journal of Cell Science* 125.Pt 19 (2012).

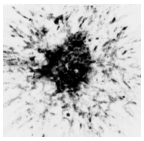

[21] Seiji Tadokoro et al. "Talin binding to integrin beta tails: a final common step in integrin activation." In: *Science (New York, N.Y.)* 302.5642 (2003).

[22] Pere Roca-Cusachs et al. "Clustering of alpha(5)beta(1) integrins determines adhesion strength whereas alpha(v)beta(3) and talin enable mechanotransduction." In: *Proceedings of the National Academy of Sciences of the United States of America* 106.38 (2009).

[23] Armando del Rio et al. "Stretching Single Talin Rod Molecules Activates Vinculin Binding". In: *Science (New York, N.Y.)* 323.5914 (2009).

[24] Mingxi Yao et al. "Mechanical activation of vinculin binding to talin locks talin in an unfolded conformation". In: *Scientific Reports* 4 (2014).

[25] Akiyoshi Kishino and Toshio Yanagida. "Force measurements by micromanipulation of a single actin filament by glass needles". In: *Nature* (1988).

[26] Radoslav Janoštiak et al. "CAS directly interacts with vinculin to control mechanosensing and focal adhesion dynamics". In: *Cellular and Molecular Life Sciences* 71.4 (2013).

[27] Casten Grashoff et al. "Measuring mechanical tension across vinculin reveals regulation of focal adhesion dynamics". In: *Nature* 466.7303 (2010).

[28] Pablo Hernández-Varas et al. "A plastic relationship between vinculin-mediated tension and adhesion complex area defines adhesion size and lifetime." In: *Nature Communications* 6 (2015).

[29] Haguy Wolfenson et al. "Actomyosin-generated tension controls the molecular kinetics of focal adhesions". In: *Journal of Cell Science* 124.9 (2011).

[30] Erik H J Danen et al. "Integrins control motile strategy through a Rho-cofilin pathway". In: *The Journal of Cell Biology* 169.3 (2005).

[31] Johanna Prast, Mario Gimona, and Victor J Small. "Immunofluorescence microscopy of the cytoskeleton: combination with green fluorescent protein tags". In: *Cell Biology: A Laboratory Handbook (3rd ed) JECelis, ed. Amsterdam* (2006).

[32] Thomas Schmidt et al. "Imaging of single molecule diffusion". In: *Proceedings of the National Academy of Sciences of the United States of America* 93.7 (1996).

[33] Thomas Schmidt et al. "Characterization of Photophysics and Mobility of Single Molecules in a Fluid Lipid Membrane". In: *The Journal of Physical Chemistry* 99.49 (1995).

[34] Frank Cichos, Christian von Borczyskowski, and Michel Orrit. "Power-law intermittency of single emitters". In: *Current Opinion in Colloid & Interface Science* 12.6 (2007).

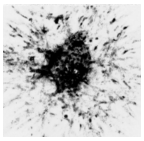

Chapter 5

Identification of genes regulating cellular traction forces, adhesion dynamics, and cell migration [1]

[1] This chapter is based on: Michiel Fokkelman*, Hayri E Balcıoğlu*, Janna E Klip, Kuan Yan, Fons J Verbeek, Erik HJ Danen, Bob van de Water *In Preparation; *:These authors contributed equally to this work.*

Abstract

Cell migration contributes to cancer metastasis and may also drive aspects of tumor growth. Here we aimed to identify genes controlling aspects of tumor cell migration, including the dynamic organization of cell matrix adhesions and cellular traction forces. In a siRNA screen, we identify 200+ genes that regulate size and/or dynamics of cell matrix adhesions in MCF7 breast cancer cells. In a subsequent screen, 11 of the 64 most effective genes are identified that regulate IGF1-induced 2D random cell migration of MCF7-IGF1R cells. For 4 of these hits (TPM1, PPP1R12B, HIPK3 and RAC2), whose silencing led to significantly enlarged adhesions and reduced cell migration, we studied their role in traction force generation. Silencing PPP1R12B, HIPK3 or RAC2 led to enhanced traction forces. Moreover, the force turnover was considerably reduced in adhesions following knockdown of these genes. Taken together, we identify genes that co-regulate cell migration, cell matrix adhesion dynamics and traction force turnover. Targeting PPP1R12B, HIPK3 or RAC2, results in large adhesions that are associated with high static traction forces and effectively blocks cell migration.

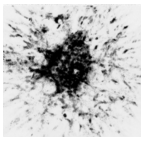

5.1 Introduction

Cell migration plays an important role in physiological processes, such as embryonic development, skin renewal and immune response. Deregulation of this cellular process plays a role in various pathologies, including cancer[1]. Tumor metastasis is the most lethal aspect of cancer progression and involves tumor cell invasion and dissemination [2]. Moreover, modeling has shown that short-range migration contributes to mixing of cell clones inside the tumor thereby promoting tumor growth [3]. Thus, oncogenic signaling pathways causing enhanced tumor cell migration *in vitro* may contain candidate targets for blocking tumor growth and metastasis formation *in vivo*. Established pathways in this respect include mitogen-activated protein kinase/extracellular signal-regulated kinase (MAPK/ERK) pathway and phosphatidylinositol 3-kinase (PI3K) [4, 5]. In addition to supporting cell survival and proliferation, these pathways also regulate cell adhesion and actin cytoskeleton [6].

Cell migration on 2D environments typically consists of several steps: protrusion, attachment, cell body movement and tail retraction [7]. Cell matrix adhesion dynamics and remodeling of the actin cytoskeleton plays a role in all of these processes [8]. Cell protrusions are driven by actin polymerization [9] and stabilized by attachment of the leading edge to the underlying surface through integrin mediated cell matrix adhesions. These adhesions contain a dynamic integrin-associated multiprotein complex that locally couples the extracellular matrix (ECM) to the actin cytoskeleton and, through cytoskeletal connections with the nuclear membrane, to the nucleus [10]. Cell body movement is driven through contractile actomyosin bundles that pull the cell body and nucleus towards the leading edge [11]. Finally the trailing edge is retracted by inducing cell matrix adhesion disassembly, possibly through microtubule signaling [12].

Formation of cell matrix adhesions and the actomyosin contractile machinery have also been shown to mediate some forms of cell migration in 3D [13]. However, the paradigm of 2D cell migration does not translate well to all 3D environments and (tumor) cells show a high level of plasticity allowing them to switch between different modes of migration in 3D [14, 15]. 3D cell confinements allow migration strategies that are independent of integrin-mediated cellular attachment [13, 16]. It has been reported that membrane protrusion formation, rather than motility in 2D corresponds to cell migration capacity in 3D [17].

Here, we aimed to understand the underlying machinery of tumor cell migration and its relation to adhesion turnover and cellular traction forces. In an siRNA screen, we identify 200+ genes that regulate size and/or dynamics of cell matrix adhesions in MCF7 breast cancer cells. In a subsequent screen, 11 of the 64 most effective genes are identified that regulate IGF1-induced 2D random cell migration of MCF7-IGF1R cells. For 4 of these hits (TPM1, PPP1R12B, HIPK3 and RAC2), whose silencing led to significantly enlarged adhesions and reduced cell migration, we studied their role in traction force generation. Silencing PPP1R12B, HIPK3 or RAC2 led to enhanced traction forces. Moreover, the force turnover was considerably reduced following knockdown of these genes. Taken together, we identify genes that co-regulate cell migration, cell matrix adhesion dynamics and traction force turnover. Targeting PPP1R12B, HIPK3 or RAC2, results in large adhesions that are associated with high static traction forces and effectively blocks cell migration.

5.2 Results

5.2.1 Larger adhesions and altered adhesion dynamics in response to knockdown of TPM1, PPP1R12B, RAC2 or HIPK3

To identify genes regulating cell matrix adhesion dynamics, a nocodazole assay was performed in MCF7 cells transfected with siRNA SMARTpools targeting adhesome genes. Four hours of nocodazole treatment resulted in disassembly of the microtubule network and after washout of nocodazole followed by incubation for 2 hours in DMSO, the microtubule network reassembled as described earlier [18] (Figure 5.1A, top). This corresponded with appearance of a more prominent actin network and larger cell matrix adhesions in the presence of nocodazole, a phenotype that was reversed after nocodazole washout (Figure 5.1A, middle and bottom). Automated quantitative analysis software was applied to identify individual adhesions and nuclei (Figure 5.1B). This confirmed growth of cell matrix adhesions in the presence of nocodazole and reversion to sizes comparable to DMSO condition upon washout (Figure 5.1C - mock). Knockdown of candidate genes with SMARTpools resulted in altered responses to nocodazole treatment and washout (Figure S1). 64 SMARTpools markedly affecting the response were further investigated.

Results of four of these SMARTpools that led to enlarged cell matrix adhesions under control conditions are shown (Figure 5.1C-E). Knockdown of HIPK3, although leading to larger adhesions did not affect the response to nocodazole or washout, indicating that cell matrix adhesion dynamics were not disturbed (Figure 5.1C). Knockdown of TPM1 did not affect cell matrix adhesion growth in response to nocodazole but shrinkage after nocodazale washout was reduced, suggesting partially impaired adhesion disassembly (Figure 5.1C). PPP1R12B knockdown led to a less prominent enlargement of adhesions in response to nocodazole and after washout adhesions were much smaller than in the DMSO condition, suggesting impaired dynamic adhesion growth (Figure 5.1C). Knockdown of RAC2 completely blocked cell matrix adhesion growth in response to nocodazole, indicating a block in general cell matrix adhesion dynamics (Figure 5.1C).

5.2.2 Knockdown of TPM1, PPP1R12B, RAC2 or HIPK3 inhibits tumor cell migration

All 64 candidate genes identified with the nocodazole assay, were silenced with siRNA SMARTpools and migration of individual MCF7-IGF1R cells stimulated with IGF1 was quantified (Figure 5.2A). Positive control si-DNM2 [19] significantly reduced cell migration when compared to mock condition as expected. The knockdown of 18 candidate genes significantly impaired cell migration whereas knockdown of 5 genes enhanced cell migration (Figure 5.2A). In a deconvolution screen using 4 individual siRNAs, 11 of the hits identified in the nocodazole and random cell migration assays were confirmed, including reduced cell migration in the presence of siRNAs targeting TPM1, PPP1R12B, RAC2 or HIPK3 (Figure 5.2B,C and data not shown). Vinculin immunostaining on cells fixed after the random migration assay further confirmed that larger adhesions were formed following the knockdown of TPM1, PPP1R12B, RAC2 or HIPK3 (Figure 5.2D-F).

5.2.3 Knockdown of PPP1R12B, RAC2 and HIPK3 results in higher traction forces and slower force turnover

After establishing the importance of TPM1, PPP1R12B, RAC2 and HIPK3 in cell matrix adhesion dynamics and cell migration, we wanted

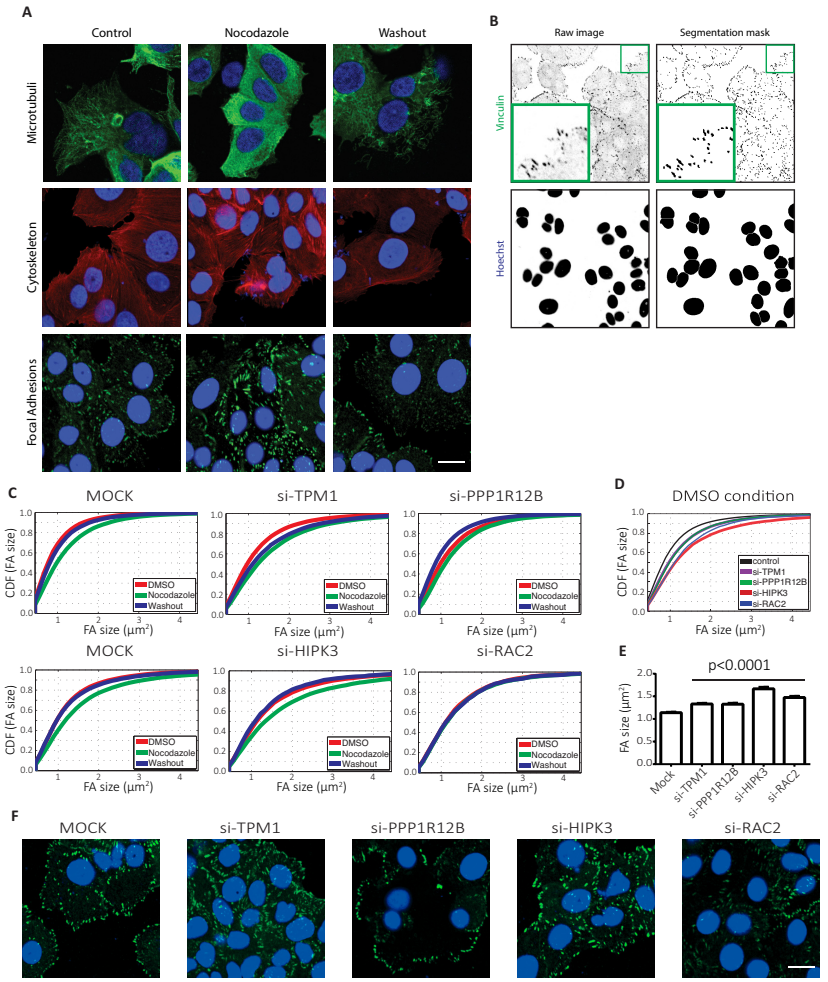

Figure 5.1

Nocodazole assay identifies genes responsible in cell-matrix adhesion dynamics. *A, MCF7 cells stained for microtubules (top), actin (middle) or vinculin (bottom) together with nucleus staining in blue in control DMSO condition (left), following 4 hours of nocodazole treatment (middle) or after washout of nocodazole and refreshment with control medium (right). B, Representative images of vinculin (top) and nucleus (bottom) on the left panel and corresponding binary images obtained following automated analysis on the right. C, Cumulative distribution functions of sizes of adhesions obtained by automated analysis shown in B, in mock condition or following siRNA knockdowns of indicated genes for the conditions mentioned in A. D-F, cumulative distribution functions of adhesion sizes in DMSO condition indicated in C (D), corresponding bar graphs showing mean and 95% confidence interval (E), and representative images showing vinculin in green and nucleus in blue (F). Scale bar is 20 µm. p value in E was calculated by comparing the knockdown conditions to the mock condition using t-test with Welch correction.*

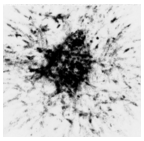

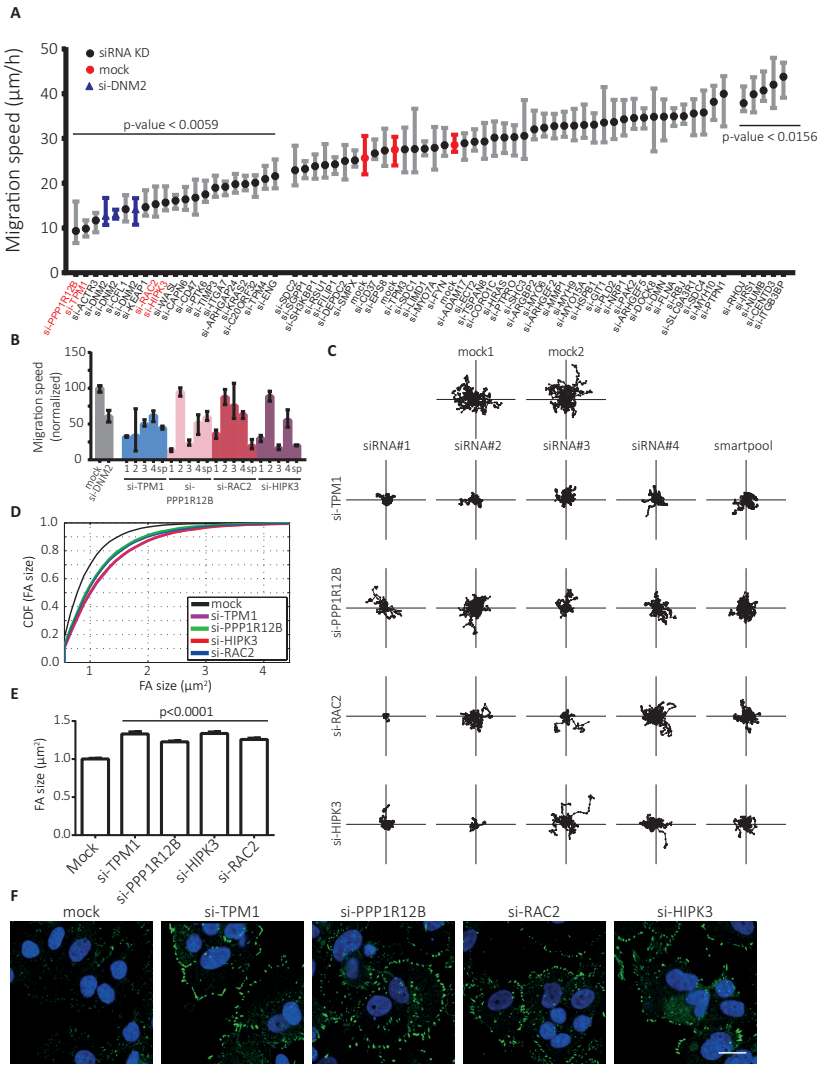

Figure 5.2

Disrupted cell matrix adhesion organization affects cell migration. *A, Quantification of single cell migration speed of MCF7-IGF1R cells after SMARTpool siRNA knockdown of 64 hits. B, C, Quantification of single cell migration speed normalized to mock following knockdown with single siRNA sequences or SMARTpool knockdown (B) and trajectories of individual cells (C). D-F, cumulative distribution functions of adhesion sizes for MCF-IGF1R cells with indicated SMARTpool knockdowns fixed after cell migration assay (D), corresponding bar graphs (E), and representative images showing vinculin in green and nucleus in blue (F). Scale bar is 20 µm. Median (A, B) or mean (E) and 95% confidence interval is shown. p values were calculated by comparing the knockdown conditions to the mock condition either with Kruskal-Wallis test with Dunn's post correction (A) or t-test with Welch correction (E).*

to study the role of these proteins in cellular force application. In order to visualize the actin cytoskeleton, MCF7-IGF1R cells were transduced with a lentiviral vector to stably express mCherry-LifeAct. Following transient transfection with siRNAs, MCF7-IGF1R-mCherry-LifeAct cells were seeded on fibronectin-stamped PDMS micropillars with an effective Young's Modulus of 47.2 kPa (bending stiffness of 65.8 nN/µm), stimulated with IGF1 and cellular forces were recorded (Figure 5.3A). The force per pillar was analyzed for the duration of the experiment (Figure 5.3B). Forces applied in PPP1R12B, RAC2 and HIPK3 knockdown conditions were significantly higher than those measured in the mock condition whereas TPM1 knockdown did not result in a significant change in magnitude of cellular traction forces (Figure 5.3C). To assess whether this reflected a general response of the entire population or whether localized increases in force were involved, we analyzed the cumulative distribution function (cdf) of measured traction forces. In addition to a shift in the population towards higher traction forces following PPP1R12B, RAC2 and HIPK3 knockdown, knockdown of each of these genes resulted in wider distributions (Figure 5.3D). This indicated that there is a larger heterogeneity in traction forces applied at different cellular regions, in response to knockdown of these genes.

Lastly, to determine the role of these genes in adhesion force turnover, we determined the autocorrelation of the force magnitudes measured at individual pillars over time. The autocorrelation function provided information on the duration of forces transduced by cellular adhesions, with faster decays indicating that the forces applied through adhesions were changing rapidly. The resulting autocorrelation functions showed the steepest decrease for the mock condition (Figure 5.3E). Quantification of the autocorrelation function halftimes showed a force halftime of ∼22 minutes for the mock condition (Figure 5.3F). The halftime was increased by ∼50% after silencing of TPM1 (although for this condition the increase was not significant), PPP1R12B or HIPK3 genes and, in addition to its most prominent attenuation of cell matrix adhesion dynamics (Figure 5.1C), knockdown of RAC2 led to doubling of the halftime up to >45 minutes (Figure 5.3F).

These findings indicate that out of 4 genes relevant for adhesion dynamics and cell migration, PPP1R12B, HIPK3 and RAC2 regulate force amplitude and turnover at cell matrix adhesions.

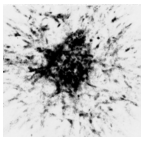

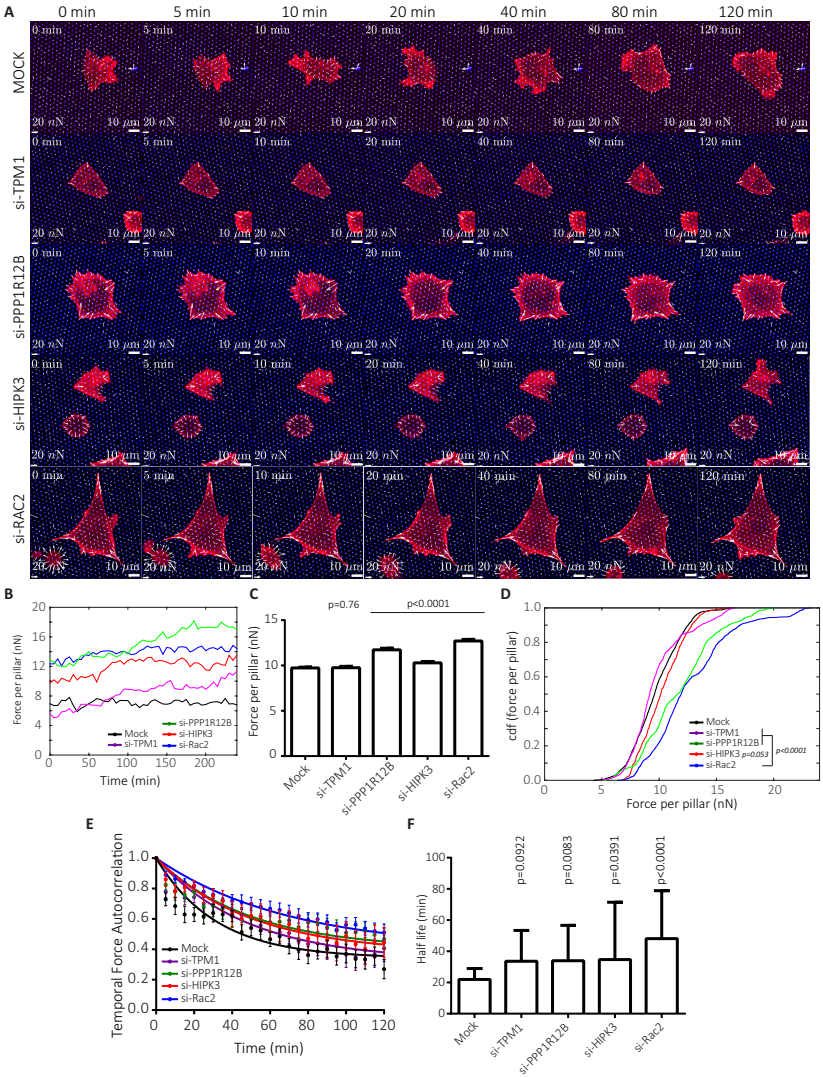

Figure 5.3

Knockdown of PPP1R12B, HIPK3 and RAC2 increases cellular force application and reduces force dynamics. *A, B, Time-lapse images of MCF7-IGF1R-mCherryLifeAct cells with indicated knockdowns together with corresponding forces at given times after IGF1 stimulation (A), and quantification of forces applied on top 5% deflected pillars followed throughout the experiment (B). C, D, bar graphs showing mean and 95% confidence interval (C), and corresponding cumulative distribution functions (D) of force per pillar for indicated SMARTpools. E, F, Force per pillar autocorrelations and corresponding fits using single exponential decay function for indicated knockdowns (E), and calculated half-times from the exponential fits with calculated errors (F). Scale bars are 20 nN and 10 µm. p values were calculated either by comparing means (C) or standard deviations (D) to mock condition using t-test with Welch's correction (C, D) or using extra sum of squares f-test (F).*

5.3 Discussion

New insights into cell adhesion and migration are a starting point for identification of drug targets implicated in cancer progression. Our findings relate the dynamics of cell matrix adhesions and the dynamics of cellular traction forces generated at these sites to tumor cell migration. We identify PPP1R12B, HIPK3 and RAC2 as regulators of each of these processes.

Even though we could not establish a role for TPM1 in traction force dynamics, the TPM1 gene was identified in our primary screen for regulators of cell matrix adhesion dynamics and TPM1 knockdown also attenuated cell migration. TPM1 gene codes for tropomyosin 1. Tropomyosin 1 takes part in muscle regulation, stabilizes actin cytoskeleton in non-muscle cells and its deregulation is implicated in cardiac illnesses [20]. Opposing findings have been reported for its function in tumor cell migration. Down-regulation of TPM1 has been shown to induce [21, 22] as well as impair cell motility. This may be related to the fact that different TPM1 isoforms have opposing effects on actin organization [23]. Therefore expression of different TPM1 isoforms in tumors of various backgrounds might act as a promoter or suppressor of cancer progression. Our findings show that down-regulation of TPM1 results in larger adhesions and impairment of cell migration. Although the siRNA SMARTpool targets multiple TPM1 species, this suggests that the main TPM1 isoform affected in MCF7 cells is the TPM1λ isoform [23]. Interestingly, despite the role of tropomyosin in actin organization and previous finding of tropomyosin inducing actomyosin contractility [20, 24], we did not find significant changes in applied forces or force dynamics upon TPM1 gene silencing.

The PPP1R12B gene, also known as MYPT2, codes for myosin phosphatase target 2 (MYPT2), which takes part in the myosin phosphatase protein complex. The myosin phosphatase protein complex, together with myosin light chain kinase, orchestrates myosin regulatory light chain phosphorylation. In heart muscle, this controls normal cardiac performance [25] and is involved in the sarcomeric architecture of actin cytoskeleton [26, 27]. Given the inhibitory effect of myosin phosphatase on myosin activity, one would expect the down-regulation of PPP1R12B to induce higher traction force generation. Indeed, we show that knockdown of PPP1R12B results in higher forces as expected. In addition, it leads to formation of larger cell-matrix adhesions and significantly im-

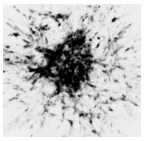

pairs force turnover. We further demonstrate that down regulation of PPP1R12B impairs tumor cell migration, possibly through its influence on cellular force machinery and adhesion dynamics.

HIPK3 encodes for the protein homeodomain interacting protein kinase 3. HIPK3 is involved in cell survival and insulin metabolism [28, 29]. Higher HIPK3 expression correlates with worse prognosis and lower sensitivity to chemotherapy [30, 31]. Here we show that knockdown of this gene also impairs tumor cell migration, induces formation of larger adhesions as well as inducing cellular force application and stability. Others have previously reported targeting HIPK3 induces sensitisization to chemotherapy[31], our findings further indicate HIPK3 as a possible target to impair tumor metastasis.

RAC2 encodes Ras-related C3 botulinum toxin substrate 2 (Rac2), and is a member of Rho family of GTPases that regulate actin cytoskeleton [32]. Rac2 knockout in the tumor stroma is known to regulate tumor growth and metastasis [33] and activating mutations have been identified in human cancer [34]. Previously, Rac2 knockout macrophages were shown to display altered migration and fewer podosomal structures, indicative of increased contractility [35, 36]. Our findings extend these studies: Rac2 is implicated in cancer cell migration and in its absence cell matrix adhesions become static and cellular traction forces at these sites are increased and very stable.

A positive correlation between adhesion size and the magnitude of cellular forces has been reported previously [37–39]. Our results confirm this notion and identify 3 important regulators of these aspects. Interestingly, these regulators also control the dynamics of traction forces: their downregulation leads to decreased force turnover rates. Small dynamic cell matrix adhesions and low dynamic traction forces go hand in hand with an active actin cytoskeleton organization that drives cellular motility. Genes, such as the ones identified here, that regulate these aspects and whose silencing causes a shift to larger adhesions with high stable traction forces causing inhibition of cell migration; encode candidate targets to interfere with tumor metastasis. Since cell motility in 3D environments is highly plastic and may follow a different set of rules [13, 14], it remains to be established what the consequences of their inhibition are under such conditions. Such studies followed by preclinical animal models will have to further establish their potential as cancer drug targets.

5.4 Materials and methods

5.4.1 Cell culture

MCF7 and IGF1R overexpressing MCF7-IGF1R cell lines described previously [40], were grown in RPMI1640 medium supplemented with 10% fetal bovine serum (GIBCO, USA), 25 U/ml penicillin and 25 µg/ml streptomycin (Invitrogen) in a 5% CO2 humidified incubator at 37°C. For visualization of the actin cytoskeleton, cells were transduced using a lentiviral mCherry-LifeAct cDNA expression vector (provided by Dr. Olivier Pertz, University of Basel, Basel, Switzerland), and were cultured in selection medium containing 2 µg/ml puromycin (Acros Organics/Fisher Scientific cat. # 227420500).

5.4.2 Cell transfection with siRNA

A custom designed SMARTpool siRNA library (Dharmacon, Lafayette, CO, USA) targeting 569 genes with known or predicted roles in cell adhesion was used. The siRNAs were diluted with serum free medium (SFM) together with DharmaFECT 4 (Dharmacon). Glass bottom 96-well plates (Greiner Bio-One, Frickenhausen, Germany) were coated with 10 µg/ml Collagen type 1 (isolated from rat tails). A 50 nM reverse transfection was performed according to manufacturer's guidelines. Complex formation time was 20 minutes and 10,000 MCF7 WT cells were added. Transfection was performed in duplicate. Each plate contained negative controls (no siRNA, mock, siGFP (D-001300-01) and non-targeting Control #2 (D-001210-02)), a positive control (si-DNM2) and transfection controls (si-KIF11, si-PXN and si-GLO Green). Plates were placed in the incubator and the medium was refreshed after 20 hours.

Cells were put on overnight serum starvation 32 hours after transfection. The next day, a nocodazole assay was performed, in which cells were exposed to one of three conditions. Cells were exposed either to 0.025% DMSO in starvation medium for 6 hours, or to 10 µM nocodazole (#74151, Fluka, Sigma-Aldrich, St.Louis, MO, USA) in starvation medium for 4 hours, or to 4 hours 10 µM nocodazole followed by a 2 hours washout with 0.025% DMSO in starvation medium. Transfection controls (si-KIF11, si-PXN and si-GLO Green) were not exposed. After treatment, cells were fixed in 4% buffered formaldehyde for 10 minutes, and washed thrice with PBS. Fixed cells were permeabilized

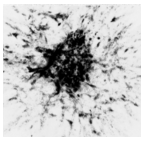

and blocked in TBP (0.1% Triton X-100, 0.5% BSA in PBS), followed by immunostaining for vinculin (V-9131, Sigma-Aldrich), tubulin (T-9026, Sigma-Aldrich) or Rhodamine Phalloidin (Invitrogen/Fisher Scientific cat. number R415), and by secondary antibody conjugated with Alexa488 (Invitrogen/Fisher Scientific cat. number A11008). Hoechst 33258 (Sigma) was used to visualize nuclei.

5.4.3 Automated microscopy

Microscopy was performed on a Nikon Eclipse Ti confocal microscope that included an automated xy-stage, an integrated Perfect Focus System (PFS) and 408, 488 and 561 Argon lasers. The system was controlled by Nikon's EZ-C1 software (version 3.90). Images were acquired using a Plan-Apochromat 20x objective with 0.75 NA, at a resolution of 512 x 512 pixels, with a pixel dwell time of 7 µs and 4x scanner zoom.

For automated imaging, a custom-written macro was used within EZ-C1 that searched for cells, focus on the focal adhesions and acquire an image. Using the Perfect Focus System, the software searches randomly for cells in Hoechst channel (408-laser) until a certain threshold is met, i.e. a number of cells per well (pre-set). The PFS is then turned off, and using a custom autofocus it focuses on the focal adhesions. Once the optimal focus is found, the system acquires the image and then continues with the next position. Between 5 and 8 images per well were acquired.

5.4.4 Image analysis

Image analysis was implemented using ImageJ version 1.43h (http://imagej.nih.gov/ij/). Acquired images were split into the original channels and the nuclei channel was used to remove empty images. The analysis was performed for one channel at a time. First, the image is passed through a Gaussian filter to normalize the CCD signal and a rolling ball is applied to remove noise. Next, segmentation was performed based on a watershed masked clustering algorithm [41]. Cell matrix adhesion features: area, perimeter, extension, dispersion, elongation, orientation, compact factor and average intensity, were obtained for objects larger than 4 pixels.

5.4.5 Random cell migration assay

MCF7-IGF1R cells were used for live cell migration assays. Transfections were performed as described above, with 15,000 cells in a standard 96-well culture plate. After 56 hours, the transfected MCF7-IGF1R cells were replated onto collagen-coated glass bottom plates and were allowed to adhere overnight. Cells were switched to starvation medium and pre-exposed for 45 minutes to 100 ng/ml Hoechst 33342. After refreshing the medium, cells were placed on a Nikon Eclipse Ti microscope fitted with a 37°C incubation chamber, 20x objective (0.75 NA), automated stage and PFS system.

Three positions per well were manually selected, and Differential Interference Contract (DIC) and Hoechst images were captured every 6 to 14 minutes with a DS-Qi1MC CCD camera with 2x2 binning (pixel size: 0.64 µm) for 7 hours using NIS software (Nikon) following stimulation with 100 ng/ml IGF1 (Increlex, Ipsen, Basking Ridge, NJ, USA). All images were sorted using custom-made R-scripts (R Foundation for Statistical Computing, Vienna, Austria). Image analysis was performed using CellProfiler (Broad Institute [42]). Briefly, images were segmented using a watershed masked clustering algorithm, after which cells were tracked based on overlap between frames. Tracking data was organized and analyzed using in-house developed R-scripts [43] to obtain single cell migration data. Single cell migration speeds were plotted using GraphPad Prism 6.0 (GraphPad Software, La Jolla, CA, USA) and changes in migration speed were evaluated by comparing cell populations (Kruskal-Wallis with Dunn's multiple comparisons post-test). For all live microscopy, experiments were performed in duplicate and results were considered significant if p-value < 0.05 for all experiments.

Visualization and analysis of cell matrix adhesions was performed as described for nocodazole assay.

5.4.6 Traction force microscopy with silicon elastomeric micropillar post arrays

MCF7-IGF1R-mCherry-LifeAct cells were transfected with siRNAs as described above. After 65h, cells were used for micropillar experiments, according to methodology described previously [44]. Nanolithography with PDMS was performed to create pillars of 4.1 µm height, 2 µm diameter, 4 µm center-to-center distance in a hexagonal lattice with spac-

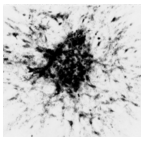

ers on the side. Pillars were calculated to have a bending stiffness of 65.8 nN/µm and an effective Young's modulus of 47.2 kPa [44]. ECM stamping was performed using a flat piece of PDMS preincubated with a 40 µl mix of [50 µg/mL unlabeled fibronectin (Sigma Aldrich) and 10 µg/mL Alexa647 (Invitrogen)-conjugated fibronectin]. Following blocking with 0.2% Pluronic (F-127, Sigma Aldrich) in PBS for 1 hour, cells were pipetted on the pillar array and were incubated for 2 hours in complete medium, and 3 hours in serum starved medium. For imaging, the pillars, with cells on top, were placed upside down in a 24 well glass bottom plate (Greiner Bio-One), mounted on a Nikon Eclipse Ti microscope, stimulated with 100 ng/mL IGF1 and imaged every 5 minutes for 400 minutes in scanning confocal mode together with a 20x magnification 0.75 NA dry air lens with internal 1.5 x magnification and 4.184 scanner zoom to obtain a pixel size of 0.2 µm.

Forces were calculated with approximately 2 nN precision from the pillar channel using specifically designed Matlab scripts (Mathworks, Natick, MA, USA) as described previously [44]. Briefly, deflections of individual pillars were calculated by relating the exact pillar locations determined from the labeled fibronectin fluorescence image to the calculated reference undeflected hexagonal grid. Movies were generated and manually checked for movies with deflections that had high signal-to-noise ratio and to remove cells that died or divided. Cell masks were generated from the mCherry-LifeAct channel by first passing the image through a Gaussian low pass filter, subtracting the background intensity and running the image through a sobel and a log-edge detection algorithm followed by image dilation and hole filling each time. Pillars were followed through the movie with in-house written Matlab script that matched pillars in subsequent frames (or 2 frames apart if a match was not found in first iteration) that were closer than 2 µm. This enabled tracking more than 90% of the pillars for the duration of the movie. Pillars that showed the top 5% deflection for the duration of the imaging and were coupled to cells were taken for further analysis. Average force per pillar was determined by averaging the pillar deflections for the whole duration of the movie for all selected cells. Autocorrelation was calculated for top 5% deflected pillars per movie using Matlab acorr function, averaged per condition and an exponential function was fit for the first 2 hours (25 data points) to obtain the half time.

5.4.7 Statistic analysis

Significance was calculated according to the method indicated at individual figure legends using GraphPad Prism 6.0.

5.5 Acknowledgements

We thank Olivier Pertz for providing the mCherry-LifeAct construct; Kees van Oord for developing an automated FA imaging macro for EZ-C1; Hans de Bont for technical assistance with live microscopy; Sandra Zovko for help with IF staining and study design; and Sylvia Le Dévédec for her helpful comments on the manuscript. This work was financially supported by grants from the EU FP7 Health Programs MetaFight project (grant agreement 201862) to B. van de Water; Systems Microscopy NoE project (grant agreement 258068) to B. van de Water; and the Netherlands Organization for Scientific Research NWO-FOM (grant number 09MMC03 to H.E.B.).

5.6 Authors' contribution

MF, HEB, EHJD and BvdW designed the research and wrote the manuscript. MF, HEB and JEK performed the experiments and analyses. KY and FJV established the FA image analysis tools.

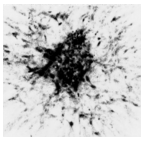

5.7 Supplemental figures

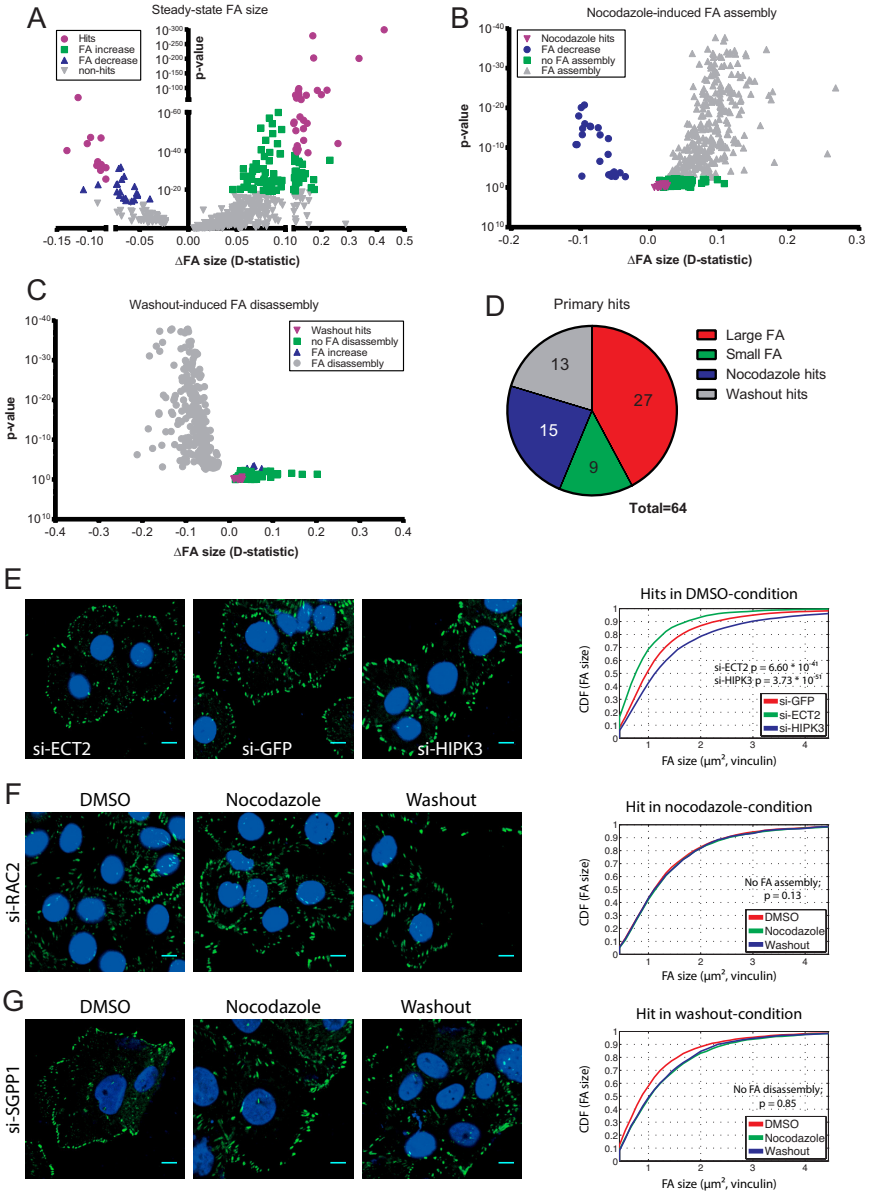

Figure S1
RNAi screen identifies novel regulators of cell matrix adhesion dynamics.

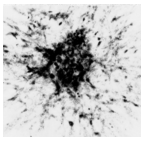

Figure S1

RNAi screen identifies novel regulators of cell matrix adhesion dynamics. *A, Cell matrix adhesion size distributions after siRNA knockdown in DMSO condition were compared to siGFP control cells. The shift in size distribution (D-statistic) is used as a measurement of change in adhesion size. A decrease in adhesion size is shown in blue and an increase in size in green. Hits remaining after stringent thresholding are shown in purple. B, Cell matrix adhesion size of siRNA knockdown cells in nocodazole condition was compared to DMSO of the same siRNA, to detect impaired adhesion assembly. siRNAs that show no change in FA size were considered as hits (purple). C, Cell matrix adhesion size of siRNA knockdown cells in washout condition was compared to nocodazole of the same siRNA, to detect impaired adhesion disassembly. siRNAs that show no change in adhesion size were considered as hits (purple). D, In total 64 hits were found to affect cell matrix adhesion morphology under steady state conditions (red and green), or to specifically impair adhesion assembly (blue) or disassembly (grey). E, Example images of adhesion size decrease (si-ECT2) and increase (si-HIPK3) after siRNA knockdown in DMSO condition. Quantification of adhesion size is shown on the right. F, Loss of RAC2 inhibited cell matrix adhesion assembly. Quantification of adhesion size shows identical distributions in the different conditions. G, Knockdown of SGPP1 impaired adhesion disassembly. Quantification of adhesion sizes confirms no change in washout condition compared to nocodazole.*

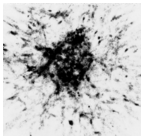

Bibliography

[1] Anne J Ridley et al. "Cell migration: Integrating signals from front to back". In: *Science (New York, N.Y.)* 302.5651 (2003).

[2] Daniela Quail and Johanna Joyce. "Microenvironmental regulation of tumor progression and metastasis". In: *Nature Medicine* 19.11 (2013).

[3] Bartlomiej Waclaw et al. "A spatial model predicts that dispersal and cell turnover limit intratumour heterogeneity". In: *Nature* 525.7568 (2015).

[4] Amardeep S Dhillon et al. "MAP kinase signalling pathways in cancer". In: *Oncogene* 26.22 (2007).

[5] Ana M Gonzalez-Angulo et al. "PI3K pathway mutations and PTEN levels in primary and metastatic breast cancer". In: *Molecular Cancer Therapeutics* 10.6 (2011).

[6] Cai Huang, Ken Jacobson, and Michael D Schaller. "MAP kinases and cell migration". In: *Journal of Cell Science* 117.20 (2004).

[7] J Thomas Parsons, Alan R Horwitz, and Martin A Schwartz. "Cell adhesion: integrating cytoskeletal dynamics and cellular tension." In: *Nature Reviews. Molecular Cell Biology* 11.9 (2010).

[8] Christophe Clainche and Marie-France Carlier. "Regulation of actin assembly associated with protrusion and adhesion in cell migration". In: *Physiological Reviews* 88.2 (2008).

[9] Corina Sarmiento et al. "WASP family members and formin proteins coordinate regulation of cell protrusions in carcinoma cells". In: *The Journal of Cell Biology* 180.6 (2008).

[10] Benjamin Geiger, Joachim Spatz, and Alexander Bershadsky. "Environmental sensing through focal adhesions". In: *Nature Reviews Molecular Cell Biology* 10.1 (2009).

[11] Hideki Yamaguchi and John Condeelis. "Regulation of the actin cytoskeleton in cancer cell migration and invasion". In: *Biochimica et Biophysica Acta (BBA) - Molecular Cell Research* 1773.5 (2006).

[12] Sandrine Etienne-Manneville. "Microtubules in cell migration". In: *Cell and Developmental Biology* 29.1 (2012).

[13] Ryan J Petrie et al. "Nonpolarized signaling reveals two distinct modes of 3D cell migration". In: *The Journal of Cell Biology* 197.3 (2012).

[14] Peter Friedl et al. "New dimensions in cell migration." In: *Nature Reviews. Molecular Cell Biology* 13.11 (2012).

[15] Hoa H Truong et al. "β1 integrin inhibition elicits a prometastatic switch through the TGFβ-miR-200-ZEB network in E-cadherin-positive triple-negative breast cancer". In: *Science Signaling* 7.312 (2014).

[16] Martin Bergert et al. "Force transmission during adhesion-independent migration." In: *Nature Cell Biology* 17.4 (2015).

[17] Aaron S Meyer et al. "2D protrusion but not motility predicts growth factor–induced cancer cell migration in 3D collagen". In: *The Journal of Cell Biology* 197.6 (2012).

[18] Ellen J Ezratty, Michael A Partridge, and Gregg G Gundersen. "Microtubule-induced focal adhesion disassembly is mediated by dynamin and focal adhesion kinase." In: *Nature Cell Biology* 7.6 (2005).

[19] Wei-Ting Chao and Jeannette Kunz. "Focal adhesion disassembly requires clathrin-dependent endocytosis of integrins". In: *FEBS Letters* 583.8 (2009).

[20] Peter Gunning, Geraldine O'neill, and Edna Hardeman. "Tropomyosin-based regulation of the actin cytoskeleton in time and space". In: *Physiological Reviews* 88.1 (2008).

[21] Hua-Qing Q Du et al. "Silencing of the TPM1 gene induces radioresistance of glioma U251 cells." In: *Oncology Reports* 33.6 (2015).

[22] Qiao Zheng, Alfiya Safina, and Andrei V Bakin. "Role of high-molecular weight tropomyosins in TGF-β-mediated control of cell motility". In: *International Journal of Cancer* 122.1 (2008).

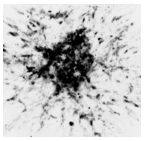

[23] Syamalima Dube et al. "Expression of tropomyosin 1 gene isoforms in human breast cancer cell lines". In: *International Journal of Breast Cancer* 2015 (2015).

[24] Hideaki Fujita et al. "The effect of tropomyosin on force and elementary steps of the cross-bridge cycle in reconstituted bovine myocardium". In: *The Journal of Physiology* 556.2 (2004).

[25] Audrey Chang et al. "Constitutive phosphorylation of cardiac myosin regulatory light chain in vivo". In: *Journal of Biological Chemistry* 290.17 (2015).

[26] Takuro Arimura et al. "Identification, characterization, and functional analysis of heart-specific myosin light chain phosphatase small subunit". In: *Journal of Biological Chemistry* 276.9 (2001).

[27] Ryuji Okamoto et al. "Characterization and function of MYPT2, a target subunit of myosin phosphatase in heart." In: *Cellular Signalling* 18.9 (2006).

[28] Véronique Rochat-Steiner et al. "FIST/HIPK3: a Fas/FADD- interacting serine/threonine kinase that induces FADD phosphorylation and inhibits fas-mediated Jun NH(2)-terminal kinase activation." In: *The Journal of Experimental Medicine* 192.8 (2000).

[29] Nobuhiro Shojima et al. "Depletion of homeodomain-interacting protein kinase 3 impairs insulin secretion and glucose tolerance in mice". In: *Diabetologia* 55.12 (2012).

[30] James F Curtin and Thomas G Cotter. "JNK Regulates HIPK3 expression and promotes resistance to Fas-mediated apoptosis in DU 145 prostate carcinoma cells". In: *Journal of Biological Chemistry* 279.17 (2004).

[31] Meng Xu et al. "miR-382 inhibits tumor growth and enhance chemosensitivity in osteosarcoma." In: *Oncotarget* 5.19 (2014).

[32] Anne J Ridley. "Rho GTPases and actin dynamics in membrane protrusions and vesicle trafficking". In: *Trends in Cell Biology* 16.10 (2006).

[33] Shweta Joshi et al. "Rac2 controls tumor growth, metastasis and M1-M2 macrophage differentiation in vivo." In: *PLoS One* 9.4 (2014).

[34] Masahito Kawazu et al. "Transforming mutations of RAC guanosine triphosphatases in human cancers." In: *Proceedings of the National Academy of Sciences of the United States of America* 110.8 (2013).

[35] Ann P Wheeler et al. "Rac1 and Rac2 regulate macrophage morphology but are not essential for migration". In: *Journal of Cell Science* 119.13 (2006).

[36] Cheng-han Yu et al. "Integrin-matrix clusters form podosome-like adhesions in the absence of traction forces". In: *Cell Reports* 5.5 (2013).

[37] Nathalie Q Balaban et al. "Force and focal adhesion assembly: a close relationship studied using elastic micropatterned substrates". In: *Nature Cell Biology* 3.5 (2001).

[38] Hedde van Hoorn et al. "The nanoscale architecture of force-bearing focal adhesions". In: *Nano Letters* 14.8 (2014).

[39] Léa Trichet et al. "Evidence of a large-scale mechanosensing mechanism for cellular adaptation to substrate stiffness". In: *Proceedings of the National Academy of Sciences of the United States of America* 109.18 (2012).

[40] Yinghui Zhang et al. "Elevated insulin-like growth factor 1 receptor signaling induces antiestrogen resistance through the MAPK/ERK and PI3K/Akt signaling routes". In: *Breast Cancer Research* 13.3 (2011).

[41] Zi Di et al. "Automated analysis of NF-KB nuclear translocation kinetics in high-throughput screening". In: *PLoS One* 7.12 (2012).

[42] Anne E Carpenter et al. "CellProfiler: image analysis software for identifying and quantifying cell phenotypes". In: *Genome Biology* 7.10 (2006).

[43] Steven Wink et al. "Quantitative high content imaging of cellular adaptive stress response pathways in toxicity for chemical safety assessment". In: *Chemical Research in Toxicology* 27.3 (2014).

[44] Hayri E Balcıoğlu et al. "The integrin expression profile modulates orientation and dynamics of force transmission at cell-matrix adhesions." In: *Journal of Cell Science* 128.7 (2015).

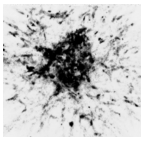

Chapter 6

General Discussion

Cells and their surrounding extracellular matrix (ECM) form a continuous network that is in constant homeostasis. This dynamic equilibrium requires complex cellular feedback mechanisms including force feedback loops. The ability of cells to sense and respond to the mechanical cues from their environment and, vice versa, to apply forces onto their environment is called cellular mechanotransduction and has been implicated in both physiological and pathological conditions. The work in this thesis is aimed at elucidating the different cellular mechanisms that take role in cellular mechanotransduction. I mainly focused on integrin mediated cell-matrix adhesions that are known to play a critical role in this process [1] (chapter 1).

Studying cell matrix adhesions in different dimensionalities In order to address the role of the cell-matrix adhesions in different contexts we made use of several techniques. 3D spheroid cultures allowed elucidation of the role of mechanotransduction at tissue level; whereas polyacrylamide gels with tunable stiffness and a cyclic cell stretcher allowed the study of the role of mechanical cues in cell function, and elastomeric PDMS micropillars with tunable stiffness allowed for measurements of cell traction forces.

In addition to developing state-of-the-art experimental techniques, extensive data (e.g. image) analysis was required. For this purpose,

scripts were written to recognize cells, nuclei, cell matrix adhesions, actin cables, collagen fibers, and determine aspects such as size and orientation. Additional computational analysis tools were developed for quantitative image analysis using information from PDMS micropillar displacements and dSTORM. Together these advances and implementations made it possible to perform this research and study the role of cell-matrix adhesions in cellular mechanotransduction.

How does the integrin composition of cell-matrix adhesions affect cellular mechanotransduction?
Alterations in expression levels of integrins have been previously related to activation of distinct cellular signaling mechanisms [2, 3] and (breast) cancer metastasis [4, 5]. It has also been shown that different integrins (e.g. those containing αv or β1 subunits) play distinct roles in generation of cellular traction forces [3, 6]. In chapter 3, we show that cells adhering to fibronectin either through integrin αvβ3 or α5β1 apply comparable levels of traction forces and are able to sense differences in environment stiffness. This appears in contrast to an earlier report showing that the complementary regulation of myosin II activity and mDia-mediated actin polymerization by these two integrins is required for rigidity sensing [3]. One way in which our work differs from this study is the fact that we expressed these integrin to levels supporting similar adhesion efficiency instead of equimolar levels. Moreover, all cells used in our model expressed some level of αv, providing a very different model system from the one used by Schiller et al [3].

We find that the integrin expression profile affects the orientation, rather than the amplitude of traction forces (chapter 3). This is accompanied by differential regulation of cytoskeletal architecture through the activity of Rho-ROCK signaling. Our findings demonstrate that cells, via altering integrin composition of their adhesions, are able to tune their inside-out force generation and outside-in force sensing possibly through Rho GTPase signaling pathways. We observe that expression of β1 integrins supports formation of long actin filaments resulting in higher centripetal orientation of forces, whereas expression of αvβ3 supports formation of shorter actin fibers, more random traction forces, and it allows cells to more robustly respond to external mechanical cues; e.g. more effective reorganization of actin cytoskeleton upon cyclic stretch and cell spreading and adhesion formation at softer substrates. Interestingly, αvβ3 frequently emerges with cancer invasion and tumor angiogenesis

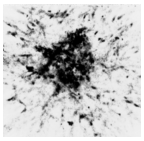

[7]. The distinct properties of this integrin in regulation of mechanotransduction as identified by us, may contribute to these aspects of cancer progression.

Regulation of the molecular composition of cell matrix adhesions with traction force application

The relationship between the molecular composition of cell matrix adhesions and force has not been unraveled. In chapter 4 of this thesis, localization analysis of super resolution images obtained with direct stochastic reconstruction microscopy (dSTORM) allowed us to quantify the number of talin, paxillin, vinculin and focal adhesion kinase (FAK) molecules in cell matrix adhesions. By combining this method with traction force microscopy we were able to obtain a quantitative relationship between the molecular composition of the adhesion and force application. We observed that there was a 1:2:2 relation with force induced recruitment of talin:paxillin:vinculin molecules on a relatively stiff substrate, whereas no relation was observed between force application and number of FAK molecules. Given the role of talin, paxillin, vinculin and FAK in transducing the force from integrins to the actin cytoskeleton [8] as well as their role in regulating the actin cytoskeleton by signaling through RhoGTPases [9], these findings indicate that changes in force levels alter adhesion mediated signaling and actin mediated force feedback control.

It has been shown that phosphorylation of paxillin and FAK as well as the interaction between and talin and vinculin are force dependent [10–12]. Combined with these findings, our data indicates that FAK phosphorylation rather than FAK recruitment is related to increased traction forces. Interestingly, lowering the stiffness of the substrate leads to dramatic change in the stoichiometry of the investigated proteins within adhesions and we show that this is mainly due to a reduced force associated with vinculin. This demonstrates that environmental stiffness modulates the relation between traction forces and the molecular composition of cell matrix adhesions. Others have demonstrated that vinculin can be recruited by paxillin without vinculin activation or by talin, leading to vinculin activation and binding to actin fibers [13]. Together with our findings, this suggests that soft substrates support force-induced vinculin-paxillin interaction leading to a pool of inactive vinculin molecules. Instead, more rigid substrates support force-induced talin-vinculin interaction leading to vinculin activation and coupling to the actin cytoskeleton and hence, a much higher force induction per re-

cruited vinculin (in chapter 1 force dependent vinculin-talin and vinculin-paxillin interactions are discussed in more detail).

We investigated a small subset of cell matrix adhesion proteins. Other molecular force sensors, including the integrins, are also present in cell-matrix adhesions as discussed in chapter 1 of this thesis. In order to fully understand the underlying molecular regulation of force-feedback control, force dependent abundance and activity of all these proteins as well as other possible candidates need to be addressed. Where antibodies are available, our dSTORM-based approach can be applied and results may be integrated with current ongoing proteomics analyses of cell matrix adhesions [14] in order to get an overview of cell matrix adhesion dynamics in relation to traction force. This is highly relevant as alterations in force feedback mechanisms can result in- and drive pathologies.

Quantification of molecules from dSTORM images: the next step in super resolution microscopy?
The method we used in chapter 4 to obtain the number of molecules from the dSTORM image can be readily applied to any super resolution image given that there is significant signal amplification (i.e. multiple localizations observed per protein). In chapter 4 we addressed any possible shortcoming or error in quantifying the number of molecules with our method apart from possible antibody under-labeling. Having used high concentrations of both primary and secondary antibodies, we believe that the numbers we reported are the best estimates possible with current technologies.

As dSTORM can be performed with commercially available antibodies no genome editing is necessary for application of our method. Therefore it does not suffer from risks associated with gene tagging such as alterations in protein localization, activity, and expression levels. Additionally, since the effect of labeling and photophysics on different localizations obtained during one acquisition cycle will be theoretically the same, and our method only relies on the positional information, it can readily be applied to the localization distributions without any prior knowledge of the setup used. Lastly, and uniquely to our approach, the fraction of a given protein in a given area (e.g. a cell matrix adhesion) undergoing certain post-translational modifications (e.g. protein phosphorylation and ubiquitination) can be addressed with this technique by using general and modification-specific antibodies against a protein of interest.

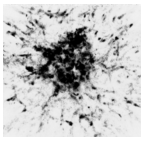

Consequences of cellular force application for cancer progression- remote collagen network orientation

The complex interplay between tumor cells, tumor stroma and the surrounding extracellular matrix (ECM) has been shown to play an essential role in tumor progression [15]. In chapter 2 we observe that tumor cells orient a collagen network through ROCK mediated contractility. Expression of β1 integrins and ROCK signaling has been implicated in tumor progression through matrix crosslinking [16]. Here, in agreement with earlier reports from others and us [4, 5], depletion of β1 integrins has very different effects depending on the cell type. Our findings suggest a direct relation between tumor expansion/cell migration and collagen reorganization that is not determined by the expression of β1 integrins. Other collagen receptors (e.g. syndecans and discoidin domain collagen receptors) or integrins binding to other ECM proteins might be important for this relation instead.

Previously, isolated cells have been shown to sense the presence of other cells up to ∼100 µm in collagen environments [17]. This was attributed to the alignment of fibrous collagen matrix induced by the cells. In our system we observed distant orientation of the collagen up to 2.5 mm. This distant orientation of collagen cannot be explained by local cellular secretion or degradation of collagen as the length scale over which we observe collagen orientation is way beyond tumor expansion areas, up to 5 times the tumor radius. This indicates that propagation of forces applied by the multicellular tumor spheroids over long distances through the fibrous collagen environment drives remote collagen alignment.

Consequences of cellular force application for cancer progression- a role for remote collagen network orientation in tumor angiogenesis?

Chemical signaling, mainly vasculature endothelial growth factor (VEGF) signaling, and its crosstalk with physical signaling have been studied in angiogenesis. It has been shown that physical cell-ECM interaction affects cellular response to VEGF [18, 19] as well as regulating VEGF expression [20, 21]. Additionally the physical properties of the matrix can alter the sprouting response to VEGF stimulation [22]. Our findings in chapter 2 further indicate that the physical signaling from the tumor cells can promote long distance directional tumor-angiogenesis. How this physical signaling compliments or controls VEGF chemical signaling remains unknown. Blocking VEGF receptor signaling or inducing

VEGF gradients in combination with sequential printing of tumor and endothelial cells in ECM scaffold can be used to address this question. Still, in chapter 2 we show that disruption of the mechanical connection between the primary tumor and the vasculature cells is sufficient to impair the directionality of vasculature cells. *In vivo*, such physical signaling by the tumor may help guide angiogenesis and thereby promote cancer progression. Therefore, interfering with mechanical tumor-ECM communication is a promising candidate approach to interfere with multiple aspects of progression including cancer growth, invasion, as well as tumor-angiogenesis.

Common signaling pathways regulating cell migration, adhesion size and cellular traction forces

In chapter 5, using 2D screens we identified 11 candidate adhesome genes that regulate cell migration and adhesion dynamics. Performing time-lapse force measurements on 4 of these candidates has shown that in addition to causing impaired cell migration and larger cell-matrix adhesions, knockdown of these genes resulted in a general trend for increased traction forces and slower force turnovers. The relation of force to adhesion size and migration has been also studied previously [23, 24]. The family of Rho GTPases and downstream ROCK signaling might play an essential role in this relation as the orchestrators of actin cytoskeleton. In chapter 2 of this thesis we have shown that high ROCK activity, in addition to formation of longer actin fibers and centripetal force generation in cells discussed in chapter 3, supports tumor expansion and tumor induced collagen reorganization. In chapter 5 we further show that high traction forces and slow force turnover, which suggest high ROCK activity, is observed in combination with impaired cell migration. Our findings together indicate that cell migration, adhesion formation and force generation are interrelated and ROCK signaling has an important role in this relation.

Concluding remarks

It follows from Newton's law of motion that force generation is essential for cell migration. Even in assays where anchorage independent migration of cells was characterized, the force generation mechanism has been shown to be necessary for cell motility [25]. Hence it is not surprising to see the altered adhesion structures, cell migration and force application being related. Rho GTPases can regulate all three of these cellular mechanisms and focusing on the cell protrusions shows how Rho GTPases can

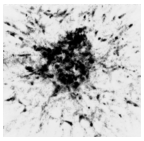

be dynamically mediated in a molecular level [26]. This regulation, together with other signaling pathways, controls mechanosensing at the molecular and multicellular level and plays an important role in both physiological and pathological conditions. With the work presented in this thesis, further understanding of molecular signaling in control of cellular mechanosensing as well as the role of mechanosensing in cancer has been achieved.

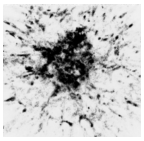

Bibliography

[1] Benjamin Geiger, Joachim Spatz, and Alexander Bershadsky. "Environmental sensing through focal adhesions". In: *Nature Reviews. Molecular Cell Biology* 10.1 (2009).

[2] Erik H J Danen et al. "The fibronectin-binding integrins α5β1 and αvβ3 differentially modulate RhoA-GTP loading, organization of cell matrix adhesions, and fibronectin fibrillogenesis". In: *The Journal of Cell Biology* 159.6 (2002).

[3] Herbert B Schiller et al. "β1- and αv-class integrins cooperate to regulate myosin-II during rigidity sensing of fibronectin-based microenvironments". In: *Nature Cell Biology* 15.6 (2013).

[4] Jenny G Parvani et al. "Targeted inactivation of β1 integrin induces β3 integrin switching, which drives breast cancer metastasis by TGF-β". In: *Molecular Biology of the Cell* 24.21 (2013).

[5] Hoa H Truong et al. "β1 integrin inhibition elicits a prometastatic switch through the TGFβ-miR-200-ZEB network in E-cadherin-positive triple-negative breast cancer." In: *Science Signaling* 7.312 (2014).

[6] Grace L Lin et al. "Activation of β1 but not β3 integrin increases cell traction forces". In: *FEBS Letters* 587.6 (2013).

[7] Jay S Desgrosellier and David A Cheresh. "Integrins in cancer: biological implications and therapeutic opportunities." In: *Nature Reviews. Cancer* 10.1 (2010).

[8] Cord Brakebusch and Reinhard Fässler. "The integrin-actin connection, an eternal love affair". In: *The EMBO Journal* 22.10 (2003).

[9] Stephan Huveneers and Erik H J Danen. "Adhesion signaling - crosstalk between integrins, Src and Rho". In: *Journal of Cell Science* 122.8 (2009).

[10] Ana M Pasapera et al. "Myosin II activity regulates vinculin recruitment to focal adhesions through FAK-mediated paxillin phosphorylation." In: *The Journal of Cell Biology* 188.6 (2010).

[11] Armando del Rio et al. "Stretching Single Talin Rod Molecules Activates Vinculin Binding". In: *Science (New York, N.Y.)* 323.5914 (2009).

[12] Jihye Seong et al. "Distinct biophysical mechanisms of focal adhesion kinase mechanoactivation by different extracellular matrix proteins." In: *Proceedings of the National Academy of Sciences of the United States of America* 110.48 (2013).

[13] Lindsay B Case et al. "Molecular mechanism of vinculin activation and nanoscale spatial organization in focal adhesions." In: *Nature Cell Biology* 17.7 (2015).

[14] Edward Horton et al. "Mechanosensitivity of integrin adhesion complexes: role of the consensus adhesome". In: *Experimental Cell Research* (2015).

[15] Michael W Pickup, Janna K Mouw, and Valerie M Weaver. "The extracellular matrix modulates the hallmarks of cancer". In: *EMBO Reports* 15.12 (2014).

[16] Kandice R Levental et al. "Matrix crosslinking forces tumor progression by enhancing integrin signaling". In: *Cell* 139.5 (2009).

[17] Xiaoyue Ma et al. "Fibers in the Extracellular Matrix Enable Long-Range Stress Transmission between Cells". In: *Biophysical Journal* 104.7 (2013).

[18] Anthony Ambesi and Paula J McKeown-Longo. "Conformational remodeling of the fibronectin matrix selectively regulates VEGF signaling". In: *Journal of Cell Science* 127.17 (2014).

[19] Akiko Mammoto et al. "A mechanosensitive transcriptional mechanism that controls angiogenesis." In: *Nature* 457.7233 (2009).

[20] Yinying Dong et al. "Increasing matrix stiffness upregulates vascular endothelial growth factor expression in hepatocellular carcinoma cells mediated by integrin β1". In: *Biochemical and Biophysical Research Communications* 444.3 (2014).

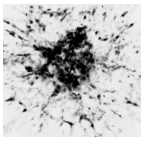

[21] Nicolas C Rivron et al. "Tissue deformation spatially modulates VEGF signaling and angiogenesis". In: *Proceedings of the National Academy of Sciences of the United States of America* 109.18 (2012).

[22] Amir Shamloo and Sarah C Heilshorn. "Matrix density mediates polarization and lumen formation of endothelial sprouts in VEGF gradients". In: *Lab on a Chip* 10.22 (2010).

[23] Nathalie Q Balaban et al. "Force and focal adhesion assembly: a close relationship studied using elastic micropatterned substrates". In: *Nature Cell Biology* 3.5 (2001).

[24] Myriam Reffay et al. "Interplay of RhoA and mechanical forces in collective cell migration driven by leader cells". In: *Nature Cell Biology* 16.3 (2014).

[25] Martin Bergert et al. "Force transmission during adhesion-independent migration." In: *Nature Cell Biology* 17.4 (2015).

[26] Matthias Machacek et al. "Coordination of Rho GTPase activities during cell protrusion". In: *Nature* 461.7260 (2009).

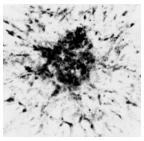

Summary

Role of integrin adhesions in cellular mechanotransduction

The ability of cells to translate between extracellular mechanical cues and intracellular signals is called cellular mechanotransduction. Cellular mechanotransduction plays an important role in cell survival, differentiation, migration and cancer progression. Mechanotransduction consists of inside-out and outside-in signaling. Outside-in signaling consists of cells sensing the mechanical cues from the environment and regulating intracellular signaling pathways accordingly. Whereas inside-out signaling is cells changing the mechanical properties of their environment through application of traction forces or secretion of extracellular material. Through these mechanisms cells are able to maintain a dynamic mechanical equilibrium with their environment. The misregulation of this equilibrium is observed frequently in pathologies such as cancer and fibrosis.

Integrin transmembrane proteins physically connect the extracellular matrix to intracellular multimolecular complexes called cell-matrix adhesions. Cell-matrix adhesions and associated proteins have been widely studied in close relation to cellular mechanotransduction. Some of these proteins take part in intracellular-extracellular force transduction by connecting integrins to the actin cytoskeleton and others respond to mechanical stress. These proteins change their activities or open cryptic interaction sites and hence induce mechanotransduction by changing their chemical activities upon physical stimuli. In this thesis I worked on the role of cellular mechanotransduction in cancer and proteins that affect mechanotransduction. I specifically focused on integrins and other integrin associated proteins.

In **chapter 2** my findings on role of mechanotransduction in cancer progression are shown. This was studied *in vitro* by microprinting tumor

cells to form spheroids (tumoroids) in 3D collagen gel and monitoring both tumor expansion and collagen organization over a course of several days. You may observe the expansion of such a tumoroid at the left bottom of the even pages of this thesis. The studies where I used more than 20 different tumor cell lines indicated that the ability to expand and locally invade into the collagen correlated with an ability to remotely reorganize the surrounding collagen. Remote organization of collagen was observed up to five times the tumoroid expansion area. Vascular cells that were printed in these areas of collagen organization showed directional migration towards the tumoroid. Ablation of the physical contact between the tumoroid and the oriented collagen network abolished this response. In conclusion, in this chapter I have shown that the physical communication of tumor cells with their environment can affect both tumor expansion and tumor angiogenesis.

In **chapter 3** the effect of integrin expression profiles on cellular mechanotransduction is studied. Cells binding to the extracellular matrix protein fibronectin showed differential inside-out and outside-in mechanotransduction depending on the predominant receptor being α5β1 or αvβ3. Expression of the latter integrin emerges during active cellular processes, e.g. on endothelial cells during angiogenesis. Even though cells were able to apply traction forces of similar magnitude and increase their areas comparably with increasing environment stiffness, cells that expressed higher levels of α5β1 prominently showed longer actin fibers and a higher fraction of centripetally oriented forces. Upon treatment with inhibitors that resulted in reduced actin fiber length, the force orientation was also reduced, which resembled the phenotype of the cells expressing higher levels of αvβ3. In contrast, cells binding to fibronectin mainly through αvβ3 showed more effective actin cytoskeleton reorganization upon application of extracellular forces as well as cell-matrix adhesion formation on softer substrates.

In **chapter 4** the relationship between the amounts of cell-matrix adhesion proteins with the applied forces is studied. In previous studies several proteins that affect cellular traction forces have been identified, but to my knowledge there are no studies on the abundance of these proteins in the adhesions. In this chapter, studies on talin, vinculin, paxillin and focal adhesion kinase are shown. These proteins have been shown to be important for integrin-actin cytoskeleton connections and biochemical signals controlling the actin cytoskeleton. These proteins

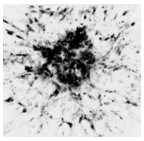

were immunostained, and studied in nanoscale resolution with super resolution techniques. From these high-resolution images, the interlocalization spacing was statistically analyzed and information with regard to number of molecules in a designated area was obtained. Using this technique, the abundance of proteins in cell-matrix adhesions was calculated. By combining this technology with traction force microscopy, this information was related to local forces applied by these adhesions on substrates of varying rigidities. No relation between the number of focal adhesion kinase molecules and force application was observed. However, higher numbers of talin, vinculin and paxillin molecules were related with larger forces. An increase of ∼60 pN on a substrate of ∼50 kPa was related with recruitment of 1 talin, 2 vinculin and 2 paxillin molecules in the adhesion. On a substrate of four times lower stiffness, the same increase in force was associated with 2 talin, 12 vinculin and 6 paxillin molecules. Here, the marked change in vinculin recruitment points to a stiffness-dependent switch in function. In conclusion, in this chapter the relation of the local abundance of cell matrix adhesion proteins and force applied by that adhesion is shown for the first time.

In **chapter 5**, studies on proteins that affect cancer cell migration, cell-matrix adhesions and cellular force application are shown. For this purpose, siRNA knockdowns were performed and the resulting effects on breast cancer cells were studied. More than 200 proteins were identified to influence cell-matrix adhesion dynamics and size. The most effective 64 proteins were tested for their effect on cell migration and 11 were shown to significantly influence cell migration. Finally, four of these proteins, encoded by genes *TPM1*, *PPP1R12B*, *HIPK3* and *RAC2*, were further studied for their role in cellular force application. Silencing *PPP1R12B*, *HIPK3* and *RAC2* resulted in increased cellular force application and reduced force turnover at adhesions. Silencing of *TPM1* did not significantly affect cellular forces. Taken together, genes encoding proteins that regulate cancer cell migration, cell-matrix adhesions and cellular force application have been identified.

Overall, the work described in this thesis unravels the role of cellular mechanotransduction in different aspects of cancer progression and reveals how the molecular composition of cell-matrix adhesions relates to traction force generation.

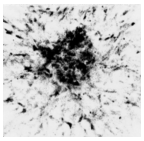

Özet

İntegrin bağlantılarının hücrenin mekanik dönüştürmesindeki rolü

Hücrelerin ekstrasellüler mekanik iletileri ve intrasellüler kimyasal sinyalleri birbirine dönüştürmesine mekanik dönüştürme denir. Mekanik dönüştürme, hücrenin yaşamını sürdürmesinde, farklılaşmasında, embriyonik göçte ve kanser gelişmesinde önemli rol oynar. Mekanik dönüştürme dıştan-içe ve içten-dışa olmak üzere ikiye ayrılır. Dıştan içe mekanik dönüştürmede, hücreler hücre dışı mekanik iletileri sezer ve bu iletileri hücre içi kimyasal sinyallere çevirir. İçten dışa mekanik dönüştürmede ise hücreler hücre dışı proteinleri çekerek veya hücre dışına protein salgılayarak hücre dışı ortamın fiziksel özelliklerini değiştirirler. Hücresel mekanik dönüştürme sayesinde hücreler ortamlarıyla dinamik bir fiziksel denge içerisinde bulunurlar. Bu dengenin bozulmasına kanserde ve lif dejenerasyonunda sıkça rastlanır.

İntegrin transmembran proteinleri, hücrelerarası madde proteinlerini fiziksel olarak hücre-matriks bağlantısı olarak adlandırılan hücre içi çok moleküllü komplekslere bağlarlar. Hücre matriks bağlantıları mekanik dönüştürmede önemli proteinlere ev sahipliği yapar. Bu proteinlerin bir kısmı integrinleri fiziksel olarak hücre iskeletine bağlayarak hücre içi - hücre dışı mekanik iletişiminde rol oynarlar. Bazı proteinler ise mekanik hassasiyet gösterir. Uygulanan kuvvet karşısında proteinlerin aktivitesi değişebilir ya da daha önce gizli olan etkileşim bölgeleri ulaşılır hale gelebilir. Bu mekanizmalar sayesinde proteinler fiziksel sinyal ile kimyasal aktivitelerini değiştirerek mekanik dönüştürmede etkili olurlar. Bu tezde hücresel mekanik değiştirmenin kanserdeki önemi ve mekanik değiştirmeyi etkileyen proteinler üzerine çalışıldı. Bahsedilen proteinlerden özellikle mekanik dönüştürmede önemli olması beklenen integrin proteini ve onunla ilişkili bazı diğer proteinler üzerine yoğunlaşıldı.

2. bölümde mekanik dönüştürmenin kanserin ilerlemesindeki rolü üzerindeki bulgular sunulmaktadır. Bunun için laboratuvarda oluşturulan üç boyutlu kollajen dokuya tümör hücresi kültüründen alınmış hücreler, bir noktaya iğneyle küresel bir şekilde koyuldu. Birkaç gün boyunca tümör hücrelerinin yayılımları ve çevreleyen kollajen dokunun düzeni incelendi. Tümöroid denilen bu kanser hücresi topluluğunun bir örneğinin, ikinci günden üçüncü güne gelişimini sayfaların sol altında görebilirsiniz. Yirmiden fazla kanser hücresi kültürü ile yapılan çalışmada, kanser tipi ve protein seviyelerinden bağımsız olarak, kollajen ortamı daha uzun mesafelerde düzenleyebilen tümöroidlerin, daha fazla büyüdüğü ve yerel yayılımda bulunduğu gözlemlendi. Bu tümöroidlerden bazıları kollajen ortamı, kendi yayılma alanlarının beş katı mesafeye kadar düzenlediler. Bu uzun mesafe düzenleme bölgesine konulan damar hücreleri, kollajeni düzenleyen tümöroide doğru ilerleme eğilimi gösterdiler. Tümöroidin damar hücreleri ile olan fiziksel bağlantısının koparılması ise bu eğilimi ortadan kaldırdı. Sonuç olarak bu bölümde tümör hücrelerinin ortamları ile olan fiziksel iletişiminin, hem tümör yayılımını hem de tümör ortamında görülen yeni damar oluşumunu etkileyebileceği gösterildi.

3. bölümde hücrelerin integrin profillerinin hücresel mekanik dönüştürmeye etkisi gösterilmektedir. Fibronektin hücrelerarası madde proteinine bağlanan hücrelerin, bu proteine integrin α5β1 veya integrin αvβ3 proteinleri ile bağlanmasının, hücrenin dıştan içe ve içten dışa mekanik dönüştürmesini etkilediği görülmektedir. αvβ3 integrinleri daha çok hücrelerin aktif olduğu süreçlerde görülür, mesela damar oluşumu sırasında endotel hücrelerinde. Her iki durumda da hücreler hem ortamlarına benzer miktarlarda kuvvetler uyguladılar, hem de hücre alanlarını ortam sertliğiyle bağlantılı olarak benzer şekilde arttırdılar. Lakin, α5β1 integrini ile fibronektine bağlanan hücrelerde, aktin hücre iskeletinin daha uzun liflerden oluştuğu, bununla bağlantılı olarak da uygulanan kuvvet doğrultularının daha düzenli olduğu gözlendi. Aktin iskeletinin ilaçlarla daha kısa liflerden oluşmasının sağlandığı durumda ise kuvvetlerin düzeninin azaldığı ve αvβ3 integrini ile bağlanan hücrelere benzediği gözlendi. Buna karşılık αvβ3 integrini ile fibronektine bağlanan hücrelerin ise hem uygulanan kuvvetler karşılığında aktin iskeletlerinin düzenini daha etkin bir şekilde değiştirdikleri görüldü, hem de daha yumuşak ortamlarda hücre-matriks bağlantıları oluşturdukları gözlemlendi.

4. bölümde hücre-matriks bağlantı proteinlerinin miktarının, uygu-

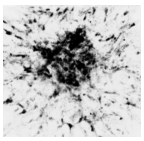

lanan kuvvetle ilişkisi incelendi. Daha önceki çalışmalarda hücresel kuvvetleri etkileyen çeşitli proteinler teşhis edilmişti. Yalnız benim bilgi dahilimde bu proteinlerin hücre bağlantılarındaki miktarları üzerine bir çalışma bulunmamaktadır. Bu bölümde talin, vinkülin, paksilin ve fokal adezyon kinaz ile çalışıldı. Bu proteinlerin daha önceki çalışmalarda integrin-hücre iskeleti bağlantısında ve bu yapıdaki kimyasal bildirimlerde önemli olduğu gözlemlenmiştir. Bu proteinler antikor boyaması ile işaretlendi. Örnekler süper çözünürlüklü floresan mikroskopu tekniği ile nanometre düzeyinde incelendi. Bu yüksek çözünürlüklü görüntülerdeki antikorlar arası mesafeler istatistiksel olarak incelenerek ilk defa belirli alanlardaki işaretlenmiş protein miktarı hesaplandı. Bu teknik ile hücre-matriks bağlantısındaki protein miktarları hesaplandı. Bu teknoloji çekiş kuvveti mikroskopu tekniği ile birlikte kullanılılarak protein miktarları farklı sertlikteki ortamlarda bağlantıların uyguladığı kuvvetlerle ilişkilendirildi. Fokal adezyon kinaz miktarının kuvvetle herhangi bir ilişkisi görülmedi. Talin, vinkülin ve paksilin miktarlarının artması ise daha yüksek kuvvetlerle özdeşleşti. 60 pN gibi bir kuvvet artışı yaklaşık 50 kPa sertliğindeki bir ortamda, 1 talin, 2 vinkülin ve 2 paksilin molekülüyle ilişkilendi. Dört kat daha yumuşak bir ortamda ise aynı kuvvet artışı 2 talin, 6 paksilin ve 12 vinkülin molekülüyle ilişkilendi. Burada vinkülin molekülündeki büyük değişim ortam sertliğiyle bağlantılı faaliyet değişikliğine işaret ediyor. Sonuç olarak bu bölümde ilk defa belirli hücre-matriks bağlantısı proteinlerinin net miktarının bir bağlantıdaki kuvveti nasıl etkilediği incelendi.

5. bölümde tümör hücrelerinin göçü, hücre bağlantısının dinamiği ve hücresel kuvvetleri etkileyen proteinler üzerine çalışıldı. Bunun için çeşitli proteinlerin kodlanmaları küçük RNA parçaları ile engellendi. Bu sayede bu proteinlerin hücredeki miktarlarının azalmasının hücre üzerindeki etkisi incelendi. 200'den fazla proteinin hücre-matriks dinamiğini ve büyüklüğünü etkilediği gözlendi. Bu proteinlerden en etkili olduğu tespit edilen 64 tanesinden 11 tanesinin hücre göçüyle de ilişkili olduğu tespit edildi. Bu proteinlerden TPM1, PPP1R12B, HIPK3 ve RAC2 genleri ile kodlanan 4 tanesinin hücresel kuvvetler üzerindeki etkisi incelendi. PPP1R12B, HIPK3 ve RAC2 genlerinin kodlanmasının engellenmesi, hücresel kuvvetlerin artmasına ve daha yavaş değişmesine sebep oldu. TPM1 geninin kodlanmasının engellenmesi sonucunda ise hücresel kuvvetlerde kayda değer bir değişim görülmedi. Böylece tümör hücrelerinin göçünü, hücre bağlantısının dinamiğini ve hücresel kuvvet-

lerin değişimini etkileyen proteinler teşhis edilmiş oldu.

Bu tezde sunulan bulgular bir bütün olarak ele alındıgında, hem hücresel mekanik dönüştürmenin kanser gelişimindeki etkilerini hem de hücre-matriks bağlantısının moleküler yapısının hücresel kuvvetlerle ilişkisini göstermektedir.

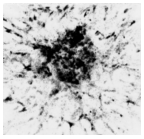

Samenvatting

De rol van integrine adhesies in cellulaire mechanotransductie.

Het vermogen van cellen om extracellulaire mechanische stimulatie in intracellulaire signalen te vertalen wordt mechanotransductie genoemd. Cellulaire mechanotransductie speelt een belangrijke rol in de overleving van cellen, cel differentiatie, cel migratie en de progressie van kanker. Mechanotransductie is een bidirectioneel proces. Cellen nemen de mechanische eigenschappen van de omgeving waar en reguleren daarmee hun intracellulaire signalen. Andersom past de cel de mechanische eigenschappen van de omgeving aan door het uitoefenen van tractie of het afscheiden van extracellulair materiaal. Door deze mechanismen kunnen cellen een dynamisch evenwicht behouden met hun omgeving. De verstoring van dit evenwicht treedt vaak op in pathologische aandoeningen als kanker en fibrose.

Integrines zijn transmembraaneiwitten die de extracellulaire matrix verbinden met het intracellulaire cytoskelet. Deze verbinding verloopt via een dynamisch multimoleculair complex en is geconcentreerd in de cel-matrix adhesie plaques. De rol van de cel-matrix adhesie plaques in mechanotransductie is uitvoerig bestudeerd. Sommige van de eiwitten in de plaques spelen een rol in de krachtoverdracht vanuit de cel naar de extracellulaire matrix en vice versa door een verbinding te vormen tussen de integrines en het actine cytoskelet. Anderen doen dit door in reactie op mechanische stress hun activiteit aan te passen of verborgen eiwit-eiwit interactiegebieden te voorschijn te brengen. Uiteindelijk zorgen deze veranderingen ook voor veranderde chemische signalen bij fysieke stimuli die de activiteit van genen kunnen reguleren. In dit proefschrift beschrijf ik de rol van cellulaire mechanotransductie in kanker en onderzoek de eiwitten die effect hebben op mechanotransductie. Ik richt me specifiek op integrines en andere met integrine geassocieerde eiwitten.

In **hoofdstuk 2** presenteer ik mijn bevindingen op het gebied van mechanotransductie in kankerprogressie. In deze in vitro studie werden tumorcellen met behulp van microprinting in een driedimensionale extracellulaire matrix bestaande uit collageen aangebracht om zo bolletjes (tumoroïdes) te vormen. De ontwikkeling van tumorexpansie en collageen organisatie werd gevolgd gedurende enige dagen. U kunt de expansie van een tumoroïde volgen in de hoek linksonder van de even pagina's van dit proefschrift. Deze studie, waarin ik circa 20 verschillende tumorcellijnen heb gebruikt, geeft aan dat het vermogen om te groeien en lokaal het collageen te doordringen correlatie vertoont met het vermogen om het collageen in de omgeving te reorganiseren. De reorganisatie van het collageen bleek op vrij grote afstand van de tumoroïde plaats te vinden, tot wel vijf maal de radius van de tumoroïde. Wanneer bloedvatcellen werden geprint in deze gebieden bewogen deze in de richting van de tumor. Het verwijderen van de verbinding tussen de tumoroïde en het gereorganiseerde collageen verstoorde die gerichte migratie. De conclusie van dit hoofdstuk is dat de fysieke communicatie tussen tumorcellen en hun omgeving effect heeft op zowel tumorgroei als het rekruteren van bloedvaten, ook wel tumor angiogenese genoemd.

In **hoofdstuk 3** wordt het effect van de expressieprofielen van integrines op cellulaire mechanotransductie gepresenteerd. Cellen werden gehecht aan het extracellulaire matrix eiwit fibronectine via ofwel integrine α5β1 of αvβ3. De cellen bleken trekkrachten van vergelijkbare grootte op het fibronectine uit te oefenen. Daarnaast pasten ze op dezelfde manier hun spreiding aan de stijfheid van de omgeving aan. Echter, cellen die fibronectine voornamelijk binden via αvβ3 vormden cel-matrix adhesie plaques al op zeer zachte substraten vormen en reorganiseerden hun actine cytoskelet relatief sterk wanneer er extracellulaire krachten werden uitgeoefend. Daarnaast, bleek dat deze cellen relatief korte actine cytoskelet draden vormden en krachten op de omgeving in allerlei richtingen uitoefenen terwijl cellen die α5β1 gebruikten langere actine cytoskelet draden vormden en hun krachten op de omgeving vooral centripetaal oriënteerden. Wanneer de cellen met α5β1 behandeld werden met een middel dat de lengte van actinedraden verkortte, raakte de centripetale oriëntatie van de krachten verstoord. Hierdoor gingen de cellen sterk lijken op de cellen die juist αvβ3 voor de hechting gebruiken. Deze studie toont aan dat cellen de mechanische koppeling met de omgeving kunnen moduleren door verschillende integrine receptoren te gebruiken

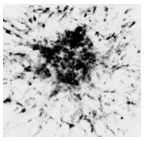

voor de interactie met de extracellulaire matrix.

In **hoofdstuk 4** wordt de relatie tussen de hoeveelheid eiwitten in de cel-matrix adhesie plaques en de uitgeoefende kracht gepresenteerd. In eerdere studies zijn verscheidene eiwitten geïdentificeerd die een effect hebben op de trekkrachten van de cel. Er zijn nog geen studies uitgevoerd die kijken naar het aantal van deze eiwitten in de adhesie. In dit hoofdstuk worden studies naar de cell-matrix adhesie componenten talin, vinculin, paxillin en focal adhesion kinase (FAK) gepresenteerd. Deze eiwitten zijn belangrijk voor de verbinding tussen integrine en actine en voor de biochemische signalen die het actine cytoskelet controleren. We hebben deze eiwitten gedetecteerd met specifieke antilichamen en bestudeerd op nanoschaal met behulp van super resolutie technieken. Uit de hoge resolutie afbeeldingen is de afstand tussen de eiwit lokalisaties statistisch geanalyseerd. Met deze techniek werd het aantal talin, vinculin, paxillin en FAK eiwitten in de cel-matrix adhesie plaques berekend. Door deze aanpak te combineren met trekkracht microscopie kon een relatie worden gelegd tussen het aantal eiwitten en de lokaal uitgeoefende kracht in een adhesie plaque. Het aantal FAK eiwitten bleek geen relatie te hebben met de uitgeoefende kracht. Een toename in talin, vinculin en paxillin moleculen bleek juist duidelijk te correleren met een toename in de uitgeoefende kracht. Voor elke ∼60 pN extra trekkracht op een substraat met een stijfheid van ∼50 kPa bleken 1 talin, 2 vinculin en 2 paxillin moleculen extra te worden gerekruteerd in de adhesie plaque. Op een substraat met een vier keer zo lage stijfheid werd een zelfde toename in kracht geassocieerd met de rekrutering van 2 talin, 12 vinculin en 6 paxillin moleculen. Dit hoofdstuk laat voor het eerst de relatie zien tussen het aantal lokaal aanwezige eiwitten in de adhesie en de kracht die uitgeoefend wordt door de adhesie. De gevonden sterke verandering in vinculin rekrutering bij verlaging van de stijfheid van het substraat wijst op een mogelijke functie als stijfheidsafhankelijke schakelaar.

In **hoofdstuk 5** wordt onderzoek beschreven naar eiwitten die een rol spelen in de migratie van kankercellen, de vorming van cel-matrix adhesie plaques en het uitoefenen van krachten door cellen. Om dit te doen zijn siRNA-knockdowns uitgevoerd en is het effect op borstkankercellen bestudeerd. Er zijn meer dan 200 eiwitten geïdentificeerd die invloed hebben op de grootte en dynamiek van cel-matrix adhesie plaques. De meest effectieve 64 eiwitten zijn getest op hun effect op cel migratie.

Van deze set hadden er 11 ook een significantie invloed op celmigratie. Tot slot zijn vier eiwitten, gecodeerd door de genen TPM1, PPP1R12B, HIPK3 en RAC2, verder bestudeerd met betrekking tot hun rol in de krachtuitoefening door de cel. Het uitschakelen van PPP1R12B, HIPK3 en RAC2 resulteerde in een toename in de krachtuitoefening door de cel en reduceerde de dynamiek van de krachten op de adhesie. Uitschakelen van TPM1 had geen significant effect op krachtuitoefening door de cel. In dit hoofdstuk zijn dus genen geïdentificeerd die coderen voor eiwitten die de migratie van kankercellen, de vorming van cel-matrix adhesies en krachtuitoefening door de cel reguleren.

Samenvattend ontrafelt dit proefschrift de rol van cellulaire mechanotransductie in de verschillende aspecten van kankerprogressie. Het toont de relatie tussen de moleculaire compositie van cel-matrix adhesies en krachtuitoefening door de cel.

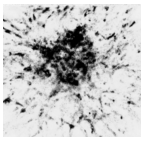

List of Abbreviations

Cas	Crk-associated substrate
CB	Cytoskeleton buffer
CCD	Charged coupled device
cdf	Cumulative distribution function
cdk	Cyclin-dependent kinase
DIC	Differential interference contrast
DMSO	Dimethyl sulfoxide
DRIE	Deep reactive ion etching
dSTORM	Direct stochastic reconstruction microscopy
ECM	Extracellular matrix
EGTA	Ethylene glycol tetraacetic acid
ERK	Extracellular signal-regulated kinases
ES	Embryonic stem
FACS	Fluorescence activated cell sorting
FA	Focal adhesion
FAK	Focal adhesion kinase
FAT	Cell matrix adhesion targeting
FERM	Four-point-one, ezrin, radixin, moesin
GFP	Green fluorescent protein
HEPES	4-(2-hydroxyethyl)-1-piperazineethanesulfonic acid acid
HIPK3	Homeodomain interacting protein kinase 3
IF	Intermediate filaments
ILK	Integrin linked kinase
IPP	ILK-Pinch-Parvin
JNK	c-Jun N-terminal kinase
KO	Knock out
LIM	Lin11, Isi-1, Mec-3
LINC	Linker of nucleoskeleton and cytoskeleton

MAP	Mitogen-activated protein
MAPK	MAP kinase
MEA	Mercaptoethylamine
MEF	Mouse embryonic fibroblast
MES	2-(N-morpholino)ethanesulfonic acid
MT	Microtubules
MYPT2	Myosin phosphatase target 2
NA	Numerical aperture
PAA	Polyacrylamide
PBS	Phosphate buffered saline
PDMS	Poly (DiMethyl)Siloxane
PFS	Perfect focus system
PI3K	Phosphatidylinositol 3-kinase
RAC2	Ras-related C3 botulinum toxin substrate 2
Rb	Retinoblastoma
ROCK	Rho kinase
RPTP-alpha	Receptor-like protein tyrosine kinase alpha
S	Synthesis
SD	Standard deviation
SFM	Serum free medium
SUN	Sad1 and UNC84
VEGF	Vascular endothelial growth factor
VEGFR	VEGF receptor

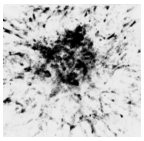

Publications

1. ”Substrate rigidity modulates the association between traction forces and molecular composition of cell matrix adhesions”
   HE Balcıoğlu[1], R Harkes[1], T Schmidt[2], EHJ Danen[2]
   in preparation

2. ”A high-throughput RNAi screen for focal adhesion dynamics”
   M Fokkelman[1], **HE Balcıoğlu**[1], JE Klip, K Yan, FJ Verbeek, EHJ Danen, B van de Water
   in preparation

3. ”Tumor-induced remote ECM network orientation steers angiogenesis”
   HE Balcıoğlu, B van de Water, EHJ Danen
   under review at Scientific Reports

4. ”Cellular mechanosensing is linked to force exertion via p130Cas”
   H van Hoorn[1], DM Donato[1], **HE Balcıoğlu**, EHJ Danen, T Schmidt
   under review at Biophysical Journal

5. "The mechanical phenotype of Ewing sarcoma cell lines predicts their metastatic niche"
   E Beletkaia, O Iendalzeva, **HE Balcıoğlu**, PCW Hogendoorn, EHJ Danen, T Schmidt
   under review at Biophysical Journal

[1] these authors contributed equally to this work
[2] shared corresponding authors

6. "A guide to mechanobiology: Where biology and physics meet"
   KA Jansen; DM Donato; **HE Balcıoğlu**; T Schmidt; EHJ Danen; GH Koenderink
   Biochim Biophys Acta, **1853** (11 Pt B), 3043-52 (2015)

7. "Integrin expression profile modulates orientation and dynamics of force transmission at cell matrix adhesions"
   HE Balcıoğlu, H van Hoorn, DM Donato, T Schmidt, EHJ Danen
   J Cell Sci, **128** (7), 1316-26 (2015)

8. "A mechanical-biochemical feedback loop regulates remodeling in the actin cytoskeleton"
   MR Stachowiak, MA Smith, E Blankman, LM Chapin, **HE Balcıoğlu**, S Wang, MC Beckerle, B O'Shaughnessy
   Proc Natl Acad Sci U S A, **111** (49), 17528-33 (2014)

9. "β1 integrin inhibition elicits a prometastatic switch through the TGFβ-miR-200-ZEB network in E-cadherin-positive triple-negative breast cancer"
   HH Truong, J Xiong, VPS Ghotra, E Nirmala, L Haazen, SE Le Dévédec, **HE Balcıoğlu**, S He, EB Snaar-Jagalska, E Vreugdenhil, et al.
   Sci Signal, **7** (312), ra15 (2014)

10. "Integrin signaling in control of tumor growth and progression"
    J Xiong, **HE Balcıoğlu**, EHJ Danen
    Int J Biochem Cell Biol, **45** (5), 1012-5 (2013)

11. "Self-organization of myosin II in reconstituted actomyosin bundles"
    MR Stachowiak, PM McCall, T Thoresen, **HE Balcıoğlu**, L Kasiewicz, ML Gardel, B O'Shaughnessy
    Biophys J, **103** (6), 1265-74 (2012)

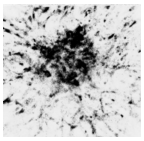

Curriculum vitae

Hayri Emrah Balcıoğlu was born on July 20, 1986 in Şişli, İstanbul, Turkey. He studied Electrical Engineering and Physics in Boğaziçi University from 2004 to 2008 with emphasis on Solid State Engineering and Solid State Physics. After obtaining bachelor degrees in both fields, he started the MS-PhD track at Applied Physics & Applied Mathematics Department in the Fu Foundation School of Engineering & Applied Science, Columbia University in the City of New York. He obtained his MSc degree in Applied Physics in 2009 and worked for some time with Prof. Ben O'Shaughnessy in the Department of Chemical Engineering at Columbia University. His work there on modeling actin stress fibers contributed to two publications.

In 2010 he started as a PhD student on a project, funded by NWO FOM (Foundation for Fundamental Research on Matter) at Leiden University under the supervision of Dr. Erik Danen. The project was part of the Dutch Mechanobiology consortium, and involved close collaboration with Prof. Thomas Schmidt at the Physics of Life Processes group in Leiden University.

In April 2016, Emrah will start a postdoctoral fellowship in the group of Prof. Benoit Ladoux at the Mechanobiology Institute, Singapore.